1980

Analysis of induction machine dynamics during power system unbalances

Thomas Howard Ortmeyer
Iowa State University

ORTMEYER, THOMAS HOWARD

ANALYSIS OF INDUCTION MACHINE DYNAMICS DURING POWER SYSTEM UNBALANCES

Iowa State University PH.D. 1980

Analysis of induction machine dynamics during power system unbalances

by

Thomas Howard Ortmeyer

A Dissertation Submitted to the
Graduate Faculty in Partial Fulfillment of the
Requirements for the Degree of
DOCTOR OF PHILOSOPHY

Major: Electrical Engineering

Approved:

Signature was redacted for privacy.

In Charge of Major Work

Signature was redacted for privacy.

For the Major Department

Signature was redacted for privacy.

For the Graduate College

Iowa State University
Ames, Iowa

1980

TABLE OF CONTENTS

NOMENCLATURE

ω_r	rotor speed
θ_r	rotor position
λ_{as}, λ_{bs}, λ_{cs}	stator phase flux linkages
λ_{ark}, λ_{brk}, λ_{crk}	kth loop rotor phase flux linkages
i_{as}, i_{bs}, i_{cs}	stator phase currents
i_{ark}, i_{brk}, i_{crk}	kth loop rotor phase currents
L_s	stator self-inductance
L_{sm}	mutual inductance between stator phases
L_r	rotor external self-inductance
L_{rm}	mutual inductance between rotor phases
L_{is-jr}	peak mutual inductance - stator to rotor
v_{as}, v_{bs}, v_{cs}	stator phase voltages
p	differential operator $\frac{d(\ )}{dt}$
r_s	stator phase resistance
R_k	kth loop rotor phase resistance
L_k	kth loop rotor internal self-inductance
θ	stator reference angle - arbitrary reference frame
$[P_\theta]$	Park's transformation of stator quantities
$[P_\beta]$	Park's transformation of rotor quantities
β	rotor reference angle - arbitrary reference frame
λ_{ds}, λ_{qs}	stator d and q axis flux linkages
i_{ds}, i_{qs}	stator axis currents
v_{ds}, v_{qs}	stator axis voltages

λ_{drk}, λ_{qrk}	rotor axis flux linkages
i_{drk}, i_{qrk}	rotor axis currents
T_e	electrical torques
T_m	mechanical load torque
P	number of poles of the machine
ω_o	rated angular frequency
ω_b	base angular frequency
H	inertia constant $\frac{MW - sec}{MVA}$
s	per unit slip
r_e	source resistance
l_e	source inductance
$v_{a\infty}$, $v_{b\infty}$, $v_{c\infty}$	phase infinite bus voltages
$v_{d\infty}$, $v_{q\infty}$	axis infinite bus voltages
b (subscript)	base quantity
M	magnetizing inductance
l_s	stator leakage inductance
$\underline{(\cdot)}$	matrix expression
j	-1
$\overline{F}$	general phasor quantity
$\overline{i}$	current density
$\overline{E}$	electric field
$\overline{H}$	magnetic field
ρ	conductivity
μ	permeability
$(\cdot)_x$	x directed component of a vector quantity

ABSTRACT

This study investigates the effects of power system unbalances on dynamic induction motor operation. It was determined that the classical induction motor dynamic models do not provide accurate results during unbalanced conditions due to the failure of these models to account for the rotor bar skin effect. A rotor bar representation which predicts the skin effect is developed. Using this representation, two mathematical models of the induction machine are introduced which are capable of accurately predicting the rotor bar skin effect during dynamic machine operation with unbalanced power system conditions. One model predicts both the electrical and motional transients while the other ignores the electrical transients and predicts only the motional transient. The developed models were used to study three important practical cases of power system imbalance: open delta motor feed, shunt, and series single phase faults on the power system. The necessity of evaluating the skin effect in the rotor representation is clearly established in each case, and the need to account for the electrical transients is evaluated.

CHAPTER I. INTRODUCTION

Induction motors form a significant portion of the power system load. In addition to the induction motor loads, the power system must also supply loads ranging from process heat to sensitive micro-electronics. The individual loads range in size from milli- or microwatts to megawatts. To meet the specific individual requirements of these diverse loads, the power system must be designed properly. This, however, can only be achieved with sufficient knowledge of both the power system and the load characteristics.

Investigations of both power system and load characteristics have been conducted for many years. These studies have involved a wide range of system conditions: dynamic and steady-state, normal and abnormal, balanced and unbalanced.

Induction Motor Analysis

Since the induction motor is of great importance, a significant portion of the analysis has been focused directly on the motor operation. Furthermore, extensive studies of induction motor operation have been continually desired for the purpose of evaluating motor design. As a result of the differing goals of these studies, differing tools of analysis have also emerged.

Induction motor analysis is conducted under either steady state or dynamic state conditions. Steady state analysis is generally approached through the use of the steady state equivalent circuits. Many forms of the induction motor equivalent circuit exist with each form designed for a specific application. Induction motor dynamic models are used during all

periods other than the steady state. Currently, two types of representation are commonly in use: models which predict the electrical transients and models which totally ignore the electrical transients. While the former is inherently more accurate, both types of models are widely used for motor-power system studies.

Motor-Power System Studies

From the power system side, important aspects of induction motor operation are motor starting characteristics and motor operating power requirements. Motor heating during both balanced and unbalanced power system conditions are also important. Analysis of motor losses and power flow are important in machine design to determine efficiency and temperature rise.

Evaluation of the electrical transients which follow system disturbances are of great interest, as are motor response to special power system conditions such as series or shunt compensation or unbalanced system conditions.

Analysis of unbalanced power system conditions is of particular interest due to their common occurrence. Steady state unbalanced conditions have been analyzed and documented. Dynamic induction motor operations during power system imbalances have not been fully analyzed, however. No suitable dynamic motor model has been proposed for use under unbalanced power system conditions. Several dynamic problems nevertheless exist. These problems include motor starting through an open delta bank; single phase to ground faults near the motor; and single phasing, or unbalanced

series faults. Since these problems are common, a definite need exists for motor-power system analysis during unbalanced dynamic motor operation. A suitable dynamic motor model must be found in order to accomplish this goal.

Research Objectives

The objectives of this research are to establish a suitable dynamic induction motor model for the analysis of motor operation during unbalanced power system conditions which will then be utilized to analyze several important operational problems. The classical dynamic induction motor models are not suitable for use in these studies, as they ignore the influences of rotor bar skin effects on motor performance. It is therefore necessary to analyze the general laws of electromagnetic phenomena as they apply in and near the rotor bar. These laws must be incorporated into the existing methods of induction motor analysis to provide a more general representation of the motor which assesses the rotor bar skin effect during dynamic periods of motor operation.

This model will be used to study specific motor operating conditions which involve dynamic operation with unbalanced power system conditions. These studies will provide information necessary for the design and implementation of the induction motor and power system equipment.

Existing dynamic machine models are evaluated in Chapter 3, where it is concluded that new dynamic models are necessary in order to properly describe the rotor bar skin effect.

In Chapter 4, a rotor bar representation is derived which describes the skin effect and is compatible with existing motor models.

Chapter 5 incorporates this rotor bar representation into a dynamic model based on the two axis theory. The representation is capable of describing both the rotor bar skin effect and the electrical transients which occur during dynamic operation. This model is referred to as the skin effect electrical transient model.

In Chapter 6, a simplified model is presented which describes the rotor bar skin effect but neglects the electrical transients. This model is referred to as the skin effect impedance model.

The motor starting transient is analyzed in Chapter 7 for motors fed through open delta transformer banks. The convergence of these models is verified, and differences between the skin effect impedance model and the skin effect electrical transient model are discussed. The overall influence of open delta banks on motor starting is also analyzed.

Chapter 8 contains a similar study concerned with single phase to ground faults at the motor terminal, while single phase series faults are analyzed in Chapter 9.

The overall conclusions of this study are presented in Chapter 10.

CHAPTER II. REVIEW OF LITERATURE

Induction motor analysis has been evolving since the introduction of the motor itself. The earliest efforts were confined to steady state analysis (16). The steady state analysis developed quickly to become extremely useful in a wide variety of induction motor studies. The usefulness of this analysis continues to grow to date (14); (52). Meanwhile, the analysis of induction motor transient performance has also received widespread attention. The equations describing the machine have been expressed in a variety of forms (39); (51); (10). The equivalence of these forms has been shown (1); and, at present, the most popular form is similar to the two axis theory of the synchronous machine (46); (47); (37). Because of the importance of synchronous machine analysis to the power system planners, the two axis theory of the synchronous machine has been widely studied and is well-documented (4); (1). Induction motor transient analysis benefited from the interest in synchronous machines, and a two axis theory for the induction motor has been developed (35); (49). Use of this induction motor model has been reported in the areas of motor starting (27); (43); (44); (23); short circuit studies (32) and with power system transient studies (17); (28); (40); (54).

Deep Bar and Double Cage Motors

The rotor bar current distribution in a squirrel cage induction motor varies from motor starting to motor running. This fact produces beneficial effects in limiting starting current while maintaining high

starting torque and low running slips. In order to maximize this effect, deep bar and double cage induction motors were introduced. The analytical techniques of induction motor analysis were expanded to include these new types of motors (2); (5); (7); (11); (12); (19); (26); (36). These techniques were limited to steady state analysis for several years. Transient motor analysis which recognized the effects of rotor bar current distribution (or skin effect) began in the late 1960's. Humpage, Durrani, and Curvalho (24) proposed to recalculate rotor resistance and inductance in the two axis theory continuously as the motor went through a transient. Klingshirn and Jordan (34) use a generalization of the steady state theory reported by Babb and Williams (5) for a dynamic model. In an approach taken from synchronous machine analysis, the short-circuit machine characteristics can be used to obtain a dynamic motor representation (30); (31); (32). Most recently, Smith and Nichols (55) propose a motor model obtained by a curve fitting procedure involving the steady state torque-speed characteristic of the motor. These motor models vary significantly. None of them has been conclusively shown to be better than the others in representing the rotor bar skin effect. Furthermore, the analysis for which they have been used has been limited to either balanced voltage conditions at operating speeds or balanced voltage conditions during motor starting.

Rotor Bar Characteristics

Many studies of rotor bar phenomena have been conducted over a long period of time. These studies have, however, been limited to steady

state conditions. Field (13) first formulated the most commonly used expressions by assuming a one-dimensional field in a rectangular rotor bar. More recent studies (41); (50); (57) investigated this assumption and identified conditions under which this assumption is valid, which encompasses a large number of practical motor designs. Studies involving varying rotor bar geometries (5); (11); (38) have further expanded the usefulness of this analysis. These studies, however, have all been limited to steady state conditions. Descriptions of rotor bar phenomena are necessary in the transient state.

Symmetrical Component Analysis

The introduction of symmetrical components (15) was quickly followed by positive and negative sequence induction motor analysis (8); (33). It was quickly noted that rotor bar current distribution significantly affects the sequence parameters. Williams (60) developed a method of quantifying this effect, and applied it to the study of heating effects in motors fed by unbalanced voltages. Further studies in this area have been undertaken, (6); (18) and motor limitations are discussed. The open delta transformer-fed motor has also been analyzed (22); (53) under steady state motor conditions. The operation of a three phase motor with one phase open was investigated, again with only steady state conditions analyzed, using the method of symmetrical components (8); (9); (21). Analysis of power system equipment is also extremely important in obtaining an accurate prediction of motor performance (3); (42); (56).

Aspects of Motor Operation

Induction motor operation when fed by unbalanced system voltages are to be investigated. Several specific areas of this operation have been analyzed.

The first area of interest is the additional motor heating due to unbalanced voltages. This area has been thoroughly investigated and appears to be understood. In the investigation of motor heating, for which account of rotor skin effect is taken, only steady state conditions are of interest.

The development of a model capable of accounting for rotor bar skin effect under dynamic operating conditions is essential for the study of several other motor problems, the most important of which are: the starting of a motor fed by open delta transformer (22); (53); the single phase to ground short circuit (58); and the sudden opening of one phase of the motor feed (8); (9); (21). These are all dynamic problems which require the development of a suitable model.

CHAPTER III. PRESENT INDUCTION MOTOR ANALYSIS UNDER UNBALANCED POWER SYSTEM CONDITIONS

Induction motor analysis is generally conducted at one of two levels. The most common type of analysis is based on the steady state equivalent circuit. Many forms of the equivalent circuit exist, each designed for a particular motor type or for a particular analytical problem. The equivalent circuits are versatile and well-documented. In many instances, they can be used for dynamic as well as steady state calculations.

The second type of analysis is intended primarily for dynamic studies. It is capable of predicting the electrical transients of the induction motor, which are neglected by the impedance type calculations of the equivalent circuits. This method of analysis is generally referred to as the two axis or dq axis theory, as it employs a change of reference to simplify the mathematical description. It can be shown that, under balanced steady state conditions, the two axis theory and the steady state impedance calculations are in agreement (43).

The use of both of these types of analysis for the study of electrically unbalanced induction motor operation has been previously reported. The study of motor heating under unbalanced steady state conditions appears to be particularly well-documented, and proposals have been developed in this area to limit overheating, which can lead to motor failure.

The Need for Analysis of Unbalanced Motor Operations

Unbalanced power system conditions produce several undesirable operating conditions in the motor. Unbalanced motor currents can be separated into two components: one component produces a magnetic flux wave in the motor air-gap which travels in the direction of motor rotation, and one produces a flux wave which travels in the reverse direction. Under balanced conditions, only the forward traveling wave is present. Under unbalanced conditions, both flux waves are present. Furthermore, the flux wave traveling in the reverse direction causes the development of a retarding torque. This retarding torque must be counteracted by increased flux levels traveling in the positive direction to develop an increased torque in the direction of rotation.

Unbalanced power system conditions therefore lead not only to unbalanced motor currents, but also to increased current levels in the motor which counteract the retarding torque. In extreme cases the retarding torque can be of sufficient magnitude to cause the motor to stall.

Additionally, the interaction of positively and negatively traveling flux waves produces a fluctuating torque of 120 hertz. This fluctuating torque can present problems if a resonance of the mechanical system occurs at or close to 120 hertz. Problems also can arise if the magnitude of these fluctuations becomes overly large.

Unbalanced operation of the induction motor is dealt with at two levels: the steady state and the dynamic state. Steady state problems are handled by ensuring that permissable levels of voltage unbalance will not cause destructive overheating of the motor, and by designing the

motor mechanical system so that no mechanical resonances occur near 120 hertz.

Practical dynamic problems caused by the interaction of an induction motor with an unbalanced power supply have not been as closely studied. Protection of the motor from these dynamic problems is largely limited to overcurrent protection to prevent motor overheating. Careful study of these problems is needed to identify and evaluate specific problem areas. A proper understanding of these phenomena will lead to better motor design and operation.

Analysis by Impedance Methods

The positive and negative sequence equivalent circuits of the induction motor are widely used to analyze machine operation under steady state conditions with unbalanced machine terminal voltages. The positive sequence equivalent circuit of the induction motor is shown in Figure 3.1 (a) and the negative sequence equivalent circuit is shown in Figure 3.1 (b). Positive and negative sequence terminal voltages can be calculated from the a, b, and c phase terminal voltages. Sequence currents and torques can then be found from the sequence voltages and the impedances of the sequence equivalent circuits. The magnitude of the 120 hertz oscillating torque can also be found from the sequence currents, although it is generally not calculated (8). Zero sequence currents are usually not allowed to flow in the motor, so evaluation of a zero sequence equivalent motor circuit is not necessary. Zero sequence voltages may exist at

the motor terminals, however, and can be of interest in studying insulation levels.

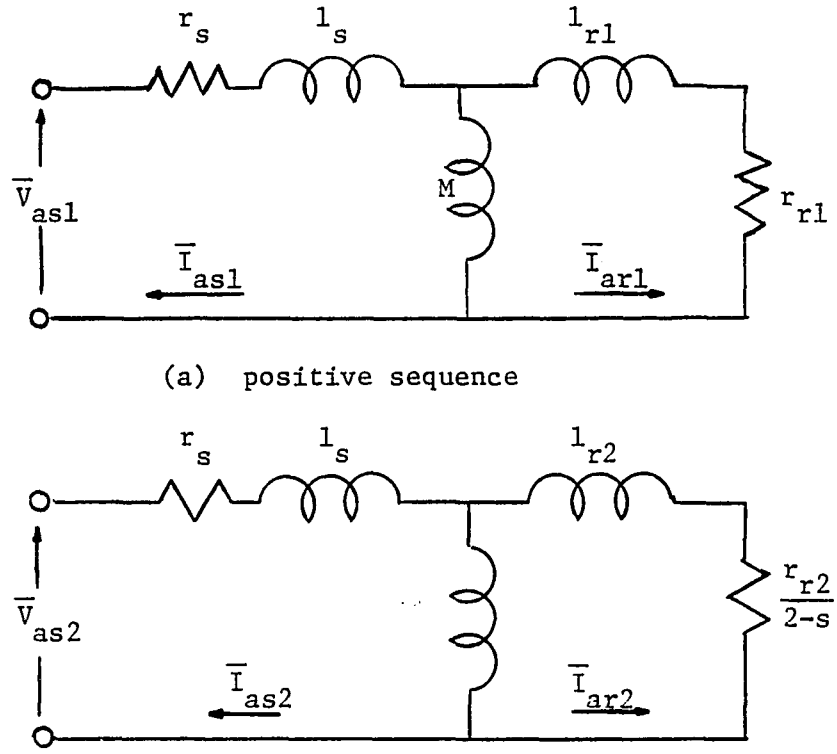

Figure 3.1. Positive and negative sequence equivalent circuits of the induction motor

The impedance calculations of the equivalent circuits, of course, neglect any electrical transients which occur in the dynamic state. It has been shown (43), however, that in many balanced cases of practical interest, evaluation of these electrical transients is not necessary. Dynamic models using the positive sequence equivalent circuit are suitable for use in a wide variety of balanced induction motor problems. An impedance model based on the positive and negative sequence equivalent

circuits will be investigated for use in studying dynamic induction motor problems under unbalanced power system conditions.

The positive sequence equivalent circuit was introduced soon after the invention of the induction motor (16). It has been thoroughly documented for use in studying a wide variety of problems, and continues to be an important tool for studying induction motor behaviour.

The negative sequence equivalent circuit was introduced soon after the introduction of symmetrical components to power system analysis (33). In fact, the forward and backward rotating fluxes in the motor air-gap provided some of the impetus for the theory of symmetrical components (14).

Early in the development of induction motors, it was noted that the dynamic impedance of the rotor conductors is influenced by the frequency of the current flowing in these bars. This phenomenon is known as the skin effect, and has been documented in many areas of electrical engineering. Approximately 30 years ago, deep bar and double cage induction motors were introduced to take advantage of the skin effect to increase starting torque and decrease inrush current.

At the same time, efforts were made to quantify this effect (5); (11). These efforts also provided methods for calculating the positive and negative sequence rotor resistance and inductance. The ratio of negative sequence rotor resistance to positive sequence rotor resistance has been reported to be as high as eight for a particular rotor design (21). This effect, which is particularly prominant in deep bar and double cage motors, is significant in all types of induction machines.

The presence of resistance and inductance in the equivalent circuits which vary with rotor speed limits the usefulness of these circuits as the basis for a dynamic model of the induction motor. It is possible, however, that such a model could be useful in problems which involve a very small range of rotor speeds.

Analysis Including the Electrical Transients

Methods which consider the electric transients during dynamic induction motor situations have also been developed. The most prominent of these methods is based on the ideal electric machine theory. This theory consists of a set of assumptions about machine operation applicable to all types of electric motors.

Using these assumptions, voltage and flux linkage equations for each motor phase can be written. These phase equations can then be simplified by Park's transformation to the odq reference frame. Because of the symmetrical natures of the induction motor, no definite physical placement of the d and q axes is necessary, and several convenient reference frames are in use. The arbitrary reference frame is an intermediate method of expressing the motor equations without specifying the particular reference frame to be used. The d and q axis of the arbitrary reference frame are shown in Figure 3.2, along with the phase windings of the stator and rotor.

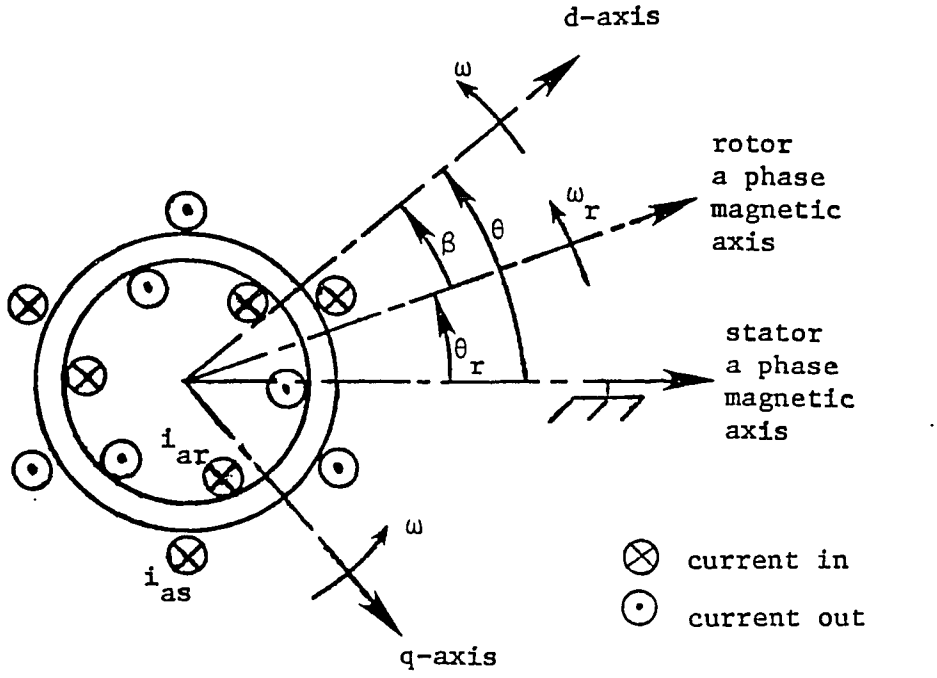

Figure 3.2. Motor with magnetic axes and arbitrary d and q axes shown

The o axis equations of the induction motor are generally neglected as o axis currents cannot flow in ungrounded induction motors. The d and q axis equations of the arbitrary reference frame are given in Equation 3.1, in per unit quantities.

$$\begin{bmatrix} v_{ds} \\ v_{dr} \\ \hline v_{qs} \\ v_{qr} \end{bmatrix} = \left[\begin{array}{cc:cc} r_s & 0 & & \\ 0 & r_r & \multicolumn{2}{c}{\underline{0}} \\ \hdashline & & r_s & 0 \\ \multicolumn{2}{c:}{\underline{0}} & 0 & r_r \end{array}\right] \begin{bmatrix} i_{ds} \\ i_{dr} \\ \hline i_{qs} \\ i_{qr} \end{bmatrix} + \left[\begin{array}{cc:cc} L_{ss} & M & & \\ M & L_{rr} & \multicolumn{2}{c}{\underline{0}} \\ \hdashline & & L_{ss} & M \\ \multicolumn{2}{c:}{\underline{0}} & M & L_{rr} \end{array}\right] \begin{bmatrix} pi_{ds} \\ pi_{dr} \\ \hline pi_{qs} \\ pi_{qr} \end{bmatrix} + \tag{3.1}$$

$$\begin{bmatrix} & \vdots & L_{ss}p\theta & Mp\theta \\ \underline{0} & \vdots & & \\ & \vdots & Mp\beta & L_{rr}p\beta \\ \cdots\cdots & \vdots & \cdots\cdots & \cdots\cdots \\ -L_{ss}p\theta-Mp\theta & \vdots & & \\ & \vdots & \underline{0} & \\ -Mp\beta-L_{rr}p\beta & \vdots & & \end{bmatrix} \begin{bmatrix} i_{ds} \\ i_{dr} \\ \cdots \\ i_{qs} \\ i_{qr} \end{bmatrix} \tag{3.1}$$

The subscripts d and q refer to the d and q axes, respectively; and the subscripts s and r refer to stator and rotor quantities, respectively. p is the differential operation d(•)/dt, and the angles θ and β are defined in Figure 3.2. The general quantities v, i, r, L, and M refer to voltage, current, resistance, self-inductance, and mutual inductance, respectively.

Equation 3.1 is a system of ordinary differential equations. If the quantities pθ and pβ are constants these equations become linear, and the principle of superposition applies to their solution. As θ and β are angular positions, pθ and pβ are angular speeds. Therefore, the machine electrical equations are linear under constant speed conditions.

Consider positive sequence voltages in the synchronously rotating reference frame. Then

$$\theta = \omega_0 t$$
$$\beta = (\omega_0-\omega_r)t = s\omega_0 t \tag{3.2}$$

where ω_o is the synchronous frequency, ω_r is the rotor speed and s is the per unit rotor slip. The axis voltages are

$$v_{ds} = \sqrt{3}\, V_1 \cos\alpha_1$$
$$v_{qs} = -\sqrt{3}\, V_1 \sin\alpha_1 \tag{3.3}$$

where V_1 is the positive sequence rms phase voltage and α_1 is the angle between a phase voltage and reference. As the voltage inputs to the equations are constants, the steady state solutions will also be constant. In the steady state, Equation 3.1 becomes

$$\begin{aligned}
\sqrt{3}\, V_1 \cos\alpha_1 &= r_s i_{ds} + \omega_0 L_{ss} i_{qs} + \omega_0 M i_{qr} \\
-\sqrt{3}\, V_1 \sin\alpha_1 &= r_s i_{qs} - \omega_0 L_{ss} i_{ds} - \omega_0 M i_{dr} \\
0 &= r_r i_{dr} + s\omega_0 M i_{qs} + s\omega_0 L_{rr} i_{qr} \\
0 &= r_r i_{qr} - s\omega_0 M i_{ds} - s\omega_0 L_{rr} i_{dr}
\end{aligned} \tag{3.4}$$

Transformation of the axis quantities to phase quantities, followed by a phasor transformation, yields

$$\bar{I}_{as} = \frac{1}{\sqrt{3}} (i_{ds} - j i_{qs}) \tag{3.5}$$

with similar expressions for $\bar{V}_{as}$ and $\bar{I}_{ar}$. The motor equations then become

$$\begin{aligned}
\bar{V}_{as} &= (r_s + j\omega_0 L_{ss})\, \bar{I}_{as} + j\omega_0 M \bar{I}_{ar} \\
0 &= \left(\frac{r_r}{s} + j\omega_0 L_{rr}\right) \bar{I}_{ar} + j\omega_0 M \bar{I}_{as}
\end{aligned} \tag{3.6}$$

As the stator and rotor self-inductances can be separated into magnetizing and leakage inductances, the equations can be rewritten as

$$\begin{aligned}
\bar{V}_{as} &= (r_s + j\omega_0 \ell_s)\, \bar{I}_{as} + j\omega_0 M(\bar{I}_{as} + \bar{I}_{ar}) \\
0 &= \left(\frac{r_r}{s} + j\omega_0 \ell_r\right) \bar{I}_{ar} + j\omega_0 M(\bar{I}_{as} + \bar{I}_{ar})
\end{aligned} \tag{3.7}$$

These equations agree with the equations of the positive sequence equivalent circuit of Figure 3.1(a).

Next, consider negative sequence voltages in a reference frame rotating at synchronous speed in the direction opposite to rotor rotation. Then

$$\theta = -\omega_0 t$$
$$\beta = -(\omega_0+\omega_r)t = -(2-s)\omega_0 t \tag{3.8}$$

Transformation of the negative sequence voltages onto this reference frame yield

$$v_{ds} = \sqrt{3}\, V_2 \cos\alpha_2$$
$$v_{qs} = \sqrt{3}\, V_2 \sin\alpha_2 \tag{3.9}$$

These voltages are constants; the reference frame will thus be referred to as the negative sequence reference frame. The steady state currents in this reference frame will be constant only if the applied voltage is purely negative sequence. The steady state equations with negative sequence applied voltage are

$$\sqrt{3}\, V_2 \cos\alpha_2 = r_s i_{ds} - \omega_0 (L_{ss} i_{qs} + M i_{qr})$$
$$\sqrt{3}\, V_2 \sin\alpha_2 = r_s i_{qs} + \omega_0 (L_{ss} i_{ds} + M i_{dr})$$
$$0 = r_r i_{dr} - (2-s)\, \omega_0 (L_{rr} i_{qr} + M i_{qs})$$
$$0 = r_r i_{qr} + (2-s)\, \omega_0 (L_{rr} i_{dr} + M i_{ds}) \tag{3.10}$$

Transformation of the axis quantities to phase quantities, followed by a phasor transformation, yields

$$\bar{I}_{as} = \frac{1}{\sqrt{3}} (i_{ds} + j i_{qs}) \tag{3.11}$$

with similar expressions for $\bar{I}_{ar}$ and $\bar{V}_{as}$. Combination of the stator equations yields

$$\bar{V}_{as} = (r_s + j\omega_0 L_{ss})\, \bar{I}_{as} + j\omega_0 M \bar{I}_{ar} \tag{3.12}$$

The rotor equations when combined and transformed to phasor quantities become

$$0 = \left(\frac{r_r}{2-s} + j\omega_0 L_{rr}\right) \bar{I}_{ar} + j\omega_0 M \bar{I}_{as} \tag{3.13}$$

Again separating the rotor and stator self-inductances into mutual and leakage components, the motor equations become

$$\bar{V}_{as} = (r_s + j\omega_0 \ell_s) \bar{I}_{as} + j\omega_0 M(\bar{I}_{ar} + \bar{I}_{as})$$

$$0 = \left(\frac{r_r}{2-s} + j\omega_0 \ell_r\right) \bar{I}_{ar} + j\omega_0 M(\bar{I}_{ar} + \bar{I}_{as}) \tag{3.14}$$

These equations agree with the equations of the negative sequence equivalent circuit of Figure 3.1.

The motor currents can be found by superposition of the solutions of the positive and negative sequence equivalent circuits. Notice, however, that the positive and negative sequence equations 3.7 and 3.14 employ the same quantities for positive and negative sequence resistance as well as inductance. The two axis theory does not, therefore, agree with the equivalent circuit analysis in the steady state, since it does not account for the rotor skin effect in any way.

The rotor bar skin effect, however, has been shown to significantly influence the motor performance. This is particularly true in cases involving unbalanced power system voltages feeding the motor. Therefore, a more general induction motor model is required in order to study these conditions. This model should be based on existing methods but must be capable of accurately predicting rotor bar current distribution and skin effect. It must be fully capable of predicting motor operation during dynamic conditions, but must agree with established methods of analysis under steady state conditions.

Summary

The existing induction motor models appear to be of limited usefulness for the study of dynamic motor operation under unbalanced power system conditions. These inadequacies are a result of assumptions made in the treatment of the skin effect on the rotor bars.

Dynamic induction motor models are needed which account for the rotor skin effect. It would be desirable to obtain both an impedance type model similar to steady state equivalent circuit analysis and a model which is capable of predicting the electrical as well as motional transients.

CHAPTER IV. ANALYSIS OF ROTOR BAR CURRENT DISTRIBUTION

In order to develop an induction motor model which is suitable for use with unbalanced power system conditions, a method of determining the rotor bar current distribution must be found. Nonuniform current distribution affects the dynamic rotor bar resistance and inductance, and significantly alters motor performance under both steady state and dynamic conditions. It is desirable that a model describing this phenomenon, which is often called the skin effect, be developed which is compatible with both equivalent circuit analysis and the two axis theory.

Several studies have been published which investigate the skin effect in rotor bars. Babb and Williams (5) and Douglas (11) present methods of calculating rotor bar impedance for various rotor bar geometries. These methods, however, are limited to steady state conditions and were not extended to any type of dynamic situation. Klingshirn and Jordan (34) extend the methods of Babb and Williams to a dynamic model for the study of motor starting under balanced voltage conditions. Smith and Nichols (55) developed a dynamic model using a curve fitting technique involving the steady state torque-speed curve. This model is also used in balanced motor starting studies. In an approach closely related to synchronous machine analysis, Kalsi and Adkins (31) develop an expanded dynamic motor model based on the short circuit parameters of the machine. This model is suitable for use in balanced power system transient analysis only.

Careful analysis of the induction motor rotor is necessary in order to select the best method of predicting the rotor performance under dynamic

unbalanced power system conditions. None of the currently available dynamic models have been evaluated for application to unbalanced power system conditions. Furthermore, in only one case (31) is a suitable justification of the dynamic model presented which allows analysis of the limitations of the model. Therefore, a detailed analysis of the rotor bar is necessary in order to determine the most appropriate representation of the rotor under dynamic conditions.

General Rotor Bar Representation

Any new model describing the rotor bar skin effect should conform with circuit theory in order for it to be compatible with the existing models of the induction motor. The equations for the skin effect model, however, must be derived from Maxwell's equations. It is general practice when computing the inductance of a circuit from Maxwell's equations to separate the inductance into two components: an external inductance and an internal inductance. The external inductance is a function of the geometry of the circuit and the materials involved, and is not a function of the currents flowing in the conductor. The internal inductance, however, is a function of the current distribution in the conductor. It will be necessary in arriving at the desired model of a rotor bar to find expressions for the internal inductance and the internal resistance of the bar.

Since the rotor bar is a good conductor, Maxwell's equations using good conductor properties will be used. Several basic properties apply to good conductors (48). In a good conductor, Ohm's law states that

$$\bar{i} = \sigma \bar{E} \tag{4.1}$$

where $\bar{i}$ is the current density, σ is the conductivity, and $\bar{E}$ is the electric field. The applicability of Ohm's law implies that no free charge exists in the conductor. The third property of a good conductor is that displacement current is negligible. Under these conditions,

$$\nabla \times \bar{H} = \bar{i}$$

and

$$\nabla \times \bar{E} = -\mu \frac{\partial \bar{H}}{\partial t} \tag{4.2}$$

Where $\bar{H}$ is the magnetic field and μ is the permeability. $\nabla x(\cdot)$ indicates the curl of a quantity.

Consider a rectangular rotor bar as is shown in Figure 4.1. The coordinate system which will be used is also shown. It is assumed that the current flows only in the x direction, and that the current density is constant at any particular value of z. The second assumption implies that the magnetic field in the y direction is the only time varying field component. The vector quantities in Equation 4.2 then simplify to the scalar equations

$$\frac{\partial E_x}{\partial Z} = -\mu \frac{\partial H_y}{\partial t} \tag{4.3}$$

$$-\frac{\partial H_y}{\partial Z} = i_x \tag{4.4}$$

These two equations form a set of partial differential equations in one space dimension and time. It is not possible to obtain exact closed form solutions of these equations with the exception of a few specialized cases. It is possible to approximate these equations with a set of ordinary

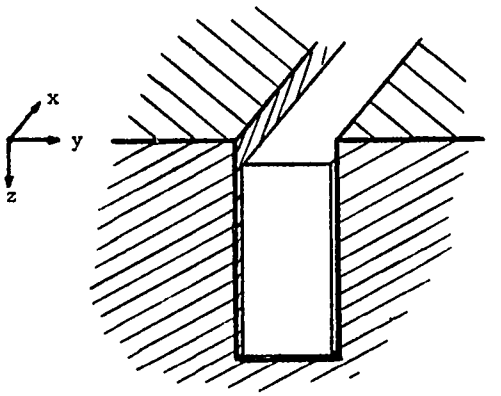

Figure 4.1 Cross section of a portion of a squirrel cage induction motor rotor showing one rotor bar

differential equations in time. This can be accomplished by dividing the bar into a finite number of segments. This set of ordinary differential equations appears to be desirable as they should be readily adaptable to step-by-step time solution in conjunction with the ordinary differential equations of the induction machine's two-axis theory. Rotor bars with variable widths can be treated as a series of rectangles of varying width by matching boundary conditions at the boundaries between rectangles. This analysis is limited to cases in which the assumption of uniform current density in the y-direction still holds.

Approximate Rotor Bar Equations

Any function of two variables, such as $f(z,t)$, can be written as

$$f(z_m+h,t) = f(z_m,t) + h\left[\frac{\partial f}{\partial z}\Big|_{z = z_m}\right] + R \tag{4.5}$$

For small h, R is small, and an approximate expression of Equation 4.5 is

$$f(z_m+h,t) = f(z_m,t) + h\left[\frac{\partial f}{\partial z}\Big|_{z=z_m}\right] \tag{4.6}$$

Let $z_o=0$ and

$$z_{m+1} = z_m + h_{m+1} \tag{4.7}$$

for m=1,2,3$\cdots$,N, where z_N is the depth of the bar. The bar, then, is divided into N segments of arbitrary depth. The depth, h_m, of each segment, however, is small enough that Equation 4.5 is a valid approximation. Then

$$\frac{\partial H_y}{\partial z}\Bigg|_{z=z_m} = \frac{1}{h_{m+1}} \left[H_y(z_{m+1},t) - H_y(z_m,t)\right] \tag{4.8}$$

For a given value of z_m, Equation 4.8 is simplified by letting

$$H_m(t) = H_y(z_m,t) \tag{4.9}$$

Then, from Equation 4.4, the current density in the rotor bar segment between z_{m-1} and z_m is

$$i_x = \frac{1}{h_m} (H_{m-1}-H_m), \quad z_{m-1} < z < z_m \tag{4.10}$$

i_x is thus a function of time only for the permissable values of z. To simplify the notation further, let

$$i_m = i_x, \text{ for } z_{m-1} < z < z_m \tag{4.11}$$

Therefore, at any instant of time, the current density between z_{m-1} and z_m is constant.

$$i_m = \frac{1}{h_m} (H_{m-1} - H_m) \tag{4.12}$$

If the current density is constant throughout a region, the electric field is also constant in that region since $\bar{i} = \sigma\bar{E}$. However, both are discontinuous at the boundary between segments.

Consider any segment k, and let the subscript $k-\frac{1}{2}$ designate the point midway between z_{k-1} and z_k. The current density in this segment is then written as

$$i_k = \sigma E_{k-\frac{1}{2}} \tag{4.13}$$

In a region in which current density is constant, the total current is current density times area, or

$$I_k = i_k A_k \tag{4.14}$$

Where A_k is the cross section area shown in Figure 4.2. Since section k is rectangular, the area can be written as

$$A_k = wh_k \tag{4.15}$$

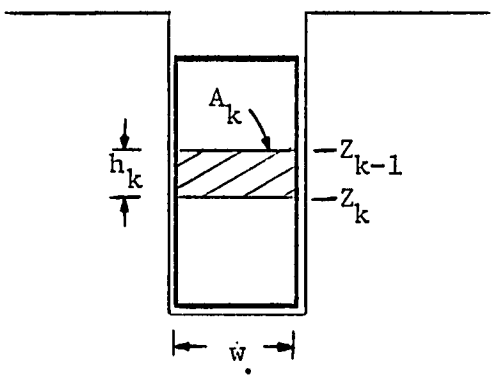

Figure 4.2 A rectangular rotor bar showing segment k of the approximation procedure

Combining Equations 4.13, 4.14, and 4.15 gives

$$E_{k-\frac{1}{2}} = \frac{I_k}{\sigma w h_k} \tag{4.16}$$

The current in segment N can be obtained by

$$I_N = w\,(H_{N-1} - H_N)$$

or

$$H_{N-1} = +H_N + \frac{1}{w} I_N \tag{4.17}$$

and

$$H_{N-2} = H_{N-1} + \frac{1}{w} I_{N-1} = H_N + \sum_{k=N-1}^{N} \frac{I_k}{w} \tag{4.18}$$

or, in general

$$H_m = H_N + \sum_{k=m+1}^{N} \frac{I_k}{w} \tag{4.19}$$

It is assumed that the permeability of iron is infinite. This assumption implies that a magnetic field cannot exist in the iron beneath the rotor bar. Because of the continuity requirements at the boundary $z=z_N$,

$$H_N = 0 \tag{4.20}$$

Equation 4.19 describes the magnetic field at the boundaries between segments. It will be assumed that the magnetic field value at a segment boundary is constant halfway into each segment it borders, or

$$H_m = \sum_{k=m+1}^{N} \frac{I_k}{w} \qquad z_{m-\frac{1}{2}} < z < z_{m+\frac{1}{2}} \tag{4.21}$$

Equation 4.3 can then be approximated over half a segment, using Equation 4.6. With a notation similar to that used in Equation 4.9, Equation 4.2 becomes

$$\begin{aligned} E_m - E_{m-\frac{1}{2}} &= -\mu \frac{h_m}{2} \frac{\partial H_m}{\partial t} \qquad z_{m-\frac{1}{2}} < z < z_m \\ E_{m+\frac{1}{2}} - E_m &= -\mu \frac{h_{m+1}}{2} \frac{\partial H_m}{\partial t} \qquad z_m < z < z_{m+\frac{1}{2}} \end{aligned} \tag{4.22}$$

Using Equation 4.21, and recognizing that the variables are functions of time only,

$$E_{m-\frac{1}{2}} - E_m = \frac{\mu h_m}{2w} \sum_{k=m+1}^{N} \frac{dI_k}{dt}$$

$$E_m - E_{m+\frac{1}{2}} = \frac{\mu h_{m+1}}{2\dot{w}} \sum_{k=m+1}^{N} \frac{dI_k}{dt} \tag{4.23}$$

The definition of voltage between two points is

$$V_{21} = -\int_1^2 \bar{E} \cdot d\bar{\ell} \tag{4.24}$$

From a rotor bar of length ℓ, the voltage at $z=z_m$ is

$$V_m = -\int_{\ell}^{0} E_m dx = E_m \ell \tag{4.25}$$

Then Equations 4.16 and 4.23 become, for section m,

$$V_{m-\frac{1}{2}} = \frac{\ell}{\sigma w h_m} I_m \tag{4.26}$$

and

$$V_{m-1} - V_{m-\frac{1}{2}} = \frac{\mu h_m \ell}{2w} \sum_{k=m}^{N} \frac{dI_k}{dt}$$

$$V_{m-\frac{1}{2}} - V_m = \frac{\mu h_m \ell}{w} \sum_{k=m+1}^{N} \frac{dI_k}{dt} \tag{4.27}$$

The equivalent circuit for section m is thus given in Figure 4.3, where

$$R_m = \frac{\ell}{\sigma w h_m} \tag{4.28}$$

$$L_m = \frac{\mu h_m \ell}{w} \tag{4.29}$$

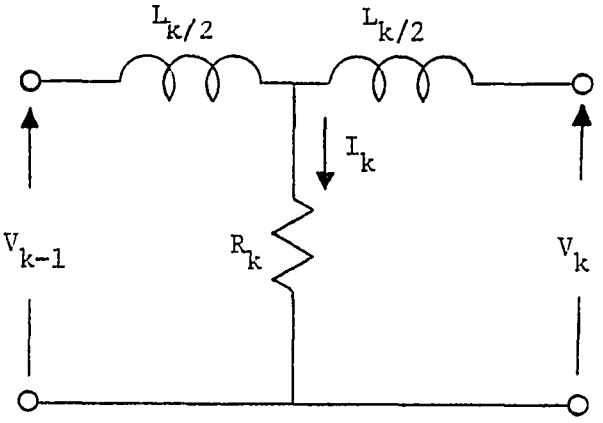

Figure 4.3 Equivalent circuit of rotor bar segment L

The rotor bar can then be represented by a series of N equivalent circuits shown in Figure 4.4. The rotor current is the sum of the current in each segment

$$i_r = \sum_{k=1}^{N} I_k \tag{4.30}$$

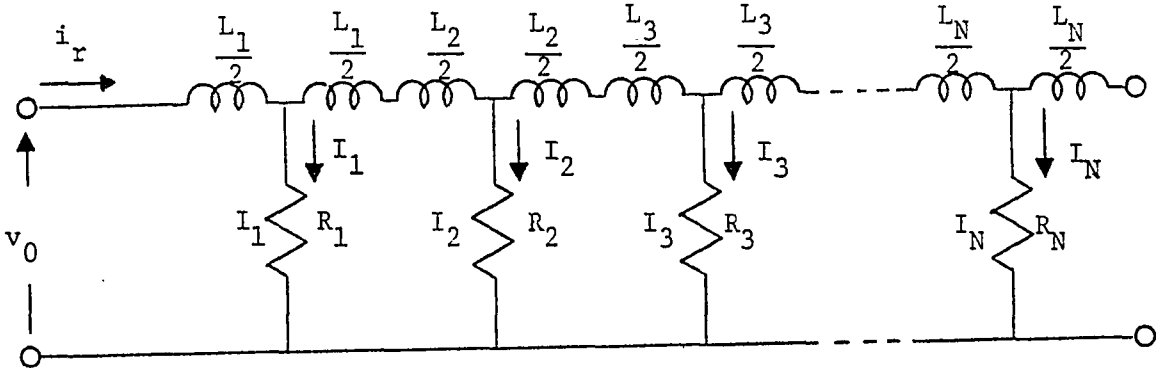

Figure 4.4 Equivalent circuit of the rotor bar

This model of the induction motor rotor bar is capable of predicting the current distribution in the bar. It also predicts the effective dynamic bar resistance and internal bar inductance. The model is valid for calculating the electrical transients in the rotor bar. It contains ordinary differential equations but no partial differential equations. Therefore, it is compatible with the two axis theory of the induction motor. Under steady state electrical conditions, the model easily simplifies to algebraic equations and is compatible with the impedance calculations of the equivalent circuits.

This rotor bar representation, although similar in configuration to one previous model [34], differs from previous efforts in that it is both based on physical representation of the machine and it has been shown to be valid under transient as well as steady state conditions. Furthermore, it is clear that the assumptions involved in arriving at this model are reasonable. The assumption of constant current density across the width of the rotor bar is a good assumption for many practical rotor bar shapes [50]. It is, however, a questionable assumption for certain rotor bar shapes. The replacement of partial differential equations by a combination of difference equations and ordinary differential equations will be accurate with a sufficient number of "T" bar representations. The proper order of the representation will be investigated by a variety of methods.

The physical basis and the reasonable assumptions of this model make it clearly a more precise representation of the induction motor rotor than the other proposed models.

Determination of Rotor Bar Parameters

A rotor bar representation has been derived which is capable of predicting the skin effect of the bar. The parameters of this representation have been found in terms of the physical properties of the bar. It is more desirable, however, to express the resistances and inductances of this rotor bar representation in terms of quantities which can be measured by electrical tests.

The rotor bar representation of Figure 4.4 is valid for both transient and steady state conditions. For strictly steady state conditions, however, a closed form solution of Equations 4.3 and 4.4 can be obtained for rectangular rotor bars [5]; [48]. The internal impedance of the bar under these conditions is

$$z = R(1+j)A\coth(1+j)A \tag{4.31}$$

where

$$A = \frac{\omega L}{2R}$$

$$R = \frac{\ell}{\sigma d w}$$

$$L = \frac{\mu \ell d}{w}$$

ω = angular frequency, radians/sec.

ℓ = bar length

d = bar depth

w = bar width (4.32)

This impedance can be measured as a function of angular frequency ω, and values of R and L determined. R and L can also be expressed in terms of rotor bar physical parameters, as indicated in Equations 4.32. Comparisons of these expressions with the rotor bar segment resistance and in-

ductance given by Equations 4.28 and 4.29 show that

$$R_m = R \frac{d}{h_m}$$

$$L_m = L \frac{h_m}{d} \tag{4.33}$$

The parameters of the rotor bar representation of Figure 4.4 can thus be determined from the electrical properties of the rotor bar.

Convergence of the Rotor Bar Model

To obtain the rotor bar representation of Figure 4.4, difference equations were used to approximate the space variable of the partial differential equations 4.3 and 4.4. These difference equations led to the representation of the rotor bar by a number of bar segments. The number of bar segments necessary to provide an accurate representation must still be determined, however.

The accuracy of a rotor bar model with a specific number of bar segments represented can be determined by comparisons of the steady solutions of the representation with the steady state closed form solution given in Equation 4.31.

The parameters that are required are R and L from Equations 4.32, the range of frequencies of interest, and the relative depth of each rotor bar segment. Babb and Williams [5] noted that convergence is faster if varying depths are used with the smallest segments near the top of the bar, where the current will be concentrated at higher frequencies. They suggest, for a four segment approximation, using the top 10% for the first segment, the next 20% for the second segment, 30% for the third segment,

and 40% for the last segment. A similar scheme will be used throughout this study.

The solution of rotor bar resistance and rotor bar inductance are given in Figure 4.5 and 4.6 respectively. For this case,

$$R = 0.025$$

$$L = 0.216 \tag{4.34}$$

which represent per unit values of a medium size motor with $r_{rn}/r_{rp}=3$. The frequency range of interest is $0<\omega<2$, where ω is also in per unit. $\omega=0$ corresponds to the rotor spinning at synchronous speed with positive sequence excitation. $\omega=1$ corresponds to the rotor at rest, and $\omega=2$ corresponds to the rotor spinning at synchronous speed with negative

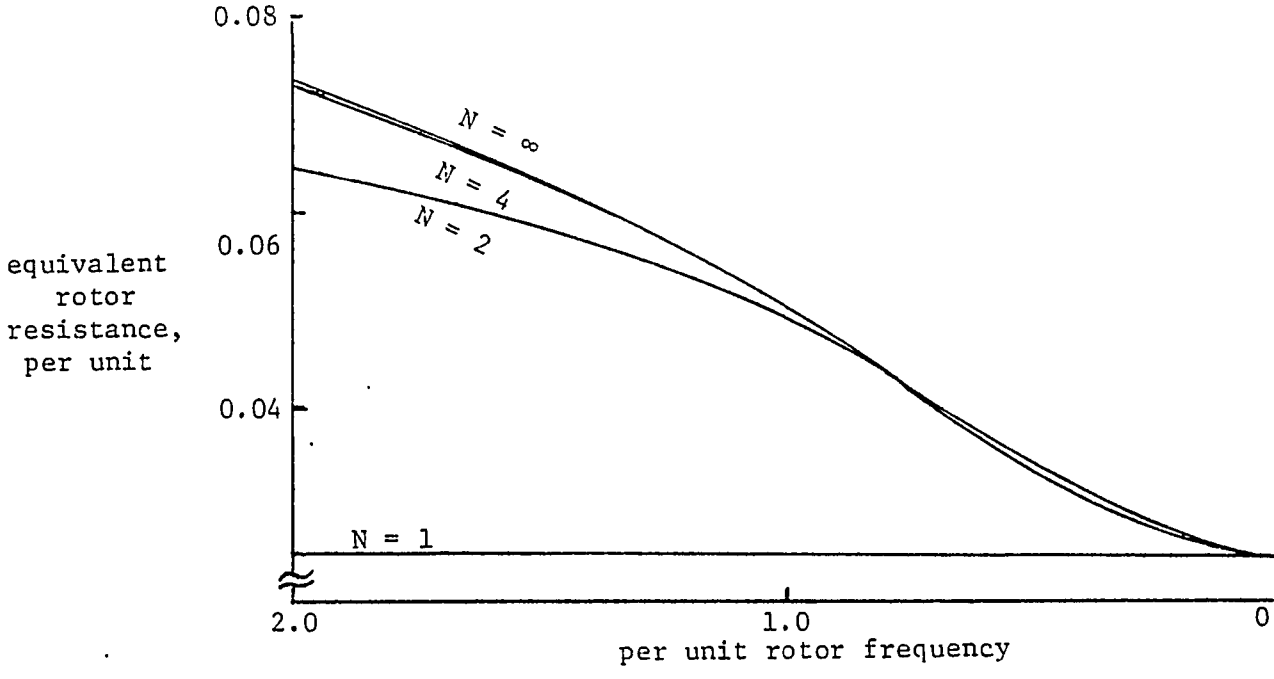

Figure 4.5 Effective rotor bar resistance predicted by 1, 2, and 4 loop models compared with the exact solution. Parameters used from Equation 4.34

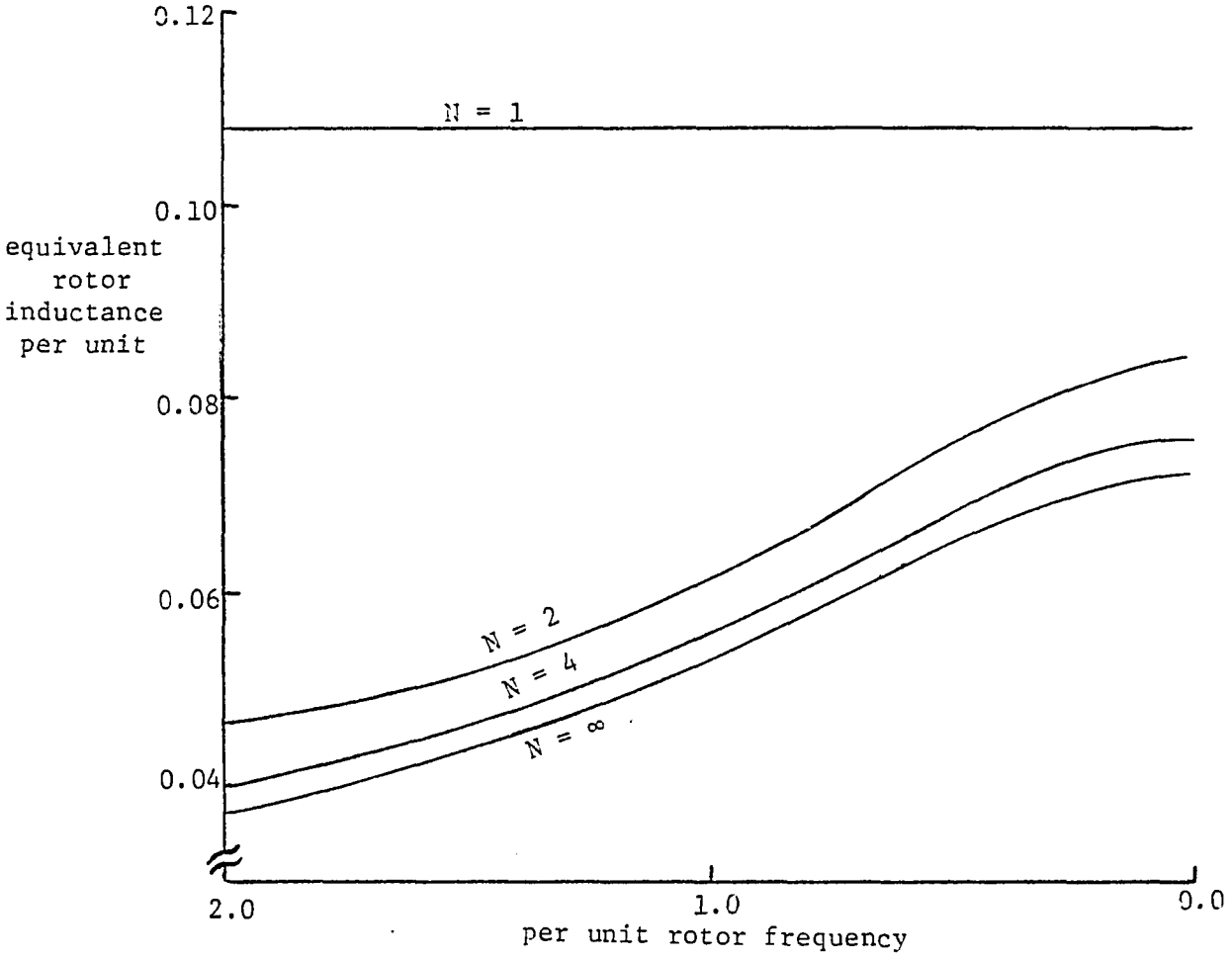

Figure 4.6 Effective rotor bar internal inductance predicted by 1, 2 and 4 loop models compared with the exact solution. Parameters used from Equation 4.34

sequence excitation from the stator. These figures show that the rotor ladder circuit of Figure 4.4 becomes a very good approximation with a moderate number of bar segments used.

Figure 4.7 and 4.8 show the results of similar calculations for

$$R = 0.0125$$

$$L = 0.045 \qquad (4.35)$$

which correspond to a rotor with $r_{rn}/r_{rp}=6$. As can be expected, the convergence of the approximate solution is slower than in the previous

case, but a good fit of the curves is still obtained without using extreme detail in the approximation.

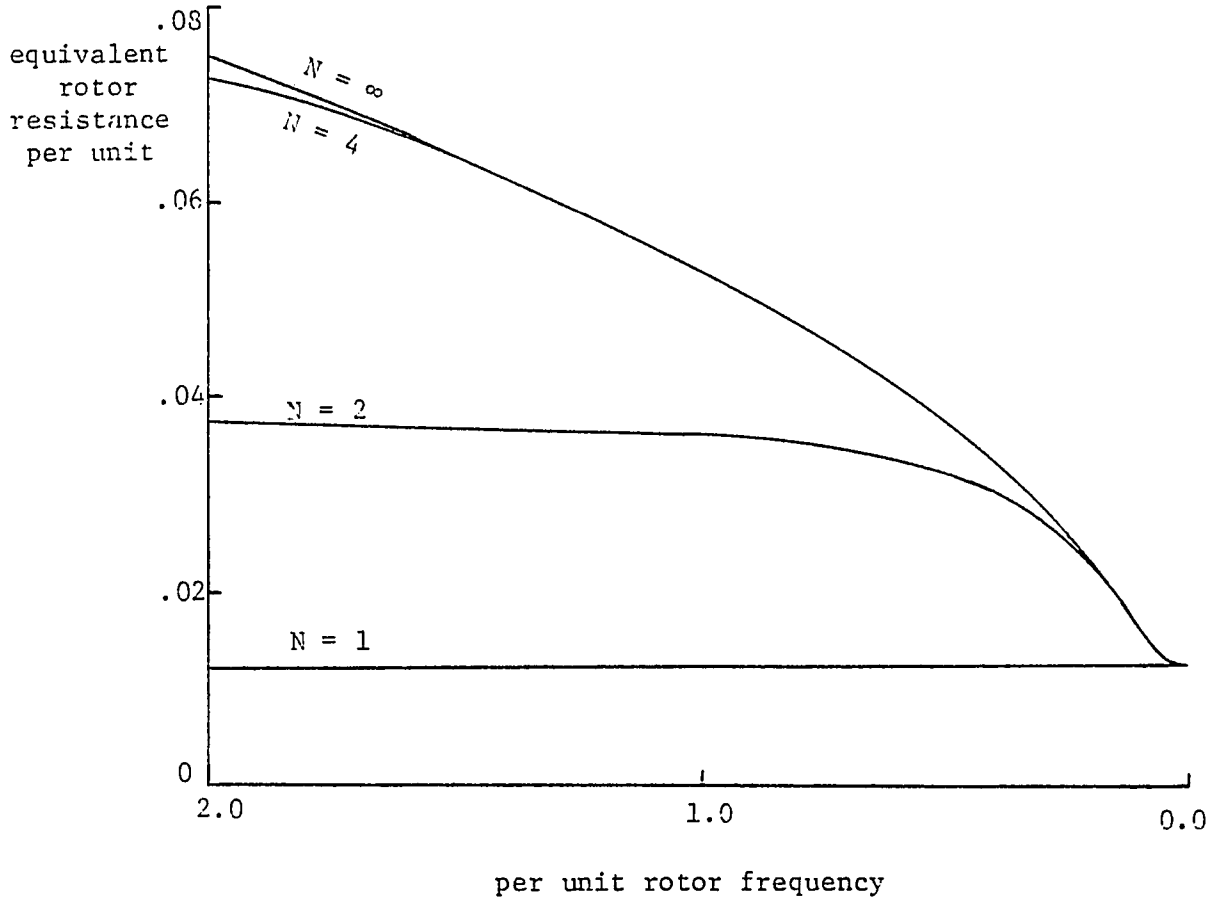

Figure 4.7 Effective rotor bar resistance predicted by 1, 2, and 4 loop models compared with exact solution. Parameters used from Equation 4.35

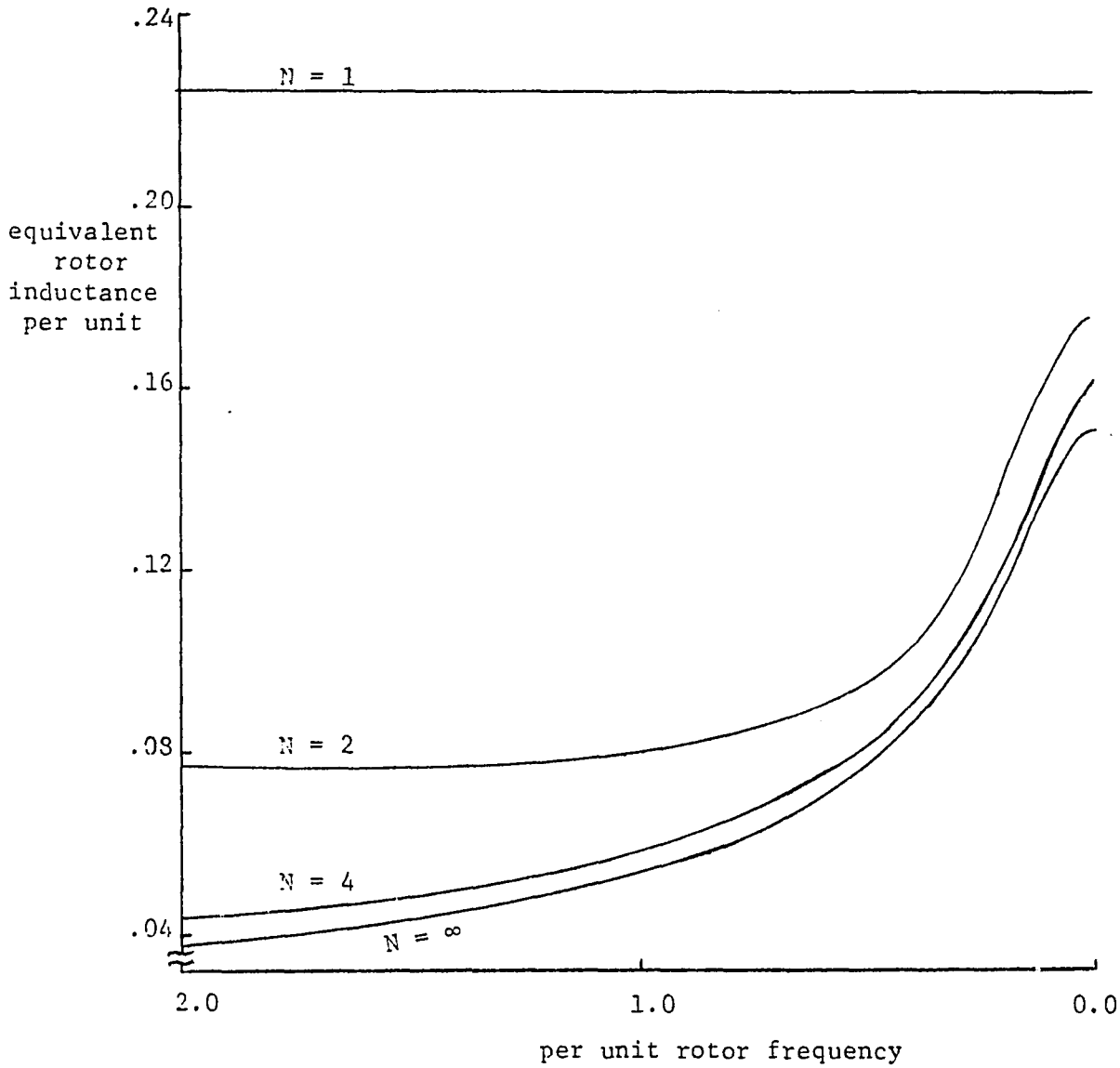

Figure 4.8 Effective rotor bar inductance predicted by 1, 2, and 4 loop models compared with the exact solution. Parameters used from Equation 4.35

Summary

A model of a rotor bar capable of predicting current distribution and effective dynamic resistance and inductance has been presented. This model is compatible with existing induction motor dynamic and steady state models. The model is based on Maxwell's equations and involves certain simplifying assumptions. The assumptions involved in arriving at Equations 4.3 and 4.4 have been widely reported and appear to be reasonable for a wide range of practical rotor bar configurations. The convergence of the difference equations of the rotor bar has been shown in the preceding section throughout the region of interest.

CHAPTER V. THE SKIN EFFECT ELECTRICAL TRANSIENT MODEL OF THE INDUCTION MOTOR

The most prominent induction motor model capable of predicting the electrical transients of the machine is based on the two axis theory. A set of common and widely accepted assumptions, often referred to as the ideal machine assumptions, is the basis of this model. The ideal machine has a uniform air gap, sinusoidal air gap MMF, and a linear magnetic circuit. Mechanical, iron, and stray load losses are neglected. The ideal induction motor is assumed to have a symmetrical cylindrical rotor and the rotor can be represented by one set of three phase windings. Additionally, the skin effects on the stator and rotor coils are neglected.

As was seen in the two preceding chapters, however, the rotor skin effect has a significant effect on induction motor operation. This is particularly true in deep bar and double cage motors. A model was developed in Chapter 4 which is capable of predicting rotor bar current distribution and effective dynamic rotor bar resistance and inductance. This rotor bar model will be incorporated into the induction motor model to describe the rotor skin effect.

The Flux Linkage Equations of the Proposed Skin Effect Model

The induction motor is represented by six equivalent coils, three each on the stator and the rotor. The location of each coil and the assumed current directions are shown in Figure 5.1. The flux linking any particular coil is a function of the current in all six coils and the

rotor position. It is assumed that flux linking one coil due to current in any other coil links the entire coil.

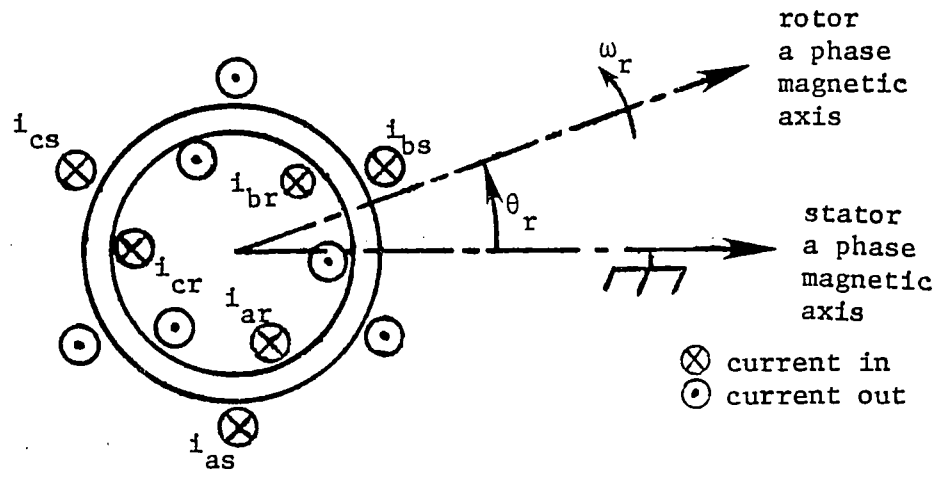

Figure 5.1 General three-phase induction motor
Winding current direction

The stator flux linkages are then

$$\begin{bmatrix} \lambda_{as} \\ \lambda_{bs} \\ \lambda_{cs} \end{bmatrix} = \left[\begin{array}{ccc|ccc} L_s & -L_{sm} & -L_{sm} & L_{as\text{-}ar} & L_{as\text{-}br} & L_{as\text{-}cr} \\ -L_{sm} & L_s & -L_{sm} & L_{bs\text{-}ar} & L_{bs\text{-}br} & L_{bs\text{-}cr} \\ -L_{sm} & -L_{sm} & L_s & L_{cs\text{-}ar} & L_{cs\text{-}br} & L_{cs\text{-}cr} \end{array}\right] \left[\begin{array}{c} i_{as} \\ i_{bs} \\ i_{cs} \\ \hline i_{ar1} \\ i_{br1} \\ i_{cr1} \end{array}\right] \qquad (5.1)$$

The subscripts s and r refer to stator and rotor quantities, respectively; a, b, and c refer to the three phase quantities.

L_s = stator phase self-inductance, which is a constant for all the three identical stator phases

L_{sm} = mutual inductance between stator phases, a positive constant

The stator to rotor mutual inductances are variables dependent on rotor position and can be expressed generally as

$$L_{is-jr} = L_{jr-is} = L_{sr}\cos\alpha_{is-jr} \tag{5.2}$$

where α_{is-jr} is the angle between stator winding i and rotor winding j for any rotor position θ_r.

The rotor flux linkages are more difficult to describe as the flux paths cut through the rotor conductors. Let λ_{arl}, λ_{brl}, and λ_{crl} denote the flux linkages which link the entire coil. Then,

$$\begin{bmatrix} \lambda_{arl} \\ \lambda_{brl} \\ \lambda_{br2} \end{bmatrix} = \left[\begin{array}{ccc|ccc} L_{ar-as} & L_{ar-bs} & L_{ar-cs} & L_r & -L_{rm} & -L_{rm} \\ L_{br-as} & L_{br-bs} & L_{br-cs} & -L_{rm} & L_r & -L_{rm} \\ L_{cr-as} & L_{cr-bs} & L_{cr-cs} & -L_{rm} & -L_{rm} & L_r \end{array}\right] \left[\begin{array}{c} i_{as} \\ i_{bs} \\ i_{cs} \\ \hline i_{arl} \\ i_{brl} \\ i_{crl} \end{array}\right] \tag{5.3}$$

The stator to rotor mutual inductances are described in Equation 5.2. L_{rm} is the mutual inductance between rotor phases, which is a positive constant. L_r is the rotor phase external self-inductance plus any internal inductance which affects the entire bar.

The remainder of the flux linking the rotor bar will link only a portion of the bar. The flux patterns in the bar are shown in Figure 5.2 Additional flux linkages will be defined in terms of the discretized variables of Chapter 4. As a result of the high permeability of iron,

flux linking any particular rotor bar segment will also link all other segments toward the rotor center, as shown in Figure 5.2.

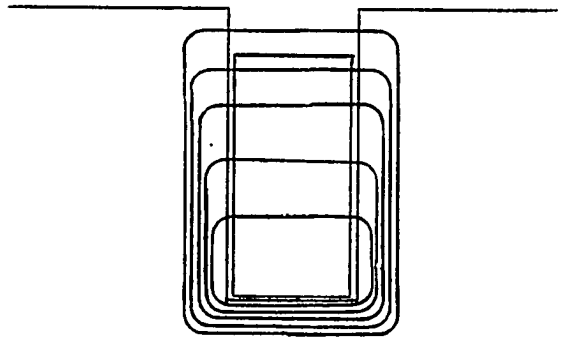

Figure 5.2 Cross-section of rotor bar showing leakage flux patterns

For convenience, the currents shown in the rotor bar equivalent circuit of Figure 5.3 will be used, rather than the currents defined in Chapter 4. The series inductances of Figure 4.4 have also been lumped together in Figure 5.3. Note that the entire rotor current passes through L_1. The flux linkage $=L_1 i_1$ therefore links the entire bar, and can be lumped with the external self-inductance of the bar. The additional flux linkages which link portions of the bar are

$$\lambda_2 = L_2 i_2$$
$$\lambda_3 = L_3 i_3$$
$$\vdots$$
$$\lambda_N = L_N i_N \tag{5.4}$$

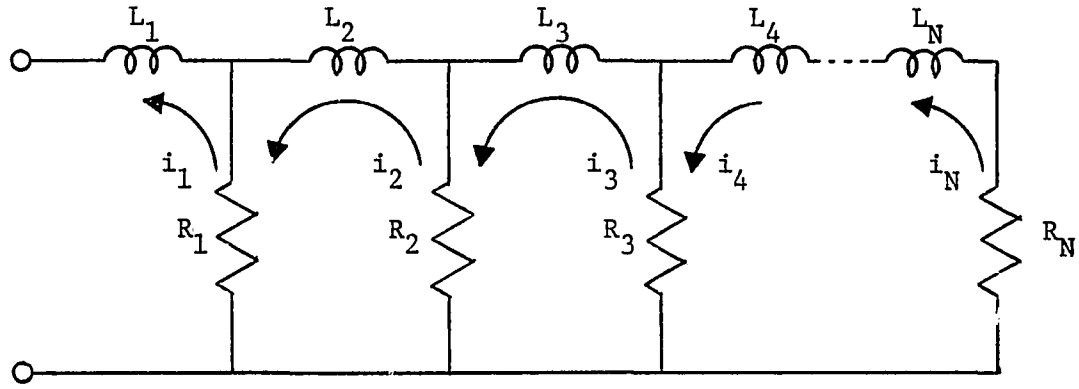

Figure 5.3 Rotor bar equivalent circuit

The flux linkage λ_k links only rotor bar segments k through N. In general, for each of the three rotor phase coils,

$$\begin{bmatrix} \lambda_{ark} \\ \lambda_{brk} \\ \lambda_{crk} \end{bmatrix} = \begin{bmatrix} L_k & 0 & 0 \\ 0 & L_k & 0 \\ 0 & 0 & L_k \end{bmatrix} \begin{bmatrix} i_{ak} \\ i_{bk} \\ i_{ck} \end{bmatrix} \tag{5.5}$$

Equations 5.1, 5.3, and 5.5 can be combined and written in matrix form as

$$\begin{bmatrix} \underline{\lambda}_{abcs} \\ \underline{\lambda}_{abcr1} \\ \underline{\lambda}_{abcr2} \\ \\ \underline{\lambda}_{abcrN-1} \\ \underline{\lambda}_{abcrN} \end{bmatrix} = \begin{bmatrix} \underline{L}_{ss} & \underline{L}_{rs} & \underline{0} & & \underline{0} & \underline{0} \\ \underline{L}_{sr} & \underline{L}_{1} & \underline{0} & \cdots\cdots & \underline{0} & \underline{0} \\ \underline{0} & \underline{0} & \underline{L}_{2} & & \underline{0} & \underline{0} \\ & & & \diagdown & & \\ \underline{0} & \underline{0} & \underline{0} & & \underline{L}_{N-1} & \underline{0} \\ \underline{0} & \underline{0} & \underline{0} & & 0 & \underline{L}_{N} \end{bmatrix} \begin{bmatrix} \underline{i}_{abcs} \\ \underline{i}_{abcr1} \\ \underline{i}_{abcr2} \\ \\ \underline{i}_{abcrN-1} \\ \underline{i}_{abcrN} \end{bmatrix} \tag{5.6}$$

where

$$\underline{\lambda}_{abc} = [\lambda_a \ \lambda_b \ \lambda_c]^T, \ i_{abc} = [i_a \ i_b \ i_c]^T$$

and each $\underline{L}(\cdot)$ is a 3x3 matrix defined in Equation 5.1, 5.3, or 5.5.

Development of the Voltage Equations for the Proposed Model

The voltage between the terminals of a coil is equal to the resistance voltage drop plus the time rate of change of the flux linking the coil. For the stator phases,

$$\begin{bmatrix} v_{as} \\ v_{bs} \\ v_{cs} \end{bmatrix} = \begin{bmatrix} r_s & 0 & 0 \\ 0 & r_s & 0 \\ 0 & 0 & r_s \end{bmatrix} \begin{bmatrix} i_{as} \\ i_{bs} \\ i_{cs} \end{bmatrix} + \begin{bmatrix} p\lambda_{as} \\ p\lambda_{bs} \\ p\lambda_{cs} \end{bmatrix} \tag{5.7}$$

For a squirrel cage induction motor, the rotor coils are closed upon themselves. The external voltages are therefore nonexistent, and only ri drops and flux linkage derivatives enter into the voltage equations. The expression of the rotor voltages is complicated, however, because the amount of flux linking the rotor coil at any given time varies across the rotor bar.

In Chapter 4, a method of segmenting the rotor bars was introduced. In this approximation procedure, the current throughout each bar segment is linked by the same amount of flux. A separate voltage equation is therefore required for each rotor segment. The flux linkages were defined in the previous section so that λ_1 links the uppermost rotor bar segment, $\lambda_1+\lambda_2$ links the next rotor bar segment, and in general, the flux linking segment k is

$$\sum_{m=1}^{k} \lambda_m \tag{5.8}$$

Then, using the currents defined in Figure 4.4,

$$\begin{aligned} R_1 I_1 &= p\lambda_1 \\ R_2 I_2 &= p\,(\lambda_1 + \lambda_2) \\ &\vdots \\ R_N I_N &= \sum_{m=1}^{N} p\lambda_m \end{aligned} \tag{5.9}$$

It is necessary to rewrite these equations in terms of the currents defined in Figure 5.3. By comparing Figures 4.4 and 5.5, Equation 5.10 is obtained.

$$\begin{aligned} I_1 &= -(i_1 - i_2) \\ I_2 &= -(i_2 - i_3) \\ &\vdots \\ I_{N-1} &= -(i_{N-1} - i_N) \\ I_N &= -i_N \end{aligned} \tag{5.10}$$

The rotor voltages are then

$$p\lambda_1 = -R_1 i_1 + R_1 i_2 \tag{5.11}$$

$$\begin{aligned} p\lambda_2 &= R_2\,(i_3 - i_2) - p\lambda_1 \\ &= R_1 i_1 - (R_1 + R_2)\, i_2 + R_2 i_3 \end{aligned} \tag{5.12}$$

The voltage for the k^{th} segment $(k=2,3,\cdots,N-1)$ is written as

$$p\lambda_k = R_{k-1} i_{k-1} - (R_{k-1} + R_k)\, i_k + R_k i_{k+1} \tag{5.13}$$

and for the bottom segment, N,

$$p\lambda_N = R_{N-1} i_{N-1} - (R_{N-1} + R_N)\, i_N \tag{5.14}$$

A set of these equations is required for each rotor phase. Applying the appropriate notation to these equations, and including the stator equations, the voltage equations for the machine are written as follows:

$$\begin{bmatrix} \underline{v}_{abcs} \\ \underline{0} \\ \underline{0} \\ \\ \\ \underline{0} \\ \underline{0} \end{bmatrix} = \begin{bmatrix} \underline{R_s} & \underline{0} & \underline{0} & & \underline{0} & \underline{0} \\ \underline{0} & \underline{R_1} & \underline{-R_1} & \cdots & \underline{0} & \underline{0} \\ \underline{0} & \underline{-R_1} & \underline{R_1+R_2} & & \underline{0} & \underline{0} \\ & \vdots & & \ddots & & \\ \underline{0} & \underline{0} & \underline{0} & & \underline{R_{N-2}+R_{N-1}} & \underline{R_{N-1}} \\ \underline{0} & \underline{0} & \underline{0} & & \underline{-R_{N-1}} & \underline{R_{N-1}+R_N} \end{bmatrix} \begin{bmatrix} \underline{i}_{abcs} \\ \underline{i}_{abcr1} \\ \underline{i}_{abcr2} \\ \\ \\ \underline{i}_{abcrN-1} \\ \underline{i}_{abcN} \end{bmatrix} + \begin{bmatrix} p\underline{\lambda}_{abcs} \\ p\underline{\lambda}_{abcr1} \\ p\underline{\lambda}_{abcr2} \\ \\ \\ p\underline{\lambda}_{abcrN-1} \\ p\underline{\lambda}_{abcrN} \end{bmatrix} \tag{5.15}$$

where each $\underline{R}_{(\cdot)}$ is a 3x3 diagonal matrix with $R_{(\cdot)}$ resistance as each diagonal term.

Equations 5.6 and 5.15 describe the electrical properties of the induction machine. Although the equations can be solved in this form, by using Park's transformation, an equivalent form can be obtained which is better suited for solution.

The dq Axis Representation of the Proposed Model

The d and the q axis are defined in Figure 5.4. The o axis is stationary, and is similar in concept to zero sequence quantities of symmetrical components. The phase quantities of both the stator and rotor will be projected onto the o, d, and q axes. Both the phase quantities

and axis quantities are three dimensional. The three axes are linearly independent (and also orthogonal) and therefore form a new basis for the expression of the motor variables. The projection of the stator variables onto the d and q axes is governed by the angle θ, as the rotor projections are a function of the angle β. These transformations, commonly referred to as Park's transformations, are

$$\begin{bmatrix} f_{os} \\ f_{ds} \\ f_{qs} \end{bmatrix} = \sqrt{\frac{2}{3}} \begin{bmatrix} \frac{1}{\sqrt{2}} & \frac{1}{\sqrt{2}} & \frac{1}{\sqrt{2}} \\ \cos\theta & \cos(\theta-\frac{2\pi}{3}) & \cos(\theta+\frac{2\pi}{3}) \\ \sin\theta & \sin(\theta-\frac{2\pi}{3}) & \sin(\theta+\frac{2\pi}{3}) \end{bmatrix} \begin{bmatrix} f_{as} \\ f_{bs} \\ f_{cs} \end{bmatrix} \tag{5.16}$$

and

$$\begin{bmatrix} f_{or} \\ f_{dr} \\ f_{qr} \end{bmatrix} = \sqrt{\frac{2}{3}} \begin{bmatrix} \frac{1}{\sqrt{2}} & \frac{1}{\sqrt{2}} & \frac{1}{\sqrt{2}} \\ \cos\beta & \cos(\beta-\frac{2\pi}{3}) & \cos(\beta+\frac{2\pi}{3}) \\ \sin\beta & \sin(\beta-\frac{2\pi}{3}) & \sin(\beta+\frac{2\pi}{3}) \end{bmatrix} \begin{bmatrix} f_{ar} \\ f_{br} \\ f_{cr} \end{bmatrix} \tag{5.17}$$

The angles θ and β in Figure 5.4 are arbitrary. For this reason, the general variables f_{os}, f_{ds}, f_{qs}, f_{or}, f_{dr}, and f_{qr} are said to belong to the arbitrary reference frame. It is convenient to use this reference frame as an intermediate step of the overall solution [35].

Equations 5.16 and 5.17 can be rewritten in matrix form as

$$\underline{f}_{odqs} = \underline{P}_{\theta}\, \underline{f}_{abcs} \tag{5.18}$$

$$\underline{f}_{odqr} = \underline{P}_{\beta}\, \underline{f}_{abcr} \tag{5.19}$$

Then the arbitrary reference frame flux linkages are written as

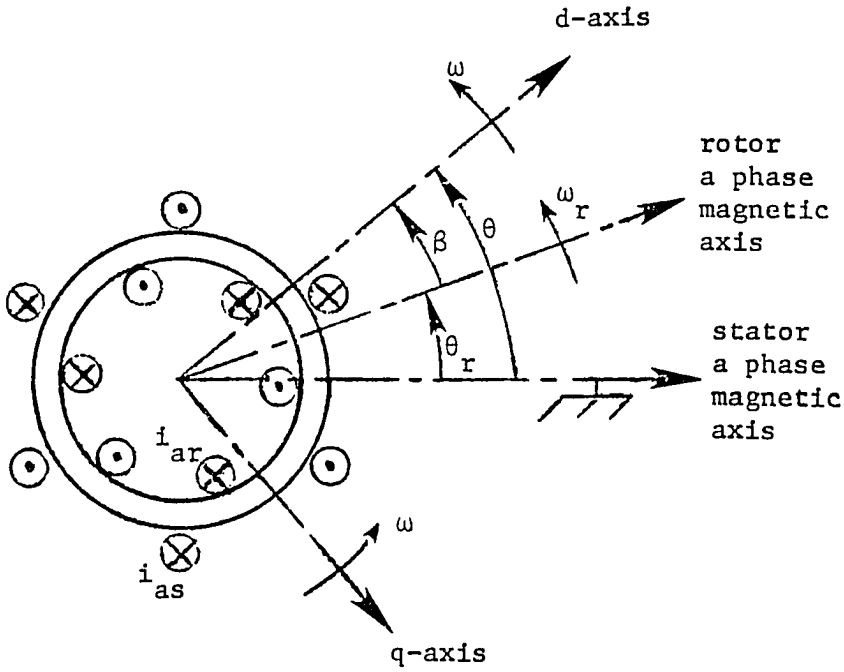

Figure 5.4 Motor with magnetic axes and arbitrary d and q axes shown

$$\begin{bmatrix} \underline{\lambda}_{odqs} \\ \underline{\lambda}_{odqr1} \\ \underline{\lambda}_{odqr2} \\ \vdots \\ \underline{\lambda}_{odqrN} \end{bmatrix} = \begin{bmatrix} \underline{P}_{\theta} & \underline{0} & \underline{0} & \underline{0} \\ \underline{0} & \underline{P}_{\beta} & \underline{0} & \underline{0} \\ \underline{0} & \underline{0} & \underline{P}_{\beta} & \underline{0} \\ & \vdots & & \vdots \\ \underline{0} & \underline{0} & \underline{0} & \underline{P}_{\beta} \end{bmatrix} \begin{bmatrix} \underline{\lambda}_{abcs} \\ \underline{\lambda}_{abcr1} \\ \underline{\lambda}_{abcr2} \\ \vdots \\ \underline{\lambda}_{abcrN} \end{bmatrix} \tag{5.20}$$

The transformation of the motor variables is then represented by the (3N+3)x(3N+3) square matrix of Equation 5.20. By referring to this transformation as $\underline{P}_M$, Equation 5.20 can be rewritten as

$$\underline{\lambda}_{odqM} = \underline{P}_M \, \underline{\lambda}_{abcM} \tag{5.21}$$

Using the transformation matrix $\underline{P}_M$, the flux linkage equation can now be transformed to the arbitrary reference frame. Using the compact matrix notation of Equation 5.21, Equation 5.6 is rewritten as

$$\underline{\lambda}_{abcM} = \underline{L}_{abcM} \, \underline{i}_{abcM} \tag{5.22}$$

Applying the transformation $\underline{P}_M$ on both sides of the equation yields

$$\underline{P}_M \, \underline{\lambda}_{abcM} = \underline{P}_M \, \underline{L}_{abcM} \, \underline{i}_{abcM} \tag{5.23}$$

Since it is also desirable to express the currents in terms of odq axis quantities, Equation 5.23 is written as

$$\underline{P}_M \, \underline{\lambda}_{abcM} = \underline{P}_M \, \underline{L}_{abcM} \, \underline{P}_M^{-1} \, \underline{P}_M \, \underline{i}_{abcM} \tag{5.24}$$

The inverse of $\underline{P}_M$ will exist due to the linear independence of the o, d, and q axes. Because the transformation is orthogonal, the inverse of the transformation matrix will equal the transpose of the transformation matrix, or

$$\underline{P}_M^{-1} = \underline{P}_M^{T} \tag{5.25}$$

The inductances using the odq variables are defined as

$$\underline{L}_{odqM} = \underline{P}_{M}\,\underline{L}_{abcM}\,\underline{P}_{M}^{-1} \tag{5.26}$$

Then Equation 5.24 is simplified to Equation 5.27

$$\underline{\lambda}_{odqM} = \underline{L}_{odqM}\,\underline{i}_{odqM} \tag{5.27}$$

Transformation 5.26 is the similarity transformation and can be written using matrix algebra as;

$$\underline{L}_{odqM} = \begin{bmatrix} \underline{P}_{\theta}\underline{L}_{ss}\underline{P}_{\theta}^{-1} & \underline{P}_{\beta}\underline{L}_{rs}\underline{P}_{\theta}^{-1} & \underline{0} & \underline{0} \\ \underline{P}_{\theta}\underline{L}_{sr}\underline{P}_{\beta}^{-1} & \underline{P}_{\beta}\underline{L}_{1}\underline{P}_{\beta}^{-1} & \underline{0} & \underline{0} \\ \underline{0} & \underline{0} & \underline{P}_{\beta}\underline{L}_{2}\underline{P}_{\beta}^{-1} & \underline{0} \\ \vdots & \vdots & & \vdots \\ \underline{0} & \underline{0} & \underline{0} & \underline{P}_{\beta}\underline{L}_{N}\underline{P}_{\beta}^{-1} \end{bmatrix} \tag{5.28}$$

where:

$$\underline{P}_{\theta}\underline{L}_{ss}\underline{P}_{\theta}^{-1} = \begin{bmatrix} L_s - 2L_{sM} & 0 & 0 \\ 0 & L_s + L_{sM} & 0 \\ 0 & 0 & L_s + L_{sM} \end{bmatrix} \tag{5.29}$$

$$\underline{P}_{\theta}\underline{L}_{sr}\underline{P}_{\beta}^{-1} = \underline{P}_{\beta}\underline{L}_{rs}\underline{P}_{\theta}^{-1} = \begin{bmatrix} 0 & 0 & 0 \\ 0 & \frac{3}{2}L_{sr} & 0 \\ 0 & 0 & \frac{3}{2}L_{sr} \end{bmatrix} \tag{5.30}$$

$$\underline{P}_{\beta}\underline{L}_{1}\underline{P}_{\beta}^{-1} = \begin{bmatrix} L_r-2L_{rM} & 0 & 0 \\ 0 & L_r+L_{rM} & 0 \\ 0 & 0 & L_r+L_{rM} \end{bmatrix} \tag{5.31}$$

and, for $k=2,3,\cdots N_1$

$$\underline{P}_{\beta}\underline{L}_{1}\underline{P}_{\beta}^{-1} \begin{bmatrix} L_k & 0 & 0 \\ 0 & L_k & 0 \\ 0 & 0 & L_k \end{bmatrix} \tag{5.32}$$

The voltage equations of the motor can be transformed to the arbitrary reference frame in a similar manner. However, this transformation is complicated by the presence of time derivatives in the equations. As

$$\underline{f}_{odq} = \underline{P}_{M}\,\underline{f}_{abc} \tag{5.33}$$

and since both $\underline{P}_M$ and $\underline{f}_{abc}$ are functions of time, the derivative of Equation 5.33 is given by

$$p\,\underline{f}_{odq} = (p\,\underline{P}_M)\,(\underline{f}_{abc}) + \underline{P}_M\,(p\underline{f}_{abc}) \tag{5.34}$$

or

$$\underline{P}_M\,(p\underline{f}_{abc}) = p\underline{f}_{odq} - (p\underline{P}_M)\,(\underline{P}_M^{-1})\,(\underline{f}_{odq}) \tag{5.35}$$

Since θ and β are functions of time, the last term of Equation 5.35 can be evaluated by using Equations 5.16 and 5.17 to yield

$$p\underline{P}_{\theta}\underline{P}_{\theta}^{-1} = \begin{bmatrix} 0 & 0 & 0 \\ 0 & 0 & -p\theta \\ 0 & p\theta & 0 \end{bmatrix} \triangleq \underline{G}_{\theta} \tag{5.36}$$

$$p\underline{P}_{\beta}\underline{P}_{\beta}^{-1} = \begin{bmatrix} 0 & 0 & 0 \\ 0 & 0 & -p\beta \\ 0 & p\beta & 0 \end{bmatrix} \triangleq \underline{G}_{\beta} \tag{5.37}$$

Using Equations 5.15, 5.26, and 5.35, the voltage equations of the motor in the arbitrary reference frame are given by Equation 5.38.

$$\begin{bmatrix} \underline{v}_{odqs} \\ \underline{0} \\ \underline{0} \\ \vdots \\ \underline{0} \\ \underline{0} \end{bmatrix} = \begin{bmatrix} \underline{R}_s & \underline{0} & \underline{0} & \cdots & \underline{0} & \underline{0} \\ \underline{0} & \underline{R}_{r1} & -\underline{R}_{r1} & \cdots & \underline{0} & \underline{0} \\ \underline{0} & -\underline{R}_{r1} & \underline{R}_{r1}+\underline{R}_{r2} & \cdots & \underline{0} & \underline{0} \\ & & \vdots & & & \\ \underline{0} & \underline{0} & \underline{0} & \cdots & \underline{R}_{rN-1}+\underline{R}_{rN-2} & -\underline{R}_{rN-1} \\ \underline{0} & \underline{0} & \underline{0} & \cdots & -\underline{R}_{rN-1} & \underline{R}_{rN-1}+\underline{R}_{rN} \end{bmatrix} \begin{bmatrix} \underline{i}_{pdqs} \\ \underline{i}_{odqr1} \\ \underline{i}_{odqr2} \\ \vdots \\ \underline{i}_{odqrN-1} \\ \underline{i}_{odqrN} \end{bmatrix}$$

$$+ \begin{bmatrix} p\underline{\lambda}_{odqs} \\ p\underline{\lambda}_{odqr1} \\ p\underline{\lambda}_{odqr2} \\ \vdots \\ p\underline{\lambda}_{odqrN-1} \\ p\underline{\lambda}_{odqrN} \end{bmatrix} - \begin{bmatrix} \underline{G}_{\theta} & \underline{0} & \underline{0} & \cdots & \underline{0} & \underline{0} \\ \underline{0} & \underline{G}_{\beta} & \underline{0} & \cdots & \underline{0} & \underline{0} \\ \underline{0} & \underline{0} & \underline{G}_{\beta} & \cdots & \underline{0} & \underline{0} \\ & & \vdots & & & \\ \underline{0} & \underline{0} & \underline{0} & \cdots & \underline{G}_{\beta} & \underline{0} \\ \underline{0} & \underline{0} & \underline{0} & \cdots & \underline{0} & \underline{G}_{\beta} \end{bmatrix} \begin{bmatrix} \underline{\lambda}_{odqs} \\ \underline{\lambda}_{odqr1} \\ \underline{\lambda}_{odqr2} \\ \vdots \\ \underline{\lambda}_{odqrN-1} \\ \underline{\lambda}_{odqrN} \end{bmatrix} \tag{5.38}$$

Because of the form of the resistance matrix, it is unaffected by the similarity transformation.

The motor representation in the arbitrary reference frame is the combination of Equations 5.27 and 5.38.

The o axis equations The induction motor windings can be connected in either delta or wye configuration. The delta wound motor has, of course, no neutral point. The neutral point of the wye wound motor is generally left floating. In either case, the sum of the phase currents is constrained to add to zero. From an examination of the transformations, if the phase currents sum to zero, then the o axis current must be zero. The o axis flux linkages are then also zero. In fact, the only o axis quantity which can be non-zero under these conditions is the stator o axis voltage. This voltage, however, is completely independent of any of the other motor variables. For this reason, the o axis equations of the motor can be neglected.

Magnetizing and leakage inductance When the equations are expressed in per unit quantities, the stator self-inductance, the rotor external self-inductance, and the stator to rotor mutual inductance can be re-defined to magnetizing and leakage inductances. The details of this process are outlined in Appendix A. With this done, the d axis flux linkages can be written as

$$\begin{bmatrix} \lambda_{ds} \\ \lambda_{dr1} \\ \lambda_{dr2} \\ \vdots \\ \lambda_{drN} \end{bmatrix} = \begin{bmatrix} M+\ell_s & M & 0 & 0 \\ M & M+L_o+L_1 & 0 & 0 \\ 0 & 0 & L_2 & 0 \\ \vdots & \vdots & \ddots & \vdots \\ 0 & 0 & 0 & L_n \end{bmatrix} \begin{bmatrix} i_{ds} \\ i_{dr1} \\ i_{dr2} \\ \vdots \\ i_{drN} \end{bmatrix} \tag{5.39}$$

L_o is the external leakage inductance of the rotor, and L_1 through L_N are defined in Figure 5.3. M is the magnetizing inductance, and ℓ_s is the stator leakage inductance. The q axis flux linkages are related to the q axis currents by the same inductance matrix.

Solution of the equations These equations form a set of non-linear ordinary differential equations. In order to analyze them, full-time solutions must be calculated with the use of either the digital or analog computer.

In order to solve these equations, a specific reference frame must be chosen. This is done by specifying consistent values for θ and β. In this study, the stationary reference frame was used exclusively. In the stationary reference frame, the d axis is taken to lie on the stator A phase magnetic axis at all times. It follows from Figure 5.4 that

$$\theta = 0$$
$$\beta = -\theta_r \qquad (5.40)$$

This completes the set of equations describing the electrical parameters of the motor.

Two other popular reference frames for the solution of these equations are known as the rotor reference frame and the synchronously rotating reference frame.

The Mechanical Equations of the Motor

The electromagnetic developed torque of the machine is known to be (43), in per unit,

$$T_e = \frac{1}{3}(\lambda_{qs} i_{ds} - \lambda_{ds} i_{qs}) \tag{5.41}$$

The rotor speed can then be found from the accelerating torque, which is the difference between T_e and the load torque T_m. The rotor speed is

$$\omega_r = \frac{1}{2H}\int (T_e - T_m)dt \tag{5.42}$$

where H and t are in seconds and ω_r, T_e and T_m are in per unit. The per unit system used is outlined in Appendix A.

Summary

A dynamic induction motor model has been derived which fully accounts for the rotor skin effect. This model is a generalization of previous induction motor models based on the two axis theory. It has the power to predict the electrical as well as motional transients; and, by accounting for the rotor skin effect, is much more versatile than previous motor models. By describing the skin effect of the rotor bars, the motor model can be used in investigating motor operating conditions which were not within the capabilities of previous models. The most significant area of these investigations concerns the motor operation under unbalanced power system conditions.

Because of the ability of this model to predict both electrical transients and skin effects, it will be referred to as the skin effect electrical transient model throughout the remainder of this text.

CHAPTER VI. THE SKIN EFFECT IMPEDANCE MODEL OF THE INDUCTION MOTOR

Induction motor models which predict the motional transient but neglect electrical transients have been and continue to be widely used. A motor model capable of calculating the rotor bar current distribution, but which neglects the electrical transients, will be developed in this chapter. It is reasonable to project that this model will be suitable for use in some dynamic motor conditions. The actual usefulness of this model will be determined in later chapters. This model will be a simplification of the skin effect electrical transient model, which was introduced in Chapter 5.

The Positive Sequence Motor Equations of the Skin Effect Model

The motor Equations 5.38 and 5.39 can be written in matrix form as

$$\underline{V} = \underline{R}\,\underline{I} + p\underline{\lambda} - \underline{G}\,\underline{\lambda} \tag{6.1}$$

and

$$\underline{\lambda} = \underline{L}\,\underline{I} \tag{6.2}$$

These equations can be combined and solved for the current derivatives.

$$p\underline{I} = \underline{L}^{-1}\,[\underline{V} - \underline{R}\,\underline{I} + \underline{G}\,\underline{L}\,\underline{I}] \tag{6.3}$$

The matrix $\underline{G}$ is a function of the time derivative of the reference frame angles θ and β. In the synchronously rotating reference frame, these angles are

$$\theta = \omega_o t$$

$$\beta = \theta - \theta_r = \omega_o t - \omega_r t \tag{6.4}$$

Then

$$p\theta = \omega_o$$

$$p\beta = \omega_o - \omega_r = s\omega_o \tag{6.5}$$

where s is the per unit slip. ω_o, the rated frequency of the system, is always constant. $s\omega_o$ is constant when rotor slip is constant. Therefore, under steady state conditions, the motor is operating at constant slip, and $\underline{G}$ becomes a constant matrix. Equation 6.3 is then a set of linear differential equations. This set of equations can therefore be solved if the voltage vector $\underline{V}$ is known.

It is most convenient to separate the voltages into sequence components before attempting a solution. Because the system is linear, the principle of superposition applies. The separate solutions can be added to arrive at a complete solution.

Consider the set of positive sequence voltages with

$$v_a = \sqrt{2}\, V_1 \cos(\omega_o t + \alpha_1) \tag{6.6}$$

These voltages can be transformed to the synchronously rotating reference frame by Equation 5.16. The axis voltages are then

$$\begin{bmatrix} v_o \\ v_d \\ v_q \end{bmatrix} = \begin{bmatrix} 0 \\ \sqrt{3}\, V_1 \cos\alpha_1 \\ \sqrt{3}\, V_1 \sin\alpha_1 \end{bmatrix} \tag{6.7}$$

The axis voltages in the synchronously rotating reference frame are therefore constants if the phase voltages contain only a positive sequence

component. The steady state currents of Equation 6.3 will then also be constant, so the time derivatives of these currents will equal zero. Under these conditions,

$$\underline{V} = (\underline{R} - \underline{G}\,\underline{L})\,\underline{I} \tag{6.8}$$

or

$$\begin{bmatrix} v_{ds} \\ v_{qs} \\ \hline 0 \\ \hline 0 \\ \hline \vdots \\ \hline 0 \\ \hline 0 \end{bmatrix} = \left[\begin{array}{cccccccc} \underline{A}_s & \underline{A}_{sr} & \underline{0} & \underline{0} & & \underline{0} & \underline{0} & \underline{0} \\ \underline{A}_{rs} & \underline{A}_r & \underline{B}_1 & \underline{0} & \cdots & \underline{0} & \underline{0} & \underline{0} \\ \underline{0} & \underline{B}_1 & \underline{A}_2 & \underline{B}_2 & & \underline{0} & \underline{0} & \underline{0} \\ \vdots & \vdots & \vdots & \ddots & & & \vdots & \\ \underline{0} & \underline{0} & \underline{0} & \underline{0} & & \underline{B}_{N-2} & \underline{A}_{N-1} & \underline{B}_{N-1} \\ \underline{0} & \underline{0} & \underline{0} & \underline{0} & & \underline{0} & \underline{B}_{N-1} & \underline{A}_N \end{array}\right] \begin{bmatrix} i_{ds} \\ i_{qs} \\ \hline i_{dr1} \\ i_{qr1} \\ \hline i_{dr2} \\ i_{qr2} \\ \hline \vdots \\ \hline i_{drN-1} \\ i_{qrN-1} \\ \hline i_{drN} \\ i_{qrN} \end{bmatrix} \tag{6.9}$$

In Equation 6.9,

$$\underline{A}_s = \begin{bmatrix} r_s & \omega_o(M+\ell_s) \\ -\omega_o(M+\ell_s) & r_s \end{bmatrix} \tag{6.10}$$

$$\underline{A}_{sr} = \begin{bmatrix} 0 & \omega_o M \\ -\omega_o M & 0 \end{bmatrix} \tag{6.11}$$

$$\underline{A}_{rs} = \begin{bmatrix} 0 & s\omega_o M \\ -s\omega_o M & 0 \end{bmatrix} \tag{6.12}$$

$$\underline{A}_{r} = \begin{bmatrix} R_1 & s\omega_o(M+L_o+L_1) \\ -s\omega_o(M+L_o+L_1) & R_1 \end{bmatrix} \tag{6.13}$$

$$\underline{A}_{k} = \begin{bmatrix} R_{k-1}+R_k & s\omega_o L_k \\ -s\omega_o L_k & R_{k-1}+R_k \end{bmatrix} \qquad k=2,3,\cdots,N \tag{6.14}$$

$$\underline{B}_{k} = \begin{bmatrix} -R_k & 0 \\ 0 & -R_k \end{bmatrix} \quad k=1,2,\cdots,N-1 \tag{6.15}$$

Equation 6.9 is a set of algebraic equations from which the motor currents may be found by matrix inversion.

It is desirable, however, to express these equations in terms of phase quantities rather than d and q axis quantities. Phase quantities can be found from the axis quantities using the inverse of Park's transformation. As only balanced positive sequence currents are being considered at this point, it is sufficient to find A phase current. A general A phase quantity f is

$$f_a = \sqrt{\frac{2}{3}} \left(f_d \cos\omega_o t + f_q \sin\omega_o t + \frac{1}{\sqrt{2}} f_o\right) \tag{6.16}$$

As o axis currents cannot flow in an ungrounded motor, the A phase current will be

$$i_a = \sqrt{\frac{2}{3}} \left[i_d \cos\omega_o t + i_q \cos\left(\omega_o t - \frac{\pi}{2}\right)\right] \tag{6.17}$$

The phasor transformation of this expression is

$$\bar{I}_a = \frac{1}{\sqrt{3}} (i_{ds} - j i_{qs}) \tag{6.19}$$

which agrees with the phasor transformation of Equation 6.6. Using these equations, the d and q axis expressions of Equation 6.9 can be transformed to phase variables. The stator equation is

$$\bar{V}_1 = \frac{1}{\sqrt{3}} (v_{ds} - j v_{qs}) = \frac{1}{\sqrt{3}} [r_s (i_{ds} - j i_{qs}) + \omega_o (M + \ell_s)(j i_{ds} + i_{qs}) + \omega_o M (j i_{dr1} + i_{qr1})] \tag{6.20}$$

or

$$\bar{V}_1 = (r_s + j\omega_o \ell_s)\, \bar{I}_{as} + j\omega_o M\, (\bar{I}_{as} + \bar{I}_{ar1}) \tag{6.21}$$

In a similar manner, the rotor equations become

$$\begin{aligned}
0 &= j\omega_o M \bar{I}_{as} + \left[\frac{R_1}{S} + j\omega_o (M + L_o + L_1)\right] \bar{I}_{ar1} - \frac{R_1}{S} \bar{I}_{ar2} \\
0 &= -\frac{R_1}{S} \bar{I}_{ar1} + \left(\frac{R_1 + R_2}{S} + j\omega_o L_2\right) \bar{I}_{ar2} - \frac{R_2}{S} \bar{I}_{ar3} \\
&\vdots \\
0 &= -\frac{R_{N-2}}{S} \bar{I}_{arN-2} + \left(\frac{R_{N-2} + R_{N-1}}{S} + j\omega_o L_{N-1}\right) - \frac{R_{N-1}}{S} \bar{I}_{arN} \\
0 &= -\frac{R_{N-1}}{S} \bar{I}_{arN-1} + \left(\frac{R_{N-1} + R_N}{S} + j\omega_o L_N\right) \bar{I}_{arN}
\end{aligned} \tag{6.22}$$

These equations describe the equivalent circuit of Figure 6.1. This circuit is the positive sequence steady state equivalent circuit of the skin effect model of the induction motor.

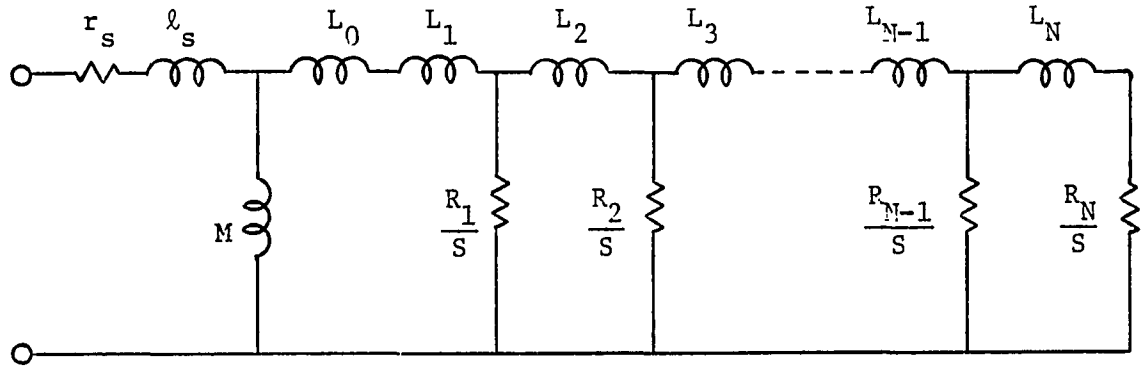

Figure 6.1 Positive sequence equivalent circuit of the skin effect impedance model

The Negative Sequence Motor Equations of the Skin Effect Model

For the purpose of analyzing the motor response to negative sequence voltages, a negative sequence reference frame will be used. In this reference frame, the d and q axes rotate at synchronous speed in the direction opposite to the rotation of the rotor. Then, from Figure 5.4,

$$\theta = -\omega_o t$$

$$\beta = -(\omega_o+\omega_r)t \tag{6.23}$$

and

$$p\theta = -\omega_o$$

$$p\beta = -(\omega_o+\omega_r) = -(2-s)\omega_o \tag{6.24}$$

Again, for constant slip, these terms are constant and the motor equations become a linear set of ordinary differential equations.

Negative sequence voltages with

$$v_a = \sqrt{2}\, V_2 \cos(\omega t+\alpha_2) \tag{6.25}$$

will have o, d, and q axis components of

$$v_o = 0$$

$$v_d = \sqrt{3}\, V_2 \cos\alpha_2$$

$$v_q = \sqrt{3}\, V_2 \sin\alpha_2 \tag{6.26}$$

in the negative sequence reference frame.

The transformation of axis quantities to phase quantities yields

$$f_a = \sqrt{\frac{2}{3}} \left[f_d \cos(-\omega_o t) + f_q \sin(-\omega_o t) + \frac{1}{\sqrt{2}} f_o \right] \tag{6.27}$$

or, in phasor terms with o axis quantities constrained to equal zero,

$$\overline{F}_a = \frac{1}{\sqrt{3}} (f_d + j f_q) \tag{6.28}$$

Equation 6.8 again describes the steady state motor operation, but matrix $\underline{G}$ is altered due to the change in reference frames. In the negative sequence reference frame, these equations are

$$\begin{bmatrix} v_{ds} \\ v_{qs} \\ \hdashline \underline{0} \\ \hdashline \underline{0} \\ \hdashline \\ \hdashline \underline{0} \\ \hdashline \underline{0} \end{bmatrix} = \begin{bmatrix} \underline{C}_s & \underline{C}_{sr} & \underline{0} & \underline{0} & \underline{0} & \underline{0} & \underline{0} \\ \underline{C}_{rs} & \underline{C}_r & \underline{D}_1 & \underline{0} & \underline{0} & \underline{0} & \underline{0} \\ \underline{0} & \underline{D}_1 & \underline{C}_2 & \underline{D}_2 & \underline{0} & \underline{0} & \underline{0} \\ \underline{0} & \underline{0} & \underline{0} & \underline{0} & \underline{D}_{N-2} & \underline{C}_{N-1} & \underline{D}_{N-1} \\ \underline{0} & \underline{0} & \underline{0} & \underline{0} & \underline{0} & \underline{D}_{N-1} & \underline{C}_N \end{bmatrix} \begin{bmatrix} i_{ds} \\ i_{qs} \\ \hdashline i_{dr1} \\ i_{qr1} \\ \hdashline i_{dr2} \\ i_{qr2} \\ \hdashline \\ \hdashline i_{drN-1} \\ i_{qrN-1} \\ \hdashline i_{drN} \\ i_{qrN} \end{bmatrix} \tag{6.29}$$

where

$$\underline{C}_s = \begin{bmatrix} r_s & -\omega_o(M+\ell_s) \\ \omega_o(M+\ell_s) & r_s \end{bmatrix} \tag{6.30}$$

$$\underline{C}_{sr} = \begin{bmatrix} 0 & -\omega_o M \\ \omega_o M & 0 \end{bmatrix} \tag{6.31}$$

$$\underline{C}_{rs} = \begin{bmatrix} 0 & -(2-s)\omega_o M \\ (2-s)\omega_o M & 0 \end{bmatrix} \tag{6.32}$$

$$\underline{C}_r = \begin{bmatrix} R_1 & -(2-s)\omega_o(M+L_o+L_1') \\ (2-s)\omega_o(M+L_o+L_1) & R_1 \end{bmatrix} \tag{6.33}$$

$$\underline{C}_k = \begin{bmatrix} R_{k-1}+R_k & =(2-s)\omega_o L_k \\ (2-s)\omega_o L_k & R_{k-1}+R_k \end{bmatrix} \quad k=2,3,\cdots,N \tag{6.34}$$

$$\underline{D}_k = \begin{bmatrix} -R_k & 0 \\ 0 & -R_k \end{bmatrix} \quad k=1,2,\cdots,N-1 \tag{6.35}$$

The transformation of the stator axis equations to a complex A phase equation yields

$$\overline{V}_2 = (r_s+j\omega_o\ell_s)\overline{I}_{as} + j\omega_o M(\overline{I}_{as}+\overline{I}_{ar1}) \tag{6.36}$$

The rotor equations are

$$0 = j\omega_o M\bar{I}_{as} + \left[\frac{R_1}{2-s} + j\omega_o(M+L_o+L_1)\right]\bar{I}_{ar1} - \frac{R_1}{2-s}\bar{I}_{ar2}$$

$$0 = -\frac{R_1}{2-s}\bar{I}_{ar1} + \left(\frac{R_1+R_2}{2-s} + j\omega_o L_2\right)\bar{I}_{ar2} - \frac{R_2}{2-s}\bar{I}_{ar3}$$

$$\vdots$$

$$0 = -\frac{R_{N-2}}{2-s}\bar{I}_{arN-2} + \left(\frac{R_{N-2}+R_{N-1}}{2-s} + j\omega_o L_{N-1}\right)\bar{I}_{arN-1} - \frac{R_{N-1}}{2-s}\bar{I}_{arN}$$

$$0 = -\frac{R_{N-1}}{2-s}\bar{I}_{arN-1} + \left(\frac{R_{N-1}+R_N}{2-s} + j\omega_o L_N\right)\bar{I}_{arN} \qquad (6.37)$$

These equations describe the equivalent circuit of Figure 6.2. This is the negative sequence steady state equivalent circuit of the skin effect model of the induction motor.

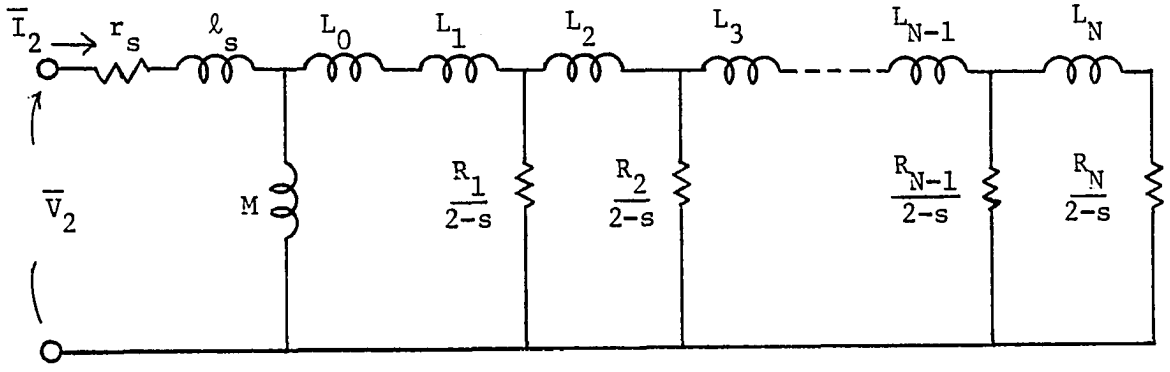

Figure 6.2 Negative sequence equivalent circuit of the skin effect impedance model

Electromagnetic Torque Developed in the Motor

An equation for finding the developed torque of the motor was presented in Chapter 5. While this equation is still valid for use with the

sequence equivalent circuits of the motor, it is far more convenient to develop an alternate torque equation expressed in terms of r.m.s. rotor currents, rotor resistance, and rotor slip.

In order to accomplish this goal, the motor currents must be separated into positive and negative sequence components. The motor torque then also consists of positive and negative sequence components. The positive sequence torque of the motor can be written as

$$T_{ep} = \sum_{k=1}^{N} \frac{R_k}{s\omega_o} I_{bkp}^2 \tag{6.38}$$

where I_{bkp} is the magnitude of the positive sequence current in the k^{th} rotor bar segment. Similarly, the negative sequence torque component is

$$T_{en} = -\sum_{k=1}^{N} \frac{R_k}{(2-s)\omega_o} I_{bkn}^2 \tag{6.39}$$

where I_{bkn} is the negative sequence current flowing in the k^{th} rotor bar segment. The motor torque is then the sum of these two torque components. Derivations of these equations are presented in Appendix E.

Steady State Analysis with the Skin Effect Model

Positive and negative sequence steady state equivalent circuits have been obtained from the skin effect electrical transient model of the induction motor. These equivalent circuits completely agree with the skin effect electrical transient model in the steady state. In so doing, these two skin effect induction motor models resolve the conflicts between the two axis theory and the steady state equivalent circuit theory found in Chapter 3. As a result, the skin effect electrical transient

model is applicable to a wide range of induction motor problems which the ordinary two axis theory cannot handle.

Because the skin effect equivalent circuits contain more elements than the equivalent circuits of Figure 3.1, they appear to be more complex. This is not necessarily true, however. The resistance and inductance values of the skin effect equivalent circuits are uniform between positive and negative sequence circuits and, more importantly, are constant for all rotor speeds. The rotor parameters of the circuits in Figure 3.1 vary from the positive to the negative sequence circuit, and also vary as the rotor speed changes. These equivalent circuits, therefore, must be readjusted as the rotor speed changes.

The added complexity of calculations involving the skin effect equivalent circuits is therefore easily justifiable by the increased generality of the circuits.

The convergence of the rotor bar internal resistance and inductance approximations was shown in Chapter 4. The convergence of the skin effect model can also be checked by steady state comparisons of the torque-speed relationship. The torque speed curve of motor M1 described in Table 6.1, is shown in Figure 6.3. The $N = \infty$ curve, which uses Equation 4.31 for the rotor bar internal impedance, is compared with the 2 and 4 loop approximations. These are referred to as models 2 and 4, respectively. The torque-speed curve of model 1A is also shown in Figure 6.3. Mode Model 1A is based on the steady state equivalent circuits of Figure 3.1 with positive and negative sequence rotor parameters equal. This model totally neglects the rotor skin effect.

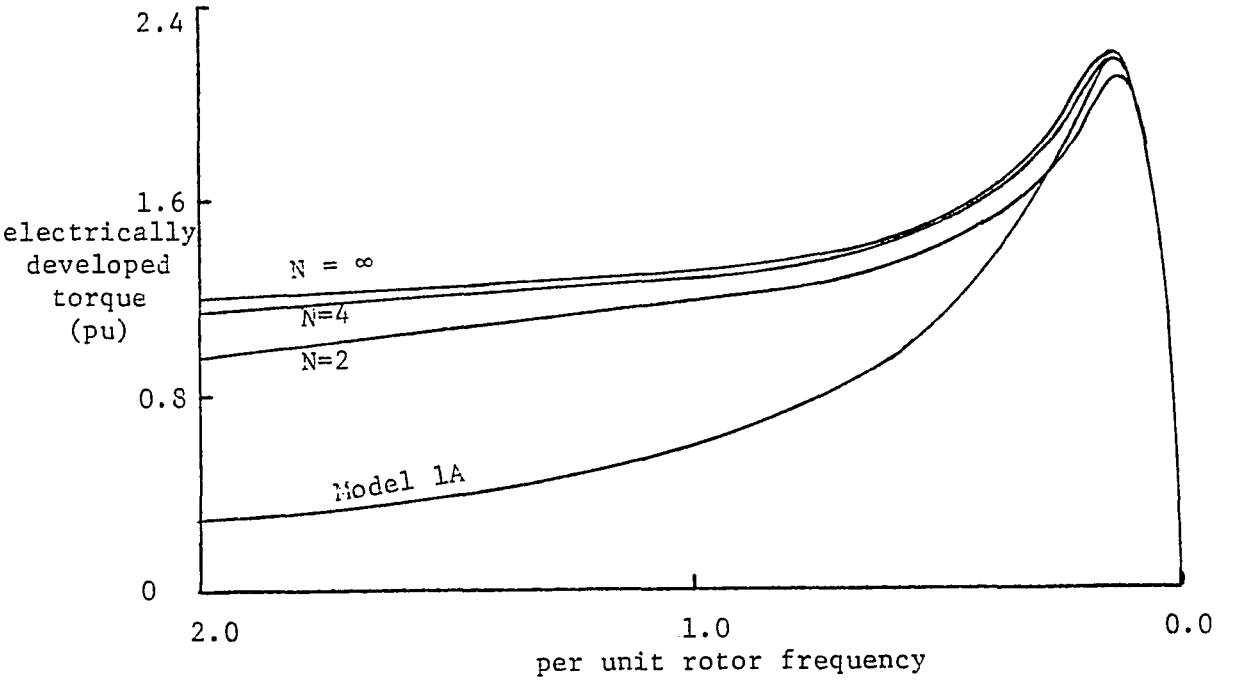

Figure 6.3 Torque-speed characteristics of motor M1 models 1A, 2 and 4 compared with exact calculations

Model 1B will also be used for comparisons in future chapters. Model 1B is also based on the equivalent circuits of Figure 3.1 with unequal positive and negative sequence rotor resistance and inductance. The evaluation of the rotor parameters are made at synchronous speed. Model 1B therefore properly accounts for the skin effect only at, or very close to, synchronous speed.

Dynamic Analysis with the Skin Effect Impedance Model

The derivation of the positive and negative sequence equivalent circuits relies heavily on the assumption that the electrical quantities involved contain only components that are sinusoidal and of the fundamental frequency, and on the assumption that rotor speed is constant.

Because of the nature of the induction machine, it is often valid to assume these conditions are approximately true in analyzing motional transients of the machine. A dynamic model based on the positive sequence equivalent circuit is widely used. The limitations of this model have been thoroughly explored [43]. These results, however, have been confined to cases with the rotor skin effect neglected.

The skin effect equivalent circuits developed in this chapter can also be used to describe the electrical action of the machine during a transient condition. This model neglects the fast electrical transient of the machine by assuming that the Lpi turns are negligibly small in the synchronously rotating reference frame for positive sequence excitation and in the negative sequence reference frame for negative sequence excitation. Because the equivalent circuits allow impedance type calculations, this model will be referred to as the skin effect impedance model in the following chapters. This model is fully capable of predicting the rotor bar skin effect. It is limited, however, in that it neglects the electrical transients. These transients may be of interest for a variety of reasons. Furthermore, the electrical and motional transients may interact under certain conditions to produce phenomena which this model is not capable of predicting.

The skin effect impedance model has been shown to be a direct simplification of the skin effect electrical transient model. Comparisons between these two models will therefore identify conditions under which the electric transients can be safely neglected and also the conditions for which the electrical transients must be evaluated.

Motor Characteristics

The skin effect models of the induction motor require more specified data than previous induction motor models. Although these data are not generally available in the form required for these models, they can be deduced from more commonly specified data if the general shape of the rotor bar is known.

Parameters of two motors are given in Table 6.1. These motors will be referred to as motors M1 and M2. Both motors have rectangular rotor bars. These motors have typical data for medium size deep bar induction motors. The positive and negative sequence rotor parameters are measured at no load operating speed, which can be assumed to be synchronous speed. The rotor resistance and leakage inductance at starting can be used in place of the negative sequence rotor values. As the rotor bars are rectangular, the internal bar impedance will be, from Equation 4.31,

$$Z_{bar} = R(1+j)A\coth(1+j)A \tag{6.40}$$

As the frequency approaches zero (which corresponds to synchronous speed of the rotor), Z_{bar} can be written as an infinite series. As $A = \sqrt{\frac{\omega L}{2R}}$, the bar impedance at low frequency is

$$Z_{bar} = R\left[1 + \frac{[(1+j)A]^2}{3} - \cdots\right]$$

$$= R + j\omega\frac{L}{3} - \cdots \tag{6.41}$$

Therefore, at $\omega=0$, the positive sequence rotor resistance is

$$R = r_{rp} \tag{6.42}$$

The positive sequence inductance ℓ_{rp} consists of external bar leakage inductance L_o plus the internal inductance at $\omega=0$.

Table 6.1 Specified motor data (per unit)

	MOTOR	M1	M2
	r_s	.02	.02
	ℓ_s	.08	.08
	M	4.0	4.0
pos. seq.	r_{rp}	.025	.0125
	ℓ_{rp}	.120	.198
neg. seq.	r_{rN}	.074	.075
	ℓ_{rN}	.085	.086
	H (sec.)	1.0	1.0

Table 6.2 Motor M1 and M2 data for the skin effect model (per unit)

MOTOR	M1	M2
r_s	.02	.02
ℓ_s	.08	.08
M	4.0	4.0
L_o	.048	.048
L	.216	.450
R	.025	.0125

$$L_o + \frac{L}{3} = \ell_{rp} \tag{6.43}$$

Finally, the values of L_o and L must be determined. These can be found at ω=2.0 p.u. from either r_{rn} or ℓ_{rn}. At ω=2.0, the real part of Equation 6.40 equals the negative sequence rotor resistance.

$$Re(Z_{bar}) = RA \frac{\sinh 2A + 2\sin 2A}{\cosh 2A - \cos 2A} = r_{rn} \tag{6.44}$$

For motor M1, from Table 6.1,

$$R = r_{rp} = 0.025$$

$$L_o + \frac{L}{3} = \ell_{rp} = 0.120 \tag{6.45}$$

In Equation 6.44, the quantity inside the brackets is approximately equal to one, so

$$A = \frac{r_{rn}}{R} = 2.95 \tag{6.46}$$

or

$$L = 8.7R = .216 \tag{6.47}$$

Then

$$L_o = .12 - \frac{.216}{3} = .048 \tag{6.48}$$

A check on the accuracy of the representation may be made by comparing the calculated and tabulated value of negative sequence inductance.

Similar calculations apply to motor M2. A summary of these values is given in Table 6.2. These data can be directly used in the skin effect induction motor models.

The parameters of motor models 1A and 1B can be taken directly from Table 6.1. These values are given in Table 6.3. These models will be

used to evaluate the necessity of considering skin effect in induction motor studies.

Table 6.3 Motor data for models 1A and 1B (per unit)

MODEL	1A		1B	
MOTOR	M1	M2	M1	M2
r_s	.02	.02	.02	.02
ℓ_s	.08	.08	.08	.08
M	4.0	4.0	4.0	4.0
r_{rp}	.025	.0125	.025	.0125
ℓ_{rp}	.12	.198	.12	.198
r_{rN}	.025	.0125	.074	.075
ℓ_{rN}	.12	.198	.085	.086

The skin effect impedance model and the skin effect electrical transient model treat the rotor bar current distribution and skin effect uniformly. They will both be used in the following chapters to predict the motor transients in a number of cases of interest to the study of induction motor operation. The necessity of evaluating the skin effect will be determined, as will the necessity of evaluating the fast electrical transients in accounting for the overall motor performance.

Summary

A representation of the induction motor has been derived which accounts for the rotor bar skin effect but neglects the electrical

transients. This model is a simplification of the skin effect electrical transient model which was derived in Chapter 5. The model consists of positive and negative sequence equivalent circuits, which are valid over the entire range of frequencies to be encountered in induction motor analysis. Previous equivalent circuits were valid only at one specific rotor speed. Because of the nature of the evaluation of the electrical effects with this model, it will be referred to as the skin effect impedance model.

The skin effect impedance model will be used in the study of steady state and dynamic motor performance. The validity of this motor model in the dynamic state will be thoroughly investigated in a variety of practical situations in which skin effect plays a prominent role. Comparisons between the skin effect impedance model and the skin effect electrical transient model will show the cases in which the evaluation of the electrical transients is necessary. Further evaluations between the skin effect models and two previous models will also be made. The first is model 1A which neglects the rotor bar skin effect. The second is model 1B, which ignores the variance of the skin effect as rotor speed varies. These comparisons will evaluate the necessity of accounting for the rotor bar skin effect in studying induction motor operation.

CHAPTER VII. STARTING TRANSIENTS IN INDUCTION MOTORS FED BY OPEN DELTA TRANSFORMERS

The open delta transformer bank is an economical method of supplying relatively small amounts of three phase load from a distribution system. The phase voltages supplied by the open delta bank become unbalanced as the transformer is loaded. This unbalance becomes increasingly severe as the loading increases, and is also affected by the load power factor.

The starting of a deep bar induction motor fed by an open delta transformer bank is of particular interest. The inrush current of the motor can lead to temporary overloads of the transformer. The unbalanced voltages of the transformer will generate positive and negative sequence currents in the motor over the full range of rotor speeds.

Analysis of the Open Delta Transformer Bank

The connection diagram for a typical open delta transformer bank is shown in Figure 7.1. With the transformer mangetization branch neglected, the open delta bank can be represented by the equivalent circuit of Figure 7.2 [22]. This equivalent circuit is valid for a three-wire load in cases where actual voltages to ground are not evaluated.

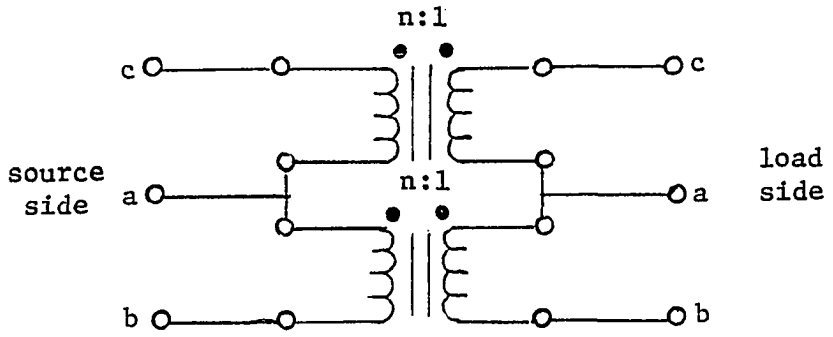

Figure 7.1 Connection diagram of an open delta transformer bank

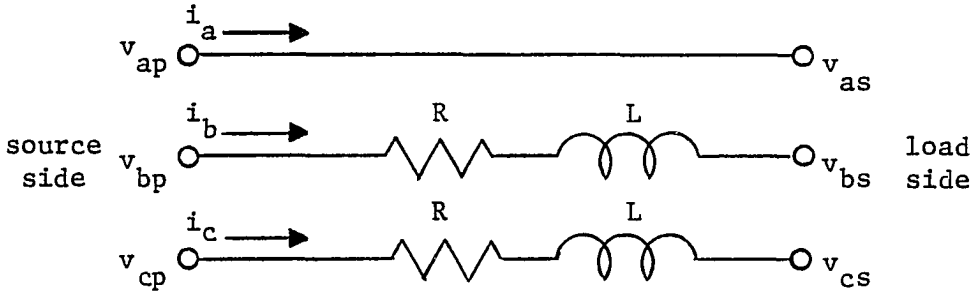

Figure 7.2 Equivalent circuit of the open delta transformer bank

The load side phase voltages will then be

$$\begin{bmatrix} v_{as} \\ v_{bs} \\ v_{cs} \end{bmatrix} = \begin{bmatrix} v_{ap} \\ v_{bp} \\ v_{cp} \end{bmatrix} - \begin{bmatrix} 0 & 0 & 0 \\ 0 & R & 0 \\ 0 & R & 0 \end{bmatrix} \begin{bmatrix} i_a \\ i_b \\ i_c \end{bmatrix} - \begin{bmatrix} 0 & 0 & 0 \\ 0 & L & 0 \\ 0 & 0 & L \end{bmatrix} \begin{bmatrix} pi_a \\ pi_b \\ pi_c \end{bmatrix} \qquad (7.1)$$

It is necessary to transform Equation 7.1 to the 012 reference frame of symmetrical components for analysis with the skin effect impedance model of the induction motor and to the odq reference frame of two axis

theory for analysis with the skin effect electrical transient model of the induction motor.

The transformation to the 012 reference frame yields, in phasor form,

$$\begin{bmatrix} \bar{V}_{0s} \\ \bar{V}_{1s} \\ \bar{V}_{2s} \end{bmatrix} = \begin{bmatrix} \bar{V}_{0p} \\ \bar{V}_{1p} \\ \bar{V}_{2p} \end{bmatrix} - \frac{1}{3} \begin{bmatrix} 2Z_t & -Z_t & -Z_t \\ -Z_t & 2Z_t & -Z_t \\ -Z_t & -Z_t & 2Z_t \end{bmatrix} \begin{bmatrix} \bar{I}_0 \\ \bar{I}_1 \\ \bar{I}_2 \end{bmatrix} \tag{7.2}$$

where $Z_t = R + j\omega L$. Zero sequence current will generally not be allowed to flow on the secondary side of the transformer. Although zero sequence voltages will be generated by positive and negative sequence currents, these can be ignored in studies concerned with the motor inrush current and starting torque. The positive and negative sequence equations are then

$$\begin{bmatrix} \bar{V}_{1s} \\ \bar{V}_{2s} \end{bmatrix} = \begin{bmatrix} \bar{V}_{1p} \\ \bar{V}_{2p} \end{bmatrix} - \begin{bmatrix} \frac{2}{3}Z_t & -\frac{1}{3}Z_t \\ -\frac{1}{3}Z_t & \frac{2}{3}Z_t \end{bmatrix} \begin{bmatrix} \bar{I}_1 \\ \bar{I}_2 \end{bmatrix} \tag{7.3}$$

The electrical transient model of the induction motor will be solved in the stationary reference frame of the two axis theory. Equation 7.1 transformed to the stationary reference frame is

$$\begin{bmatrix} v_{os} \\ v_{ds} \\ v_{qs} \end{bmatrix} = \begin{bmatrix} v_{op} \\ v_{dp} \\ v_{qp} \end{bmatrix} - \begin{bmatrix} \frac{2R}{3} & \frac{-\sqrt{2}R}{3} & 0 \\ \frac{-\sqrt{2}R}{3} & \frac{R}{3} & 0 \\ 0 & 0 & R \end{bmatrix} \begin{bmatrix} i_o \\ i_d \\ i_q \end{bmatrix} - \begin{bmatrix} \frac{2L}{3} & \frac{-\sqrt{2}L}{3} & 0 \\ \frac{-\sqrt{2}L}{3} & \frac{L}{3} & 0 \\ 0 & 0 & L \end{bmatrix} \begin{bmatrix} pi_o \\ pi_d \\ pi_q \end{bmatrix} \tag{7.4}$$

The o axis current, as is the case with the 0 sequence current, is not allowed to flow in the secondary of the transformer. Also, in many studies the o axis voltages need not be evaluated. The d and q axis equations, under these conditions are

$$\begin{bmatrix} v_{ds} \\ v_{qs} \end{bmatrix} = \begin{bmatrix} v_{dp} \\ v_{qp} \end{bmatrix} - \begin{bmatrix} \frac{R}{3} & 0 \\ 0 & R \end{bmatrix} \begin{bmatrix} i_d \\ i_q \end{bmatrix} - \begin{bmatrix} \frac{L}{3} & 0 \\ 0 & L \end{bmatrix} \begin{bmatrix} pi_d \\ pi_q \end{bmatrix} \tag{7.5}$$

Equations 7.3 and 7.5 can be coupled with the sequence or axis equations of the induction motor and the power system in order to obtain the complete model.

System Parameters

Motor starting transients will be evaluated using two motors - M1 and M2. The parameters of these motors were given in Table 6.1 It is assumed that both machines are rated at 100 kVA and 480 volts.

The transformer banks will consist of single phase 12 kV-480 V transformers with series impedance of $Z_t = .01+j.05$ pu to the transformer base. An open delta bank is not capable of supplying its nameplate rated kVA to the load [22]. Such a bank supplying only the motor will need to consist of two transformers rated at least 60 kVA. Although this is a non-standard size, 60 kVA transformers will be used for this study to provide a consistent comparison with the three phase transformer bank. The three phase bank will be of any configuration and consist of 3-33 kVA units.

The per phase impedance of the three phase bank will then be

$$Z_t = .01+j.05 \text{ pu} \tag{7.6}$$

to the machine base. The b and c phase impedance of the open delta bank will be

$$Z_t = (.01+j.05)\frac{100}{60} = .017+j.0835 \text{ pu} \tag{7.7}$$

to the machine base. For larger transformer banks supplying both motor and additional load, similar procedures are folowed.

Skin Effect Impedance Model Analysis

An extensive study was conducted of the motor starting transient of an induction motor supplied by an open delta bank. The study had goals of supplying information on the use of the skin effect impedance model of the induction motor, and of supplying information on the effect of open delta transformers on motor starting performance. Comparisons between the skin effect impedance model and the skin effect electrical transient model will also be made.

A one line diagram of the system studied is shown in Figure 7.3. The infinite bus voltage and the power system back up impedance are con-

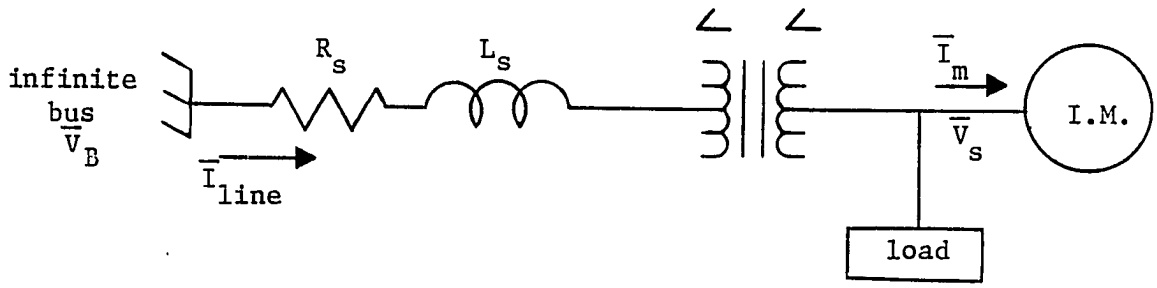

Figure 7.3 One line diagram of the system under study

sidered to be balanced. The load adjacent to the induction motor, when considered, is assumed to be constant impedance type of balanced load. The positive and negative sequence equations for this system are

$$\begin{bmatrix} \bar{V}_{1B} \\ 0 \end{bmatrix} = \begin{bmatrix} Z_s & 0 \\ 0 & Z_s \end{bmatrix} \begin{bmatrix} \bar{I}_{1L} \\ \bar{I}_{2L} \end{bmatrix} + \begin{bmatrix} \frac{2}{3}Z_t & -\frac{1}{3}Z_t \\ -\frac{1}{3}Z_t & \frac{2}{3}Z_t \end{bmatrix} \begin{bmatrix} \bar{I}_{1L} \\ \bar{I}_{2L} \end{bmatrix} + \begin{bmatrix} \bar{V}_{1s} \\ \bar{V}_{2s} \end{bmatrix} \tag{7.8}$$

As the positive and negative sequence equivalents of the induction motor are independent, as are the sequence equivalents of the load, the transformer secondary voltage can be expressed in terms of the secondary currents and equivalents of the positive and negative sequence loads.

$$\begin{bmatrix} \bar{V}_{1s} \\ \bar{V}_{2s} \end{bmatrix} = \begin{bmatrix} Z_{1eq} & 0 \\ 0 & Z_{2eq} \end{bmatrix} \begin{bmatrix} \bar{I}_{1L} \\ \bar{I}_{2L} \end{bmatrix} \tag{7.9}$$

The currents are then found to be

$$\begin{bmatrix} \bar{I}_{1L} \\ \bar{I}_{2L} \end{bmatrix} = \begin{bmatrix} Z_{1eq} + Z_s + \frac{2}{3}Z_t & -\frac{1}{3}Z_t \\ -\frac{1}{3}Z_t & Z_{2eq} + Z_s + \frac{2}{3}Z_t \end{bmatrix}^{-1} \begin{bmatrix} \bar{V}_{1B} \\ 0 \end{bmatrix} \tag{7.10}$$

and the negative sequence current is

$$\bar{I}_{2L} = \frac{\frac{1}{3}Z_t \, \bar{V}_{1B}}{(Z_{1eq}+Z_s+\frac{2}{3}Z_t)(Z_{2eq}+Z_s+\frac{2}{3}Z_t) - \frac{1}{9}Z_t^2} \tag{7.11}$$

It can be seen from Equation 7.11 that the negative sequence current will be greatest when the source impedance Z_s is small. For a given installation, with induction motor and adjacent load, the negative sequence

current will be greatest with the load switched on, as this will reduce Z_{1eq} and Z_{2eq} while Z_t will remain constant. In general, however, the presence of load adjacent to the motor will affect transformer rating and therefore transformer impedance, and the overall effect on negative current is not readily apparent.

Evaluation of Skin Effect Model Of primary importance in the use of the skin effect impedance model is the determination of the number of rotor loops required to yield accurate analysis. Although results were obtained on the accuracy of the model considering only the rotor bars, results showing the effects of detailed skin effect modeling on overall motor performance predictions are necessary. Table 7.1 gives the run-up time, inrush current, and developed torque of the motor M1 starting transient with a number of different rotor representations. Also given are the predictions of motor models 1A and 1B. Model 1A neglects the skin effect entirely, while model 1B uses a single evaluation of skin effect at running speed to distinguish between positive and negative sequence rotor impedances. Models 2 through 8 are the skin effect impedance model predictions with the model number corresponding to the number of rotor loops represented. It can be seen from Table 7.1 that the convergence of the solution in this case is quite rapid, but the need for skin effect modeling is apparent.

Table 7.2 illustrates the results of a similar study conducted with motor M2. As motor M2 has a higher deep bar effect than motor M1, a slower convergence is to be expected. This is indeed the case, as comparison of any of the columns of Table 7.2 with the corresponding

Table 7.1 Motor M1 starting performance with open delta feed. Free acceleration, $Z_s=0$

Model	Run-up time (95% of synch. speed)	Inrush current (pu at locked rotor) Positive Sequence (rms)	Inrush current (pu at locked rotor) Negative Sequence (rms)	Developed torque (pu at locked rotor) Positive Sequence	Developed torque (pu at locked rotor) Negative Sequence
1A	2.97 sec	3.918	.432	.362	.004
1B	3.06 sec	3.918	.466	.362	.016
2 loop	2.05 sec	3.975	.444	.733	.009
3 loop	1.99 sec	4.034	.457	.768	.010
4 loop	1.96 sec	4.059	.463	.780	.010
5 loop	1.95 sec	4.072	.466	.786	.010
6 loop	1.95 sec	4.080	.468	.789	.010
7 loop	1.95 sec	4.082	.468	.789	.010
8 loop	1.95 sec	4.086	.468	.791	.010

Table 7.2 Motor M2 starting performance with open delta feed. Free acceleration, Z_s=0

Model	Run-up time (95% of synch. speed)	Inrush current (pu at locked rotor) Positive Sequence (rms)	Inrush current (pu at locked rotor) Negative Sequence (rms)	Developed torque (pu at locked rotor) Positive Sequence	Developed torque (pu at locked rotor) Negative Sequence
1A	9.43 sec	3.079	.268	.108	.001
1B	10.20 sec	3.062	.358	.106	.009
2 loop	2.77 sec	3.760	.398	.478	.005
3 loop	2.21 sec	3.935	.436	.755	.009
4 loop	2.13 sec	3.984	.446	.790	.010
5 loop	2.10 sec	4.012	.453	.807	.010
6 loop	2.08 sec	4.030	.457	.816	.010
7 loop	2.07 sec	4.040	.459	.822	.011
8 loop	2.07 sec	4.048	.461	.825	.011

figures in Table 1 shows. This is further confirmed in Figure 7.4, where the percent errors in run-up time of the two motors are compared with respect to the detail of rotor representation. In this figure, model 8 is taken as the basis for comparison.

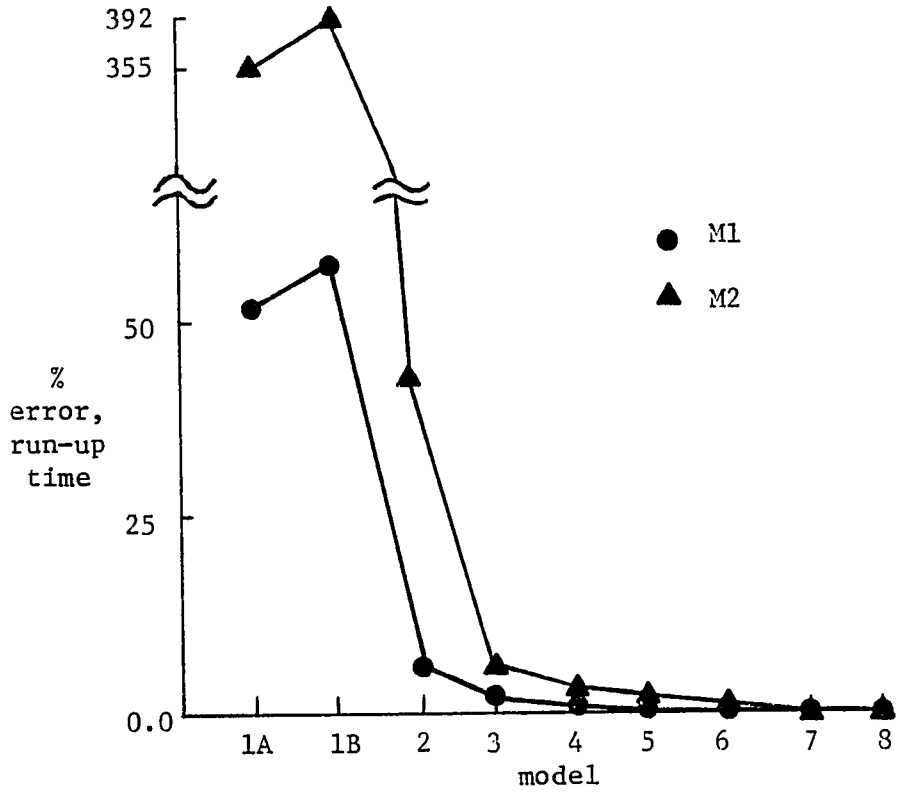

Figure 7.4 Comparison of the convergence of motor M1 and M2 run-up time predictions

The Skin Effect Electrical Transient Model

A motor starting study using the skin effect electrical transient model was conducted which analyzed the same motor and power system conditions as the studies in the previous section. This model has two

advantages over the impedance model: it evaluates the electrical transients and it provides more accurate values of inrush current, torque, and run-up time.

Figure 7.5 shows the inrush current, torque and speed predictions of the skin effect electrical transient model for motor M1 starting when fed by an open delta bank. The rotor in this study was represented by four loops. Also shown in Figure 7.5 are the torque, speed, and A phase current predictions of the skin effect impedance model. As can be seen by comparing these results, the two models agree closely in their predictions.

Figure 7.6 shows the results of a similar study of the motor starting transient of motor M2. The same power system was used for this case. Again, the comparison of results between the skin effect electric transient model and the skin effect impedance model shows close agreement. In motor studies which do not require explicit knowledge of the electrical transients or the torque fluctuations, use of the skin effect impedance model would be desirable as it is easier to implement, it yields results which are easy to interpret, and it is nearly as accurate as the skin effect electric transient model.

Motor Starting - Open Delta Feed vs. Three Phase Feed

An important aspect in the application of open delta transformer banks is the evaluation of any detrimental effects which may occur as a result of its use. The open delta bank is known to supply unbalanced

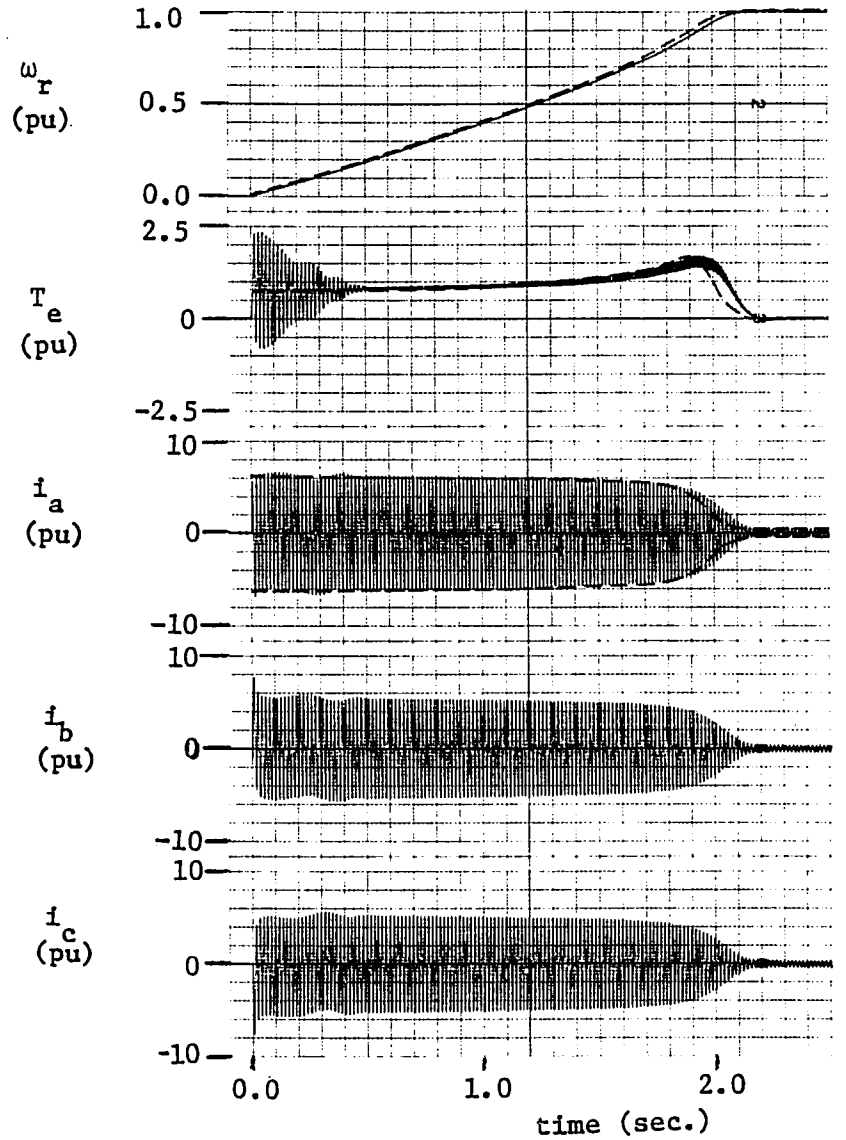

– – – – – – – – skin effect - impedance model

_____ skin effect - electric transient model

Figure 7.5 Motor starting transient of motor M1 with open delta bank

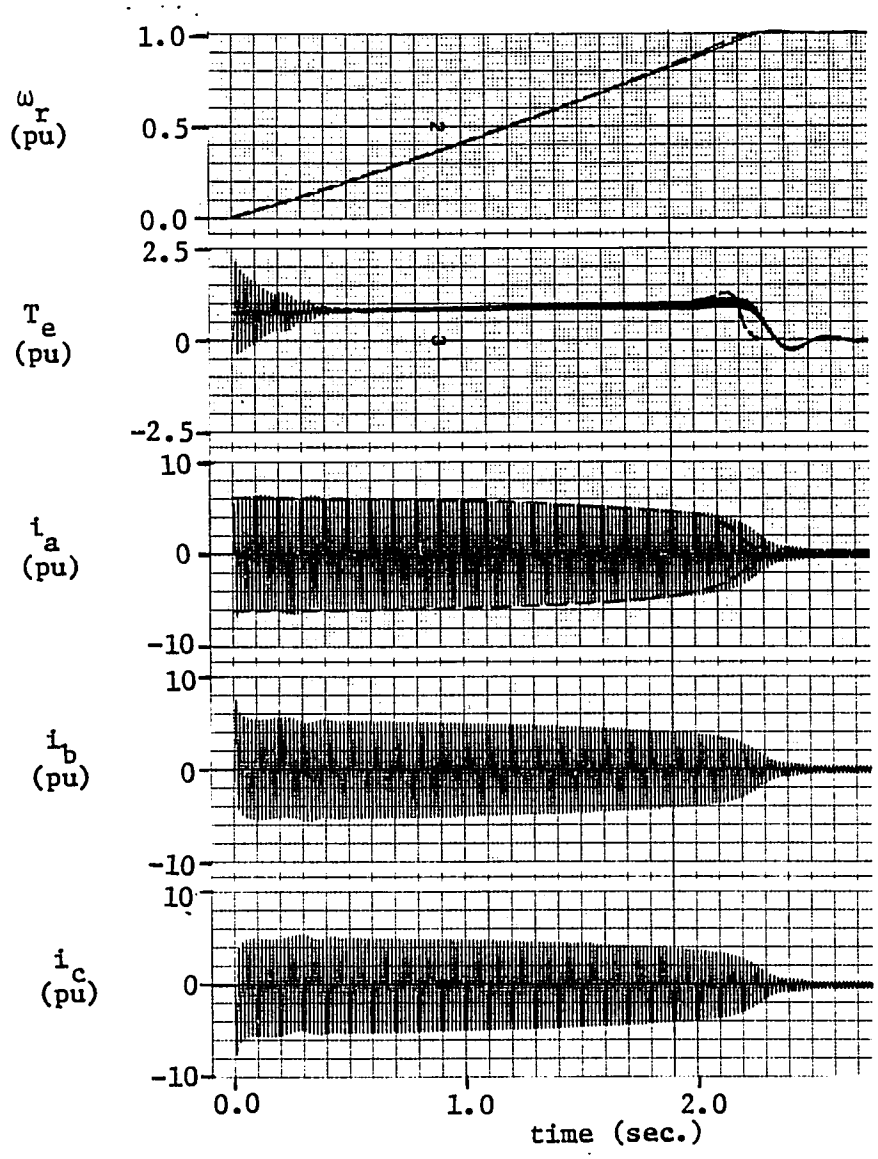

– – – – – – – skin effect - impedance model

_____ skin effect - electric transient model

Figure 7.6 Motor starting transient of motor M2 with open delta bank

voltages to its load, particularly when the bank is heavily loaded. The loading of the transformers can be expected to be heaviest when a large induction motor fed by the bank is being started. It is desirable to know whether the resulting voltage unbalance will significantly affect the motor starting transient.

In the two preceding sections, the studies involved a 100 kVA motor supplied by an open delta transformer bank consisting of 2-60 kVA transformers. In this section, the motor starting transient with this open delta bank will be compared with the motor starting transient of a motor fed by a three phase, 100 kVA transformer. All calculations for both motors and both the impedance and electric transient model use the four rotor loop model of the motor.

Motor run-up characteristics for both open delta and three phase feeds are given for motor M1 in Table 7.3 and for motor M2 in Table 7.4. The current, torque and voltage values are given with the rotor at rest. The positive sequence torque and voltage increase as the rotor gains speed, while the current decreases slowly through most of the machine run-up. With the open delta feed, the negative sequence torque, current and voltage decline as rotor speed increases. The data in Tables 7.3 and 7.4 therefore represent the highest values of negative sequence torque and voltage with respect to positive sequence values. It can be seen from these tables that the negative sequence torque is negligible, as are the differences in run-up time between the open delta and three phase bank cases. The matters of concern in the starting of a motor with an open delta feed are then the flow of negative sequence current

Table 7.3 Motor M1 starting: open delta vs. three phase feeds

Type of feed	Run-up time (95% of synch. speed)	Inrush current (pu at locked rotor) Positive Sequence (rms)	Inrush current (pu at locked rotor) Negative Sequence (rms)	Developed torque (pu at locked rotor) Positive Sequence	Developed torque (pu at locked rotor) Negative Sequence	Terminal voltage (pu at locked rotor) Positive Sequence	Terminal voltage (pu at locked rotor) Negative Sequence
Open delta	1.96 sec	4.059	.463	.780	.010	.784	.089
Three phase	1.91 sec	4.107	0.0	.799	0.0	.793	0

Table 7.4 Motor M2 starting: open delta vs. three phase feeds

Type of feed	Run-up time (95% of synch. speed)	In rush current (pu at locked rotor) Positive Sequence (rms)	In rush current (pu at locked rotor) Negative Sequence (rms)	Developed torque (pu at locked rotor) Positive Sequence	Developed torque (pu at locked rotor) Negative Sequence	Terminal voltage (pu at locked rotor) Positive Sequence	Terminal voltage (pu at locked rotor) Negative Sequence
Open delta	2.13 sec	3.984	.446	.790	.010	.787	.088
Three phase	2.07 sec	4.03	0.0	.809	0.0	.797	0

in the motor and the effect of negative sequence voltage on adjacent load.

The major concern in guarding motors against negative sequence currents is the additional motor heating which results [60]. Although many references exist on these effects during steady state operating conditions, there appear to be none concerning unbalanced heating during motor starting. While the values of negative sequence voltages present at the motor terminals are above recommended limitations for steady operating conditions, it should be recognized that these are transient conditions which last for only a matter of seconds. Furthermore, while these negative sequence currents are nearly half the value of the rated positive sequence current, they amount to only slightly over 10% of the value of positive sequence inrush current. Although little data are available on motor heating effects over such short periods of time, it would appear that this amount of current unbalance would be acceptable.

Table 7.5 compares the run-up time predictions of the electric transient model with the impedance model predictions from the above study. There is also close correlation between these models in the current, voltage, and torque predictions.

The effects of motor starting with adjacent load connected are important as most banks supply more than one motor. A 200 kVA transformer bank supplying the 100 kVA motor M1 with varying amounts of parallel load was studied. Again, comparisons are made between an open delta bank and a comparable three phase bank. The results of this study are given in Table 7.6. All calculations were made using the four loop

Table 7.5 Comparison of skin effect models

Type of feed	Model	Run-up time (95% of synch. speed) Motor M1	Motor M2
Open delta	impedance	1.96 sec	2.13 sec
	electric transient	2.01 sec	2.19 sec
Three phase	impedance	1.91 sec	2.07 sec
	electric transient	1.95 sec	2.12 sec

skin effect impedance model. As was the case with no parallel load, the positive sequence components of current, voltage and torque, as well as run-up time, are not strongly affected by the use of an open delta bank. Furthermore, in all cases studied, the negative sequence voltage component is smaller in these cases than the negative sequence voltages of Table 7.3, which considered the motor as the only load of a smaller transformer bank. As some of the cases shown in Table 7.6 involve significant overloads of the transformer bank, the cases outlined by Table 7.3 and 7.4 appear to represent the worst case situation of motor starting with an open delta feed.

Comments

The conclusions to be drawn from these results are quite general. While the calculations in this chapter involved a 100 kVA motor, the

Table 7.6 The effect of parallel load on run-up characteristics: motor M1

Parallel load	Type of feed	Run-up time (sec)	Transformer current (pu at locked rotor) Positive Sequence (rms)	Transformer current (pu at locked rotor) Negative Sequence (rms)	Developed torque (pu at locked rotor) Positive Sequence	Developed torque (pu at locked rotor) Negative Sequence	Terminal voltage (pu at locked rotor) Positive Sequence (rms)	Terminal voltage (pu at locked rotor) Negative Sequence (rms)
40 kvar reactive	open delta	1.68	4.628	.304	.934	.004	.873	.057
	3 phase	1.64	4.674	0	.953	0	.882	0
120 kvar reactive	open delta	1.87	4.835	.332	.845	.004	.867	.060
	3 phase	1.83	4.884	0	.862	0	.876	0
300 kvar reactive	open delta	2.61	5.426	.417	.623	.004	.851	.065
	3 phase	2.52	5.484	0	.636	0	.860	0
300 kW	open delta	2.08	5.378	.410	.790	.005	.859	.066
	3 phase	2.02	5.439	0	.808	0	.869	0

motor parameters are typical of motors in the size range of importance in the study of open delta transformer banks.

Large differences were shown to exist between the skin effect models and previous techinques, which were outlined in Chapter 3. These differences increase as the deep bar effect increases.

These results show that the skin effect impedance model and the skin effect electrical transient model agree closely in the areas which the impedance model is capable of predicting. The accuracy of the impedance model, however, depends on motor and system parameters, and the impedance model may not yield results as accurate as these in other cases. Use of this model would be preferable, therefore, in most studies.

Machine run-up times were not significantly affected by the presence of an open delta feed. This type of feed, however, did affect the machine currents and terminal voltages. These effects were not deemed to be serious considering the current levels and the relatively short period of time the starting transient persists.

In conditions where the transformer feeds more than one motor, the voltage unbalance during starting of one motor in extreme cases can be at or slightly above the steady state limitations. Again, this is a short term effect and motor starting should not cause heating problems in adjacent motors already running.

CHAPTER VIII. ANALYSIS OF SINGLE PHASE TO GROUND FAULTS USING THE SKIN EFFECT MODEL OF THE INDUCTION MOTOR

The contribution of current from induction motors to power system faults is an area which is often neglected in fault studies. Recent papers [32]; [58] have outlined the need for closer analysis of these currents due to faster clearing times, more stringent circuit breaker clearing capacities, and the general trend toward larger induction motors.

Induction motor fault analysis has, in general, been limited to three phase fault conditions. With a three phase fault at the motor terminals, the induction machine loses its external source of excitation. The machine excitation then comes from the stored energy in the machine's magnetic circuit, which decays very rapidly. The fault current from the machine lasts only during this period, which is normally only a matter of a few cycles.

With single phase to ground faults, however, the motor remains excited by the two unfaulted phases. Fault currents, therefore, will not decay to zero in a few cycles. This source of excitation remains until the action of a three phase circuit breaker in clearing the fault also removes the source of machine excitation. The analysis of induction motor performance during single phase to ground faults has been almost entirely neglected, largely due to the lack of an adequate dynamic model of the induction motor. One recent study [58] which did analyze the single phase to ground fault at the terminals of an induction motor was limited in that the two unfaulted phases were tripped two cycles after

the fault occurred, which severely limited the amount of post-fault motor excitation.

The skin effect models of the induction motor developed in Chapters 4, 5, and 6 have the power to determine rotor bar current distribution throughout the operating region of interest in studying unbalanced faults. With this capability, the skin effect models effectively remove the major obstacle to analytic investigations of induction motor fault performance.

The Single Phase to Ground Fault

A study of induction motor performance during single phase to ground faults has been conducted using the skin effect models of the induction motor. The fault has been treated uniformly throughout the study by assuming that a solidly grounded fault occurs at the A phase motor terminal and that the power system is strong enough and well grounded so that the other two phase voltages are unaffected. The fault inception will always occur with the motor operating under normal steady state conditions.

Under these conditions with A phase faulted, the post fault terminal voltages will be

$$v_a = 0$$

$$v_b = \sqrt{2}\ V \cos(\omega t+\alpha-\frac{2\pi}{3})$$

$$v_c = \sqrt{2}\ V \cos(\omega t+\alpha+\frac{2\pi}{3}) \qquad (8.1)$$

The positive and negative sequence voltages are then

$$\bar{V}_1 = \frac{2}{3} V \angle \alpha$$

$$\bar{V}_2 = \frac{-1}{3} V \angle \alpha \qquad (8.2)$$

and the d and q axis voltages in the stationary reference frame are

$$v_{ds} = \frac{1}{\sqrt{3}} V \cos(\omega t+\alpha)$$

$$v_{qs} = -\sqrt{3} V \sin(\omega t+\alpha) \qquad (8.3)$$

These voltage equations are linked with the motor equations of the skin effect impedance model and the skin effect electric transient model, respectively, for solutions of motor performance during single phase to ground faults.

The Initial Post Fault Period

The first few cycles immediately following fault inception are of particular importance. Large transient currents and torques occur immediately after fault inception. In many instances, fault interruption will also occur during this period.

Table 8.1 shows the initial fault current predictions of the skin effect impedance model. These values are compared with models 1A and 1B, the previously available impedance type models. Again, as was shown in previous chapters, the solution of the skin effect model converges with a relatively small number of rotor bar segments represented. The predictions of positive sequence fault currents show close agreement for all models used. The negative sequence current pre-

dictions, however, show a wide range of values. The predictions of model 1B are very close to the results from the higher order skin effect models. This can be expected only when the motor is operating at small slip.

Table 8.1 Skin effect impedance model predictions of sequence currents at the inception of a single phase to ground fault

Motor	M1				M2			
Load torque (pu)	0.1		$0.1 + .96\omega^2$		0.1		$0.1 + .96\omega^2$	
Initial rotor speed (pu)	0.999		0.967		0.999		0.967	
	Motor Current - rms (pu)				Motor Current - rms (pu)			
Motor model	Pos. Seq.	Neg. Seq.	Pos. Seq.	Neg. Seq.	Pos. Seq.	Neg. Seq.	Pos. Seq.	Neg. Seq.
1A	.165	1.674	.854	1.674	.172	1.235	1.421	1.235
1B	.165	1.918	.854	1.916	.172	1.918	1.418	1.916
2	.165	1.856	.851	1.852	.172	1.631	1.363	1.631
3	.165	1.885	.850	1.881	.172	1.843	1.378	1.840
4	.165	1.904	.852	1.900	.172	1.866	1.384	1.862
5	.165	1.913	.852	1.909	.172	1.885	1.388	1.881
6	.165	1.919	.852	1.914	.172	1.896	1.391	1.892
7	.165	1.920	.852	1.916	.172	1.903	1.392	1.899
8	.165	1.923	.852	1.919	.172	1.908	1.393	1.904

The time solutions of the skin effect impedance model and the skin effect electric transient model are of particular importance. These solutions for motor M1 with a small load torque are shown in Figure 8.1.

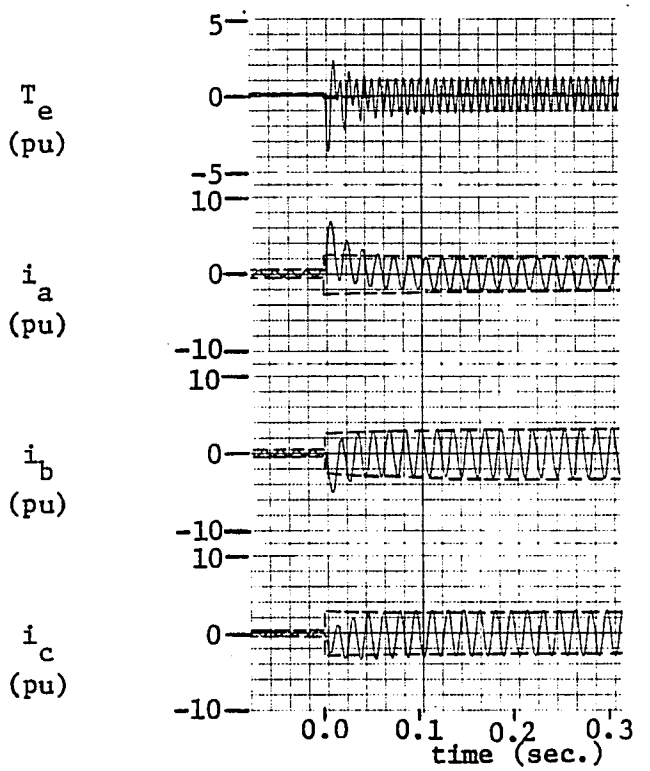

——————— electric transient model

- - - - - - - - impedance model

Figure 8.1 Skin effect electric transient and skin effect impedance model predictions of motor current during a phase to ground fault. Motor M1. T_m=0.1 pu. 4 loop models used

The switching angle of the fault in this case led to a large d.c. offset of the electrical transient. The fast electrical transients quickly subside, however, and the impedance model and electric

transient model agree closely following this initial period. Also of interest is the electrical transient model prediction of the electromagnetic torque both during the fast electrical transient and the steadily fluctuating torque during the following period.

The same fault conditions are shown in Figure 8.2 with the motor fully loaded at the time of the fault. Again, the solutions of the two models agree closely after the fast electrical transients decay. In this case however, after the electrical transients decay, the mechanical transient is just beginning. The mechanical transient has slight effects on the current comparisons between the models, which is most noticeable in B phase current in this case. It is interesting to note that in both of these cases, current in the faulted phase is lowest of the three phase currents. It is also interesting that the currents are highest when the motor is loaded, but the 120 hertz torque component is largest when the motor is lightly loaded.

Similar fault conditions for motor M2 are shown in Figure 8.3 and 8.4. In Figure 8.4, the fault occurred with very little d.c. offset. This change affects only the fast electrical transients and the initial torque, and the comparison between solutions is again good following this initial period.

At light loads (Figures 8.1 and 8.3) the fault currents for the two motors are quite similar. At full load, however, much of this similarity has disappeared due to the varied deep bar effect of the two motors.

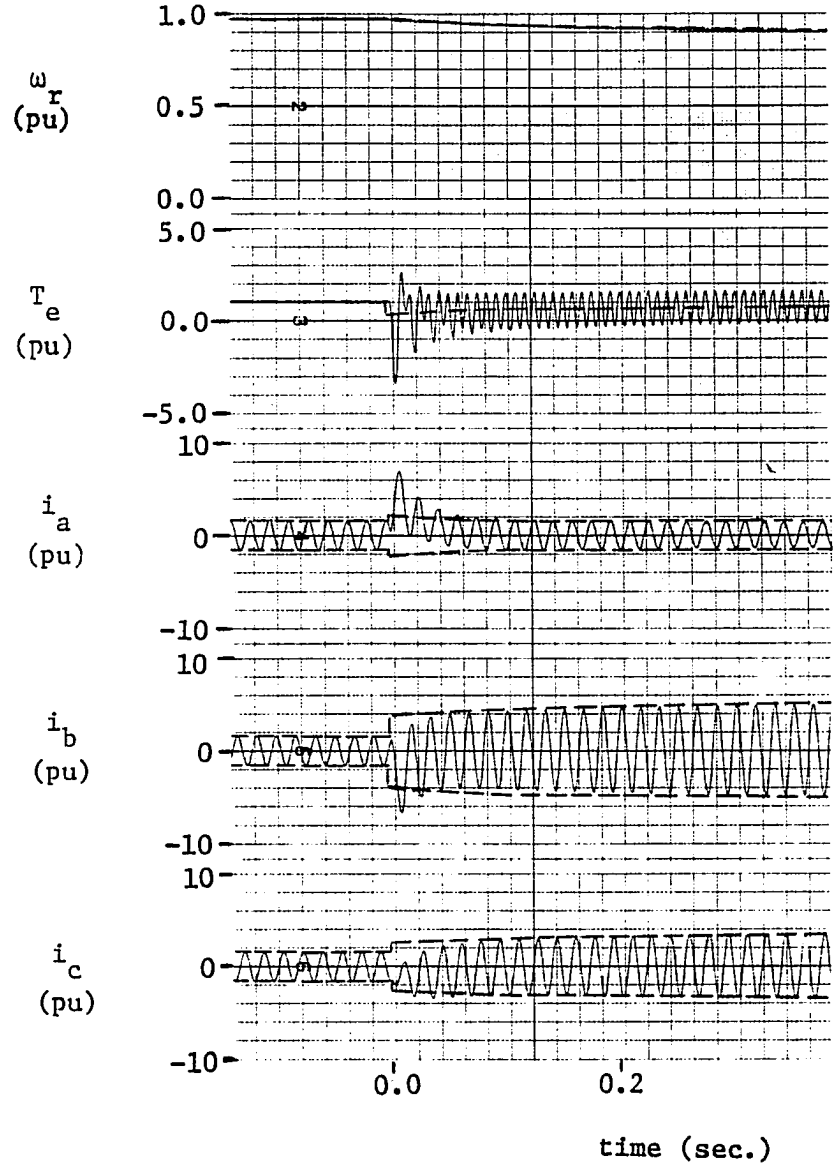

Figure 8.2 Skin effect electric transient and skin effect impedance model predictions of motor current during A phase to ground fault. Motor M1. $T_m = 0.1 + .96\omega_r^2$ pu. 4 loop models used

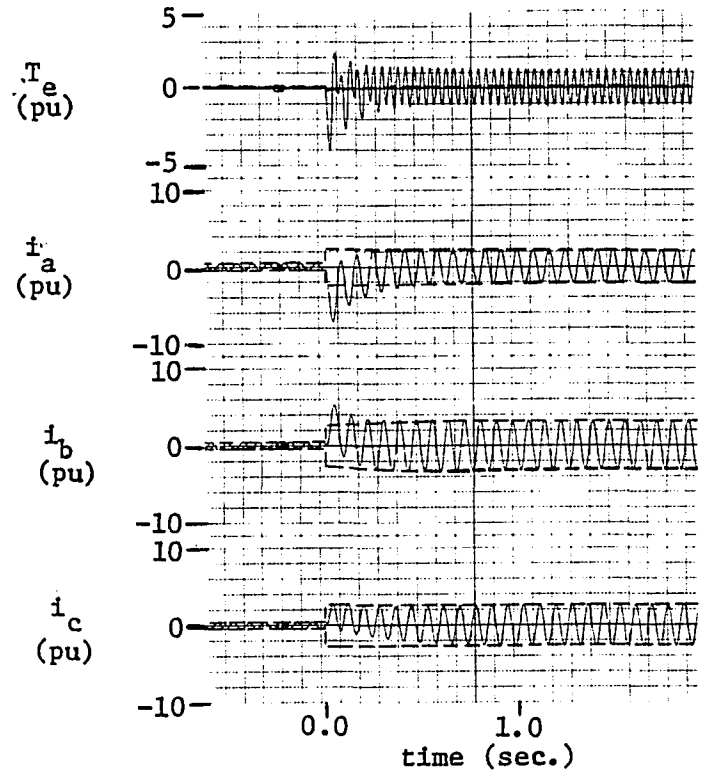

——————— electric transient model

– – – – – – skin effect model

Figure 3.3 Skin effect electric transient and skin effect impedance model predictions of motor current during A phase to ground fault. Motor M2. T_m = 0.1 pu. 4 loop models used

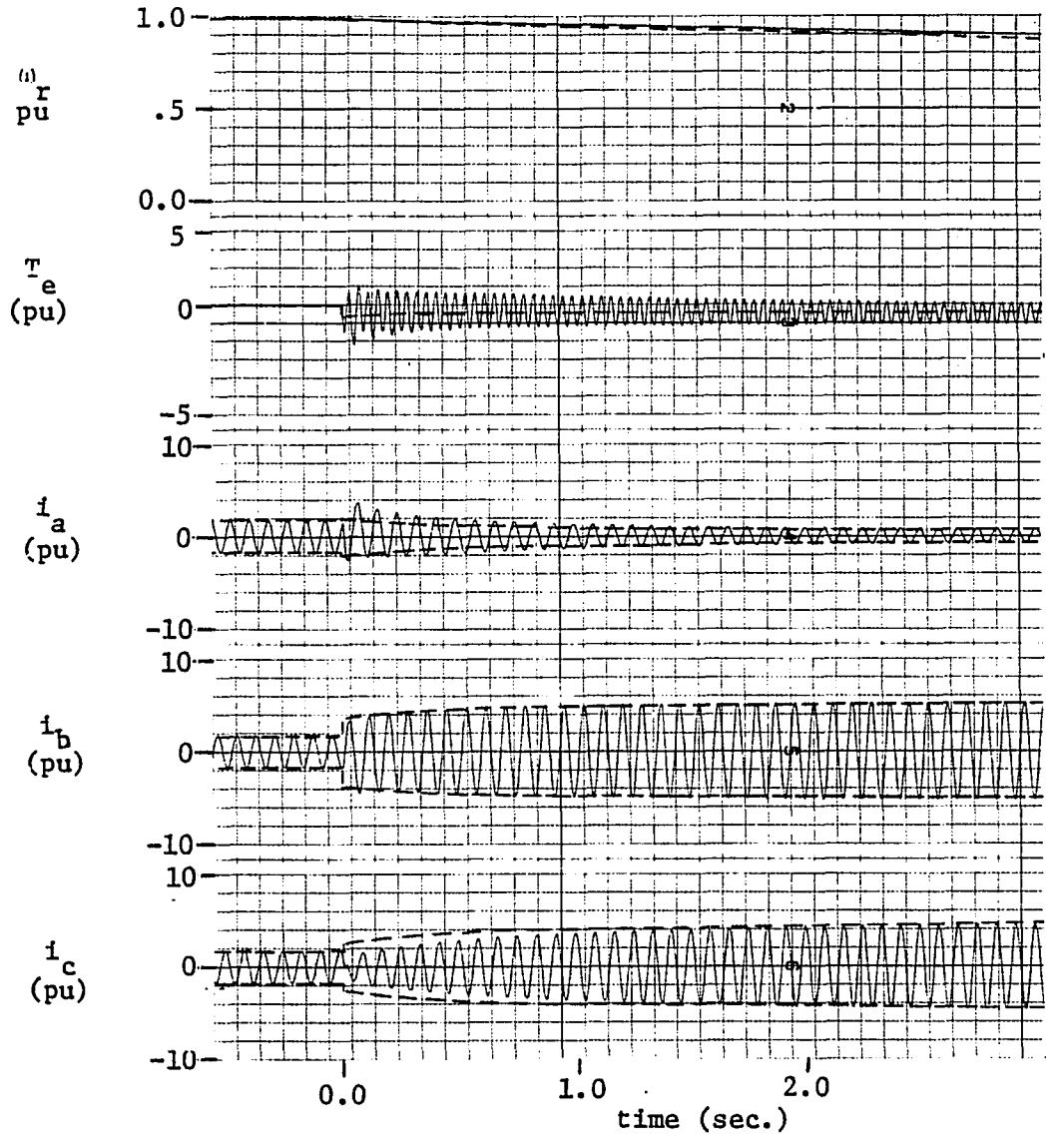

——————— electric transient model

– – – – – – – skin effect model

Figure 8.4 Skin effect electric transient and skin effect impedance model predictions of motor current during A phase to ground fault. Motor M2. $T_m = 0.1 + 0.96\omega_r^2$. 4 loop models used.

Long Term Faults

The evaluation of motor performance for longer periods of time is also important. The fault may last longer than a few cycles for a variety of reasons, and evaluation of motor performance becomes more important as the duration of the fault increases.

Depending on the motor parameters and motor loading, the motor will settle onto a new operating point or it will stall. In either case, motor current levels can be high enough to cause motor overheating.

The final values of motor currents, torques and speed are given in Tables 8.2-8.5. As the operating points are stable, the solutions of the impedance model and the electrical transient model agree at the points in these tables. The cases examined are the same as considered in the previous section. The results of model 1B again agree with the results of the skin effect model in three of the cases. In the fourth case, model 1B predicts motor stall while the skin effect model predicts a stable operating point at a rotor speed of approximately 0.65 p.u. In general, motor model 1B will approximate the skin effect model only when the transient is confined to small values of rotor slip.

In all cases considered above, including both lightly loaded and fully loaded machines, the phase currents are above rated values and care must be taken to protect the motor from overheating during this type of power system fault.

The various induction motor models also predict varying mechanical transients. Figure 8.5 shows the rotor speed predictions for motor M1 with a constant load torque of 1.0 p.u. While all models predict motor

Table 8.2 Steady state values of motor current during A phase to ground fault. Motor M1 T_m = 0.1 pu

Model	Phase currents (rms, pu) I_a	I_b	I_c	Sequence currents (rms, pu) I_1	I_2	Rotor speed (pu) ω_r	Developed torque (pu) Pos. Seq.	Neg. Seq.
1A	1.480	1.927	1.649	.266	1.674	.992	.133	-.033
1B	1.637	2.307	1.877	.407	1.917	.986	.233	-.133
2	1.600	2.207	1.814	.368	1.854	.988	.206	-.106
3	1.613	2.260	1.843	.392	1.884	.987	.223	-.123
4	1.628	2.283	1.861	.398	1.902	.986	.227	-.127
5	1.635	2.295	1.870	.400	1.911	.986	.229	-.129
6	1.640	2.302	1.876	.402	1.917	.986	.230	-.130
7	1.641	2.304	1.877	.402	1.919	.986	.230	-.130
8	1.643	2.308	1.880	.403	1.921	.986	.231	-.131

Table 8.3 Steady state values of motor current during Aϕ to ground fault. Motor M1. $T_m = 0.1 + 0.96\omega_r^2$ (pu)

	Phase currents (rms, pu)			Sequence currents (rms, pu)		Rotor speed (pu)	Developed torque (pu)	
Model	I_a	I_b	I_c	I_1	I_2	ω_r	Pos. Seq.	Neg. Seq.
1A	1.330	3.524	2.215	1.888	1.673	.910	.930	-.035
1B	1.006	3.989	3.052	2.259	1.909	.877	.977	-.140
2	1.018	3.925	3.004	2.259	1.840	.867	.926	-.109
3	1.014	3.942	3.006	2.254	1.869	.872	.953	-.125
4	1.021	3.949	2.991	2.228	1.888	.876	.963	-.129
5	1.025	3.956	2.988	2.224	1.897	.877	.968	-.130
6	1.029	3.958	2.983	2.218	1.902	.878	.971	-.131
7	1.031	3.956	2.976	2.212	1.904	.879	.972	-.132
8	1.032	3.956	2.973	2.210	1.907	.879	.973	-.132

Table 8.4 Steady state values of motor current during Aϕ to ground fault. Motor M2. T_m = 0.1 pu

Model	Phase currents (rms, pu)			Sequence currents (rms, pu)		Rotor speed (pu)	Developed torque (pu)	
	I_a	I_b	I_c	I_1	I_2	ω_r	Pos. Seq.	Neg. Seq.
1A	1.057	1.459	1.225	.239	1.235	.997	.109	-.009
1B	1.621	2.312	1.892	.414	1.918	.993	.233	-.133
2	1.421	1.905	1.608	.289	1.631	.996	.147	-.047
3	1.576	2.199	1.813	.374	1.843	.994	.206	-.106
4	1.580	2.244	1.838	.399	1.865	.993	.223	-.123
5	1.595	2.269	1.858	.405	1.884	.993	.226	-.126
6	1.604	2.283	1.869	.408	1.896	.993	.229	-.129
7	1.609	2.292	1.876	.410	1.902	.993	.230	-.130
8	1.614	2.298	1.881	.411	1.908	.993	.231	-.131

Table 8.5 Steady state values of motor current during A phase to ground fault. Motor M2. $T_m = 0.1 + 0.96\omega_r^2$ (pu)

Model	Phase currents (rms, pu)			Sequence currents (rms, pu)		Rotor speed (pu)	Developed torque (pu)	
	I_a	I_b	I_c	I_1	I_2	ω_r	Pos. Seq.	Neg. Seq.
1A	1.232	3.260	3.260	2.464	1.232	.000	.069	-.012
1B	1.039	3.259	4.073	2.464	1.833	.000	.069	-.241
2	1.133	3.936	3.565	2.684	1.620	.628	.534	-.056
3	.977	4.070	3.826	2.738	1.795	.628	.595	-.116
4	.974	4.101	3.875	2.762	1.816	.635	.616	-.128
5	.962	4.123	3.897	2.769	1.835	.640	.626	-.132
6	.958	4.139	3.912	2.776	1.846	.642	.631	-.134
7	.952	4.145	3.917	2.777	1.853	.645	.634	-.135
8	.950	4.151	3.922	2.788	1.858	.647	.636	-.136

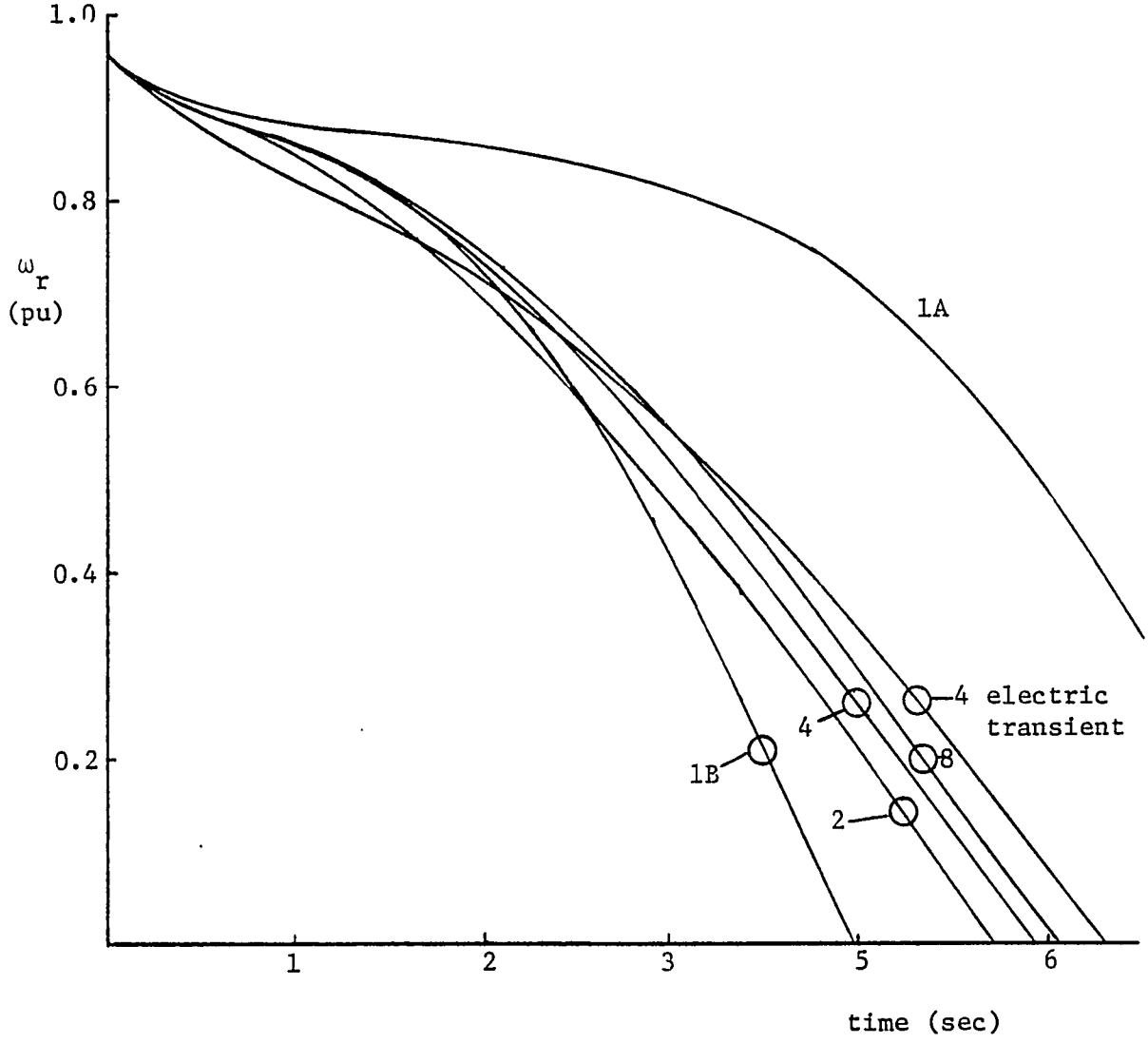

Figure 8.5 Motor M1 speed following single phase to ground fault. T_m = 1.0 pu. Skin effect impedance model prediction except where noted

stall, the predicted paths to zero rotor speed vary widely. The comparison between the four loop models of the impedance and electric transient models are most interesting. The electric transient model predicts rapid deceleration during the initial period, while the impedance model predicts more rapid deceleration during later periods.

Figure 8.6 shows motor M2 stalling under the same conditions. The deceleration is much quicker in this case and the comparisons are correspondingly closer. Note that models 1A and 1B cannot be counted on to give consistently optimistic or pessimistic results.

Comments

The skin effect models of the induction motor converge to solutions of the single phase to ground fault with a modest number of rotor loops represented.

The skin effect electrical transient model predicts the electrical transients which occur and is therefore inherently more accurate than the skin effect impedance model. The difference between these models is most profound in the period immediately following the fault inception. It appears that this fast transient decays rapidly and does not significantly affect the overall motor performance, but this period does produce the highest instantaneous current and torque levels. In all cases studied, the predictions of the impedance and electrical transient models show good agreement after these initial transients subside.

These calculations have shown that high current levels exist during the fault, particularly in the unfaulted phases. These high current

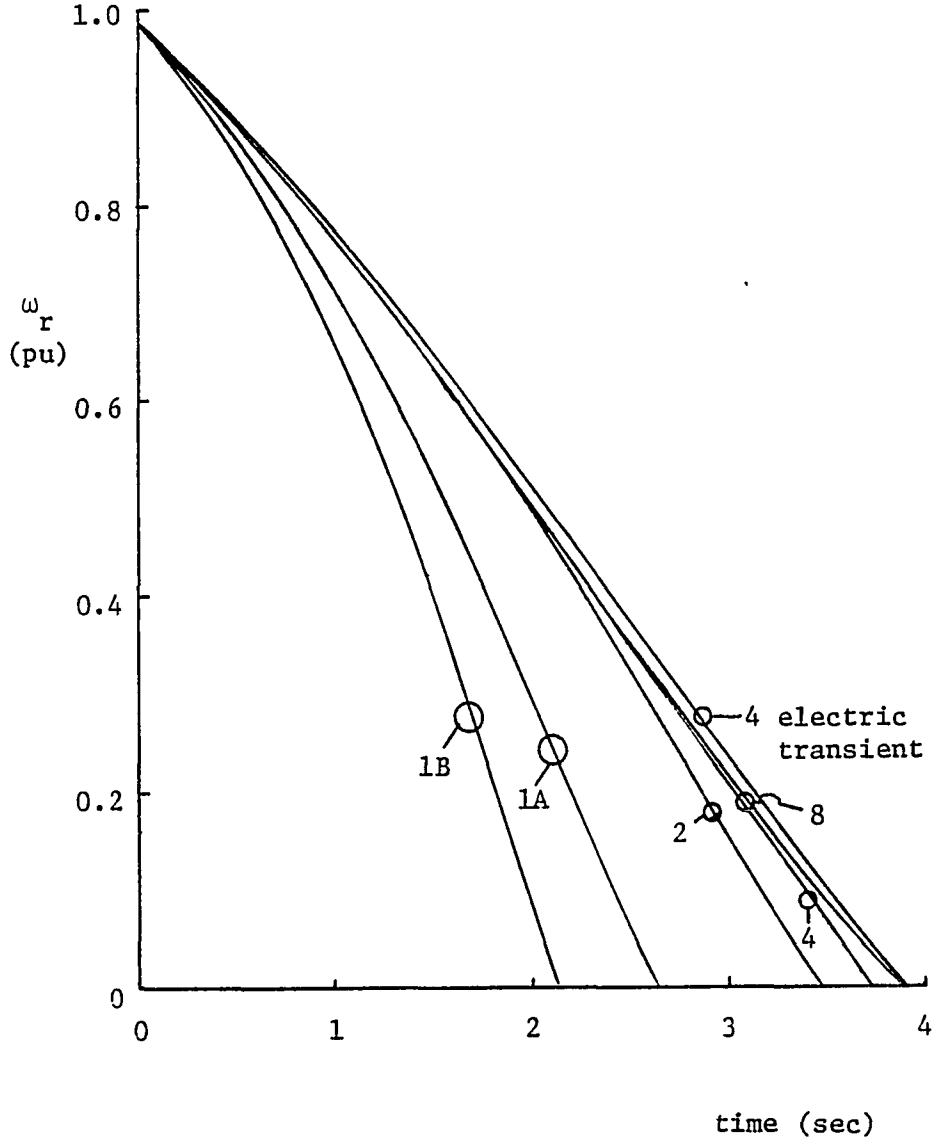

Figure 8.6 Motor M2 speed following single phase to ground fault. T_m = 1.0 pu. Skin effect impedance model predictions except where noted

levels are of concern in cases of slow fault clearing, where overheating may lead to motor damage.

CHAPTER IX. MOTOR TRANSIENTS FOLLOWING THE SUDDEN OPENING OF ONE PHASE

Under certain conditions, one phase of a three phase feed may suddenly open while the other two phases remain energized. This may result from a number of causes. The ungrounded three phase induction motor fed by the remaining phases will then experience a transient which can be harmful to the motor.

This condition, often referred to as single phasing or as a single phase series fault, can lead to stable motor operation or to motor stall, depending on conditions of the motor, motor loading, and power system. Analysis of single phasing has generally been limited to a steady state determination, by means of symmetrical component analysis, of possible low slip motor operating points.

The skin effect model of the induction motor is suitable for use in both the transient and steady state periods following the sudden opening of one phase of the motor feed.

The Power System Equations: One Phase Open

Because of the symmetries of both the symmetrical component transformation and Park's transformation, it will be assumed throughout the study that the affected phase is A phase. The faulted power system segment is shown in Figure 9.1. It follows from the figure that

$$i_a = 0 \tag{9.1}$$

and

$$v_{bs} - v_{bL} = 0$$

$$v_{cs} - v_{cL} = 0 \tag{9.2}$$

describe this unbalanced line segment. These equations will be transformed to the odq axes and the 012 sequences, where they can be coupled to the other system equations.

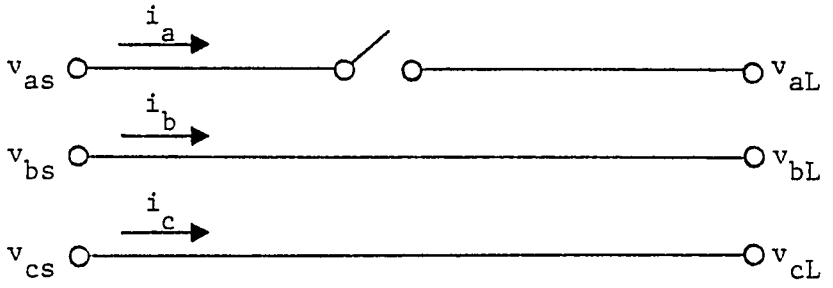

Figure 9.1 The power system segment containing the open phase

Sequence Networks

The transformation of phase voltages to sequence voltages is

$$\begin{bmatrix} \overline{V}_{0s} - \overline{V}_{0L} \\ \overline{V}_{1s} - \overline{V}_{1L} \\ \overline{V}_{2s} - \overline{V}_{2L} \end{bmatrix} = \frac{1}{3} \begin{bmatrix} 1 & 1 & 1 \\ 1 & a & a^2 \\ 1 & a^2 & a \end{bmatrix} \begin{bmatrix} \overline{V}_{as} - \overline{V}_{aL} \\ \overline{V}_{bs} - \overline{V}_{bL} \\ \overline{V}_{cs} - \overline{V}_{cL} \end{bmatrix} \tag{9.3}$$

where a is the phasor operation $1\underline{|120°}$ and the voltages are expressed in terms of phasor quantitites. The sequence voltages, from Equations 9.2 and 9.3, are then

$$\overline{V}_{0s} - \overline{V}_{0L} = \overline{V}_{1s} - \overline{V}_{1L} = \overline{V}_{2s} - \overline{V}_{sL} = \frac{1}{3}(\overline{V}_{as} - \overline{V}_{aL}) \tag{9.4}$$

The phase currents can be found, from the sequence currents to be

$$\begin{bmatrix} \bar{I}_a \\ \bar{I}_b \\ \bar{I}_c \end{bmatrix} = \begin{bmatrix} 1 & 1 & 1 \\ 1 & a^2 & a \\ 1 & a & a^2 \end{bmatrix} \begin{bmatrix} \bar{I}_0 \\ \bar{I}_1 \\ \bar{I}_2 \end{bmatrix} \tag{9.5}$$

As A phase current is zero,

$$0 = \bar{I}_0 + \bar{I}_1 + \bar{I}_2 \tag{9.6}$$

The sequence diagram which satisfies these conditions is shown in Figure 9.2. Note that each sequence current leaving the source side is constrained to equal the corresponding sequence current entering the load side of the network. This constraint could be expressed with ideal 1:1

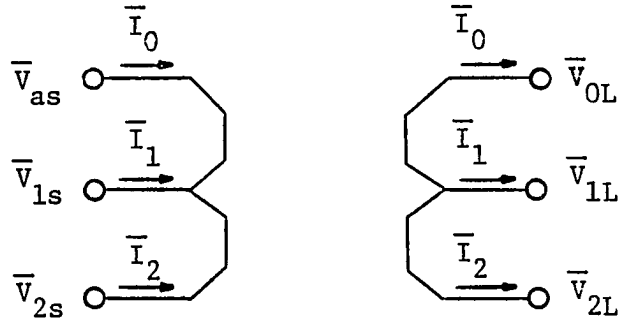

Figure 9.2 The sequence diagram equivalent to the phase diagram of Figure 9.1

current transformers in each phase. This is generally unnecessary, however, as the external connections to this diagram generally force the equality of sequence currents entering and leaving the network. This sequence diagram will be coupled with the sequence diagrams of the induction motor and the power system to find the overall solution.

A typical power source for an induction motor can be treated as a positive sequence voltage source with balanced source impedance. Power

factor correction capacitors may be present at the motor terminals. The one line diagram of this system is shown in Figure 9.3.

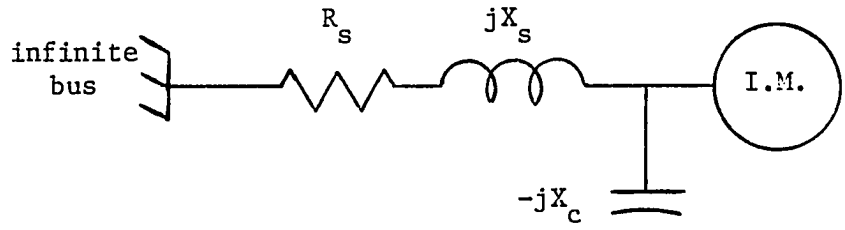

Figure 9.3 One line diagram of typical motor feed

The sequence diagrams for source impedance and shunt capacitance are well known. The sequence diagrams of the motor were derived in Chapter 6. The motor sequence impedances will be referred to as Z_{pm} and Z_{nm} for simplicity. The sequence diagram for A phase open circuit at the source side of the capacitors is then shown in Figure 9.4. It is assumed that both motor and capacitor are ungrounded, so zero sequence current cannot flow.

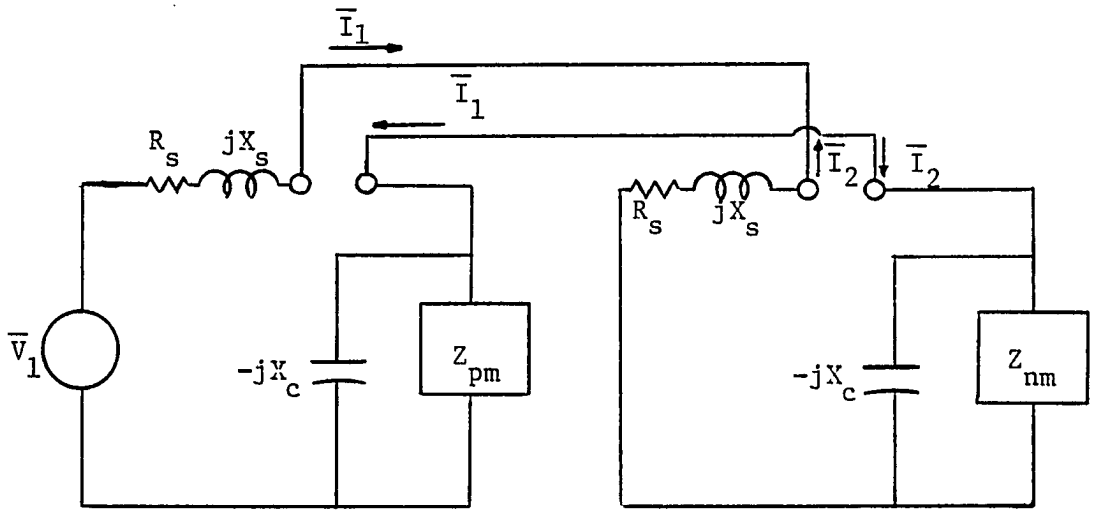

Figure 9.4 Sequence diagrams for A phase open with typical motor feed

The Axis Networks

The odq axis equivalent of Figure 9.1 will be found in the stationary frame. In this reference frame, the phase currents are related to the axis currents by Equation 9.7.

$$\begin{bmatrix} i_a \\ i_b \\ i_c \end{bmatrix} = \sqrt{\frac{2}{3}} \begin{bmatrix} \frac{1}{\sqrt{2}} & 1 & 0 \\ \frac{1}{\sqrt{2}} & -\frac{1}{2} & -\frac{\sqrt{3}}{2} \\ \frac{1}{\sqrt{2}} & -\frac{1}{2} & \frac{\sqrt{3}}{2} \end{bmatrix} \begin{bmatrix} i_o \\ i_d \\ i_q \end{bmatrix} \tag{9.7}$$

When $i_a=0$, with o axis currents constrained to equal zero,

$$i_d = 0 \tag{9.8}$$

The axis voltages are related to phase voltages by Equation 9.9.

$$\begin{bmatrix} v_{os} - v_{oL} \\ v_{ds} - v_{dL} \\ v_{qs} - v_{qL} \end{bmatrix} = \sqrt{\frac{2}{3}} \begin{bmatrix} \frac{1}{\sqrt{2}} & \frac{1}{\sqrt{2}} & \frac{1}{\sqrt{2}} \\ 1 & -\frac{1}{2} & -\frac{1}{2} \\ 0 & -\frac{\sqrt{3}}{2} & \frac{\sqrt{3}}{2} \end{bmatrix} \begin{bmatrix} v_{as} - v_{aL} \\ v_{bs} - v_{bL} \\ v_{cs} - v_{cL} \end{bmatrix} \tag{9.9}$$

Recognizing the b and c phase voltage relationships of Equation 9.2,

$$v_{qs} - v_{qL} = 0 \tag{9.10}$$

and

$$v_{ds} - v_{dL} = \sqrt{\frac{2}{3}} (v_{as} - v_{aL}) \tag{9.11}$$

The axis diagram equivalent to the phase diagram of Figure 9.1 can be found from Equations 9.8 and 9.10. This equivalent circuit is given in Figure 9.5.

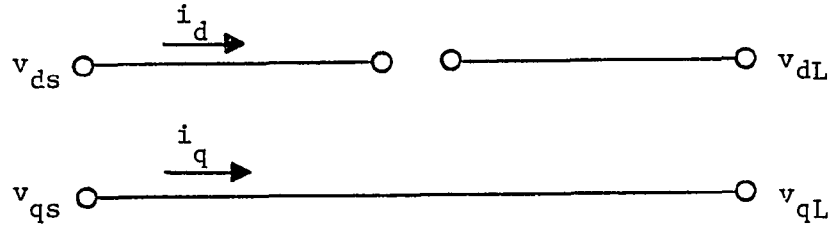

Figure 9.5 The stationary reference frame axis diagrams equivalent to the phase diagrams of Figure 9.1

These equations can be coupled with the axis equations of the power system and induction motor in order to obtain a prediction of motor operation with one phase of the three phase feed open. In cases where the motor and all other loads on the motor side of the fault are ungrounded, no o axis current can flow through the faulted section.

Skin Effect Model Analysis of the Series Fault

A single phase series fault has long been recognized as an important problem in induction motor operation. Under these conditions, the high currents of shunt faults are not developed, but currents can result which have the potential of causing motor overheating yet which are below minimum fault current levels used for protection purposes.

A study was conducted involving the necessity of using the skin effect model in calculating the transient following a series fault. Table 9.1 and 9.2 contain the final operating point predictions for motors M1 and M2 with a small mechanical load. Models 1A, 1B and the skin effect models 2 through 8 are considered. In each case, all models agree closely. This is a result of the lack of severity of the fault when the machine is lightly loaded. In both cases, the fault has caused a slight reduction of positive sequence current and a very small increase in rotor slip. The only major change is the presence of negative sequence current in the motor following the fault.

Tables 9.3 and 9.4 involve the same motors and power system conditions, but a larger motor load torque. All motor models of both motors in this case predict motor stall. The motor current, torque and voltage at stall are given in Tables 9.3 and 9.4. In these cases, a much wider range of predictions occur among the motor models investigated. The sequence torque predictions show particularly large differences between models 1A, 1B and the skin effect model.

Comparisons between the skin effect impedance model and electrical transient model show close agreement. The solutions of the two models are presented in Figure 9.6 for motor M1 with load torque T_m=1.0 pu. Both models use four rotor loop representations. In computing the electrical transient model, it is assumed that the phase opening occurs as the current passes through zero. In this case, as in cases involving lighter loads, the impedance and electrical transient model agree closely with the single exception of the torque oscillations which the impedance

Table 9.1 Final operating conditions of motor M1 following the sudden opening of A phase. T_m=0.1

Model	Phase current (pu, rms) I_a	I_b	I_c	Sequence current (pu, rms) I_1	I_2	Rotor speed (pu) ω_r	Developed torque (pu) Pos. Seq.	Neg. Seq.	Terminal voltage (pu, rms) V_a
1A	0.0	.438	.438	.253	.253	.997	.101	.001	.813
1B	0.0	.441	.441	.255	.255	.997	.102	.002	.826
2	0.0	.441	.441	.255	.255	.997	.102	.002	.822
3	0.0	.441	.441	.255	.255	.997	.102	.002	.824
4	0.0	.441	.441	.255	.255	.997	.102	.002	.825
5	0.0	.441	.441	.255	.255	.997	.102	.002	.825
6	0.0	.441	.441	.255	.255	.997	.102	.002	.826
7	0.0	.441	.441	.255	.255	.997	.102	.002	.826
8	0.0	.441	.441	.255	.255	.997	.102	.002	.826

Table 9.2 Final operating conditions of motor M2 following the sudden opening of A phase. T_m=0.1

Model	Phase current (pu, rms) I_a	I_b	I_c	Sequence current (pu, rms) I_1	I_2	Rotor speed (pu) ω_r	Developed torque (pu) Pos. Seq.	Neg. Seq.	Terminal voltage (pu, rms) V_a
1A	0.0	.435	.435	.252	.252	.998	.100	.000	.769
1B	0.0	.443	.443	.256	.256	.998	.102	.002	.825
2	0.0	.441	.441	.254	.254	.998	.101	.001	.808
3	0.0	.443	.443	.255	.255	.998	.102	.002	.820
4	0.0	.443	.443	.256	.256	.998	.102	.002	.822
5	0.0	.443	.443	.256	.256	.998	.102	.002	.823
6	0.0	.443	.443	.256	.256	.998	.102	.002	.824
7	0.0	.443	.443	.256	.256	.998	.102	.002	.824
8	0.0	.443	.443	.256	.256	.998	.102	.002	.825

Table 9.3 Final operating conditions of motor M1 following the sudden opening of A phase. $T_m = 0.1 + .96\omega_r^2$

Model	Phase current (pu, rms) I_a	I_b	I_c	Sequence current (pu, rms) I_1	I_2	Rotor speed (pu) ω_r	Developed torque (pu) Pos. Seq.	Neg. Seq.	Terminal voltage (pu, rms) V_a
1A	0.0	3.383	3.383	1.953	1.953	0.0	.090	.090	.500
1B	0.0	3.478	3.478	2.008	2.008	0.0	.095	.288	.497
2	0.0	3.414	3.414	1.971	1.971	0.0	.180	.180	.500
3	0.0	3.461	3.461	1.999	1.999	0.0	.189	.189	.500
4	0.0	3.483	3.482	2.011	2.011	0.0	.191	.191	.500
5	0.0	3.493	3.493	2.017	2.017	0.0	.193	.193	.500
6	0.0	3.500	3.500	2.021	2.021	0.0	.193	.193	.500
7	0.0	3.502	3.502	2.022	2.022	0.0	.194	.194	.500
8	0.0	3.505	3.505	2.024	2.024	0.0	.194	.194	.500

Table 9.4 Final operating conditions of motor M2 following the sudden opening of A phase. $T_m = 0.1 + .96\omega^2$

Model	Phase current (pu, rms) I_a	I_b	I_c	Sequence current (pu, rms) I_1	I_2	Rotor speed (pu) ω_r	Developed torque (pu) Pos. Seq.	Neg. Seq.	Terminal voltage (pu, rms) V_a
1A	0.0	2.676	2.676	1.545	1.545	0.0	.027	.027	.500
1B	0.0	3.075	3.075	1.775	1.775	0.0	.036	.225	.371
2	0.0	3.243	3.243	1.872	1.872	0.0	.119	.119	.500
3	0.0	3.379	3.379	1.951	1.951	0.0	.185	.185	.500
4	0.0	3.419	3.419	1.974	1.974	0.0	.194	.194	.500
5	0.0	3.441	3.441	1.987	1.987	0.0	.198	.198	.500
6	0.0	3.456	3.456	1.995	1.995	0.0	.200	.200	.500
7	0.0	3.464	3.464	2.000	2.000	0.0	.201	.201	.500
8	0.0	3.470	3.470	2.004	2.004	0.0	.202	.202	.500

model neglects. In Figure 9.7, the rotor speed of the electrical transient model is compared with the skin effect impedance model and models 1A and 1B. The differences between skin effect models are so slight that they do not show up on the graph. Similar predictions for motor M2 are given in Figures 9.8 and 9.9. Larger differences between impedance and electrical transient models exist during the first few cycles with this motor. The overall agreement between the impedance and electrical transient models remains, however.

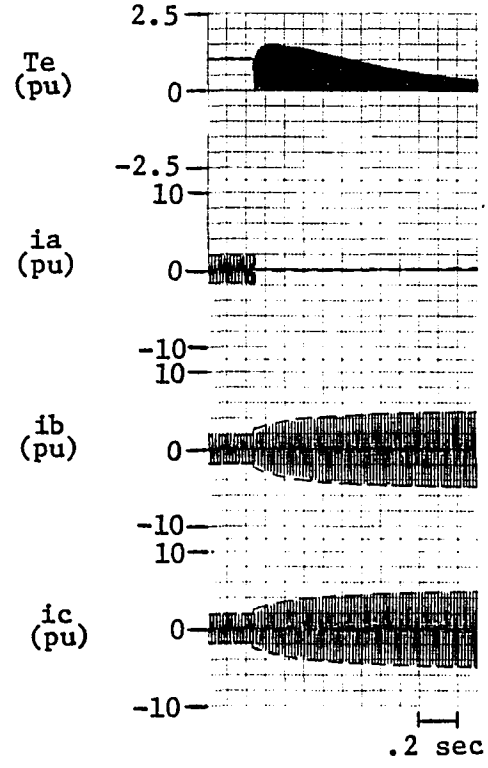

skin effect model

———— electric transient

- - - - - - impedance

Figure 9.6 Motor M1 stator current and developed torque following the sudden opening of A phase feed. T_m=1.0. Four rotor loop representation used.

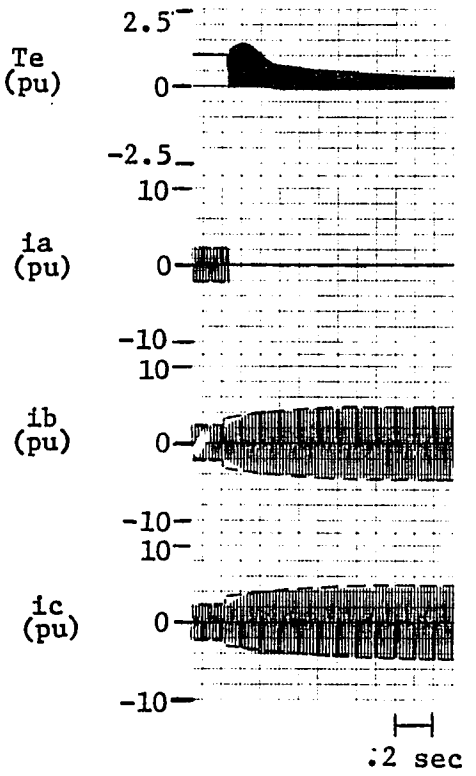

skin effect model

———— electrical transient

- - - - - - impedance

Figure 9.7 Motor M2 stator current and developed torque following the the sudden opening of A phase feed. T_m=1.0. Four rotor loop representation used.

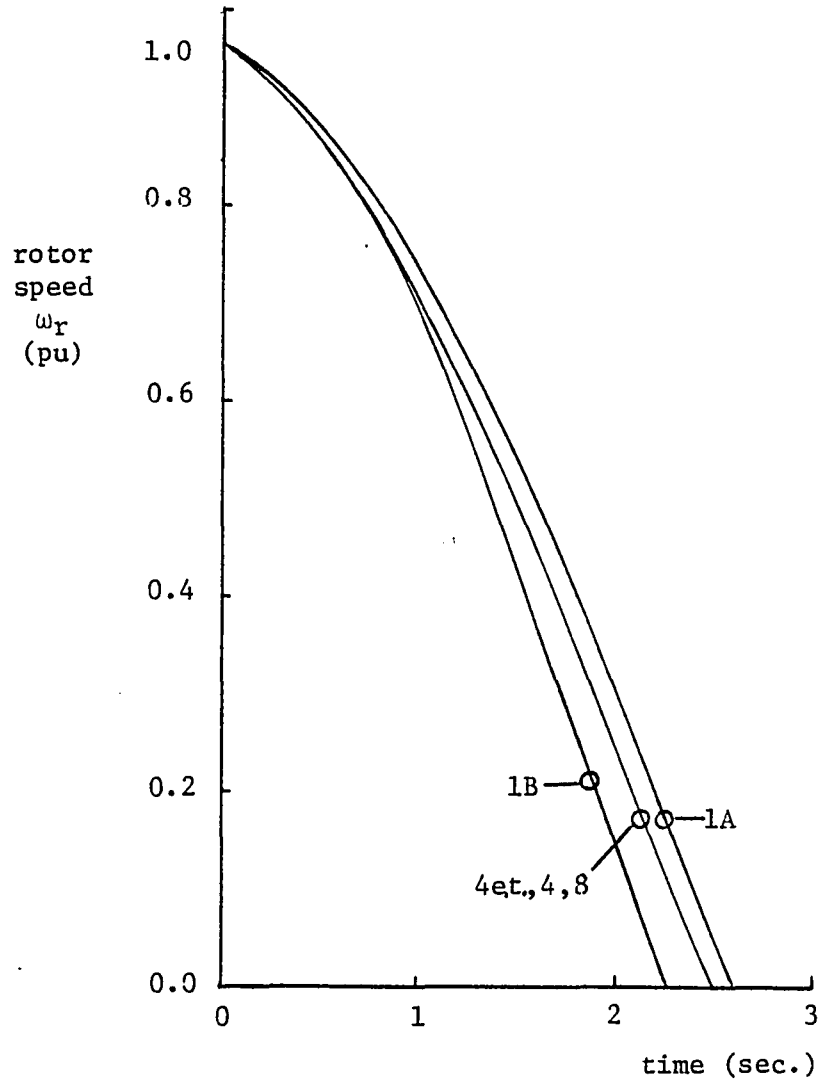

Figure 9.8 Motor M1 rotor speed following the sudden opening of A phase feed. T_m=1.0. Impedance model predictions except as noted

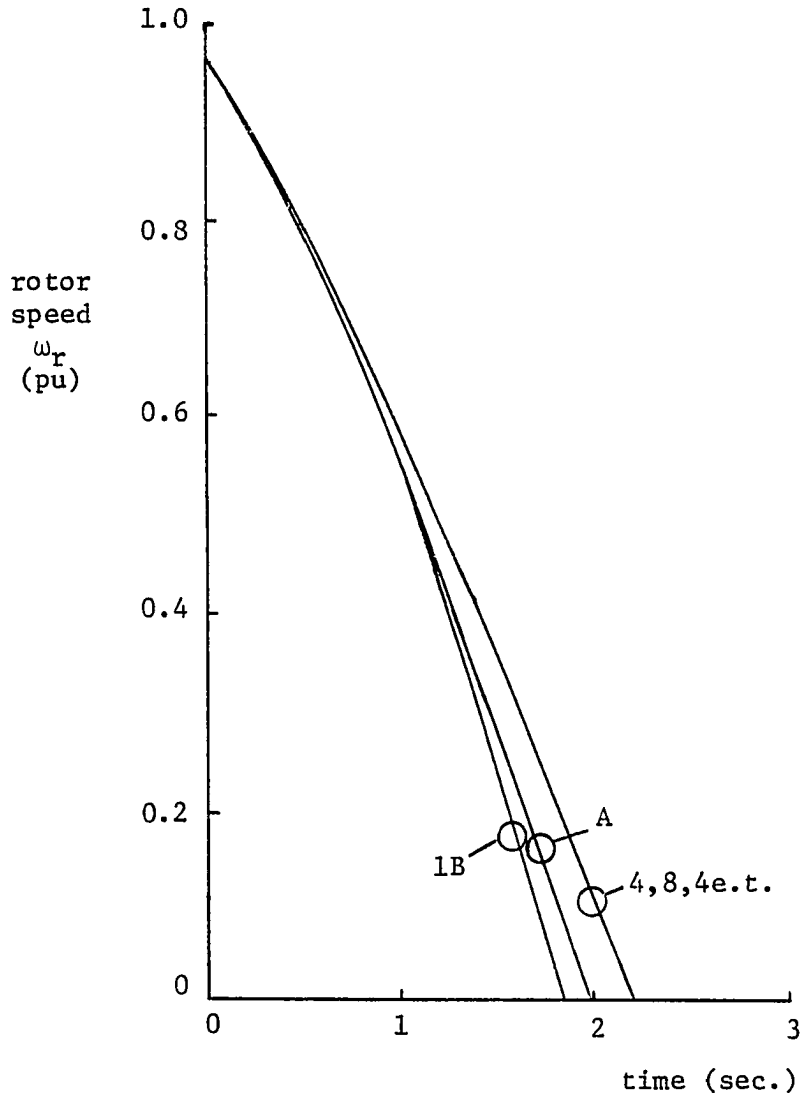

Figure 9.9 Motor M2 rotor speed following the sudden opening of A phase feed. T_m=1.0. Impedance model predictions except as noted

The Series Fault with Shunt Compensation

In many instances, when a single phase series fault occurs, a shunt compensation capacitor will be isolated from the power system with the motor terminal. The shunt compensation is assumed to consist of a balanced set of three phase capacitors with the neutral point ungrounded. The skin effect electrical transient model predictions with two levels of compensation are shown in Figure 9.10. In both cases, the load torque is taken to equal zero. Case A involves a shunt capacitance of x_c=4.05 p.u. per phase. In this case, the capacitance provides nearly all the motor excitation, and the transient is negligible. In case B, the capacitive reactance is x_c=2.0 p.u., which will fully compensate the motor at full load. In this case, a larger shift occurs in the motor operation when one phase is opened. In both cases, the impedance model prediction is very close to the electrical transient model predictions.

With smaller values of capacitive reactance, these effects are amplified. Figure 9.11 contains two cases of interest. The solutions of both the impedance and electrical transient models are shown in this figure, and correspondingly higher values of current and torque oscillations occur as the value of capacitive reactance declines. Figure 9.12 presents the solutions of the skin effect model for a still lower value of capacitive reactance. In this case, the current and torque levels have become exceedingly high. There also exist increasing differences between the impedance and electrical transient models as the capacitive reactance declines. It is apparent from these figures that in studies involving this range of shunt compensation, both current levels and

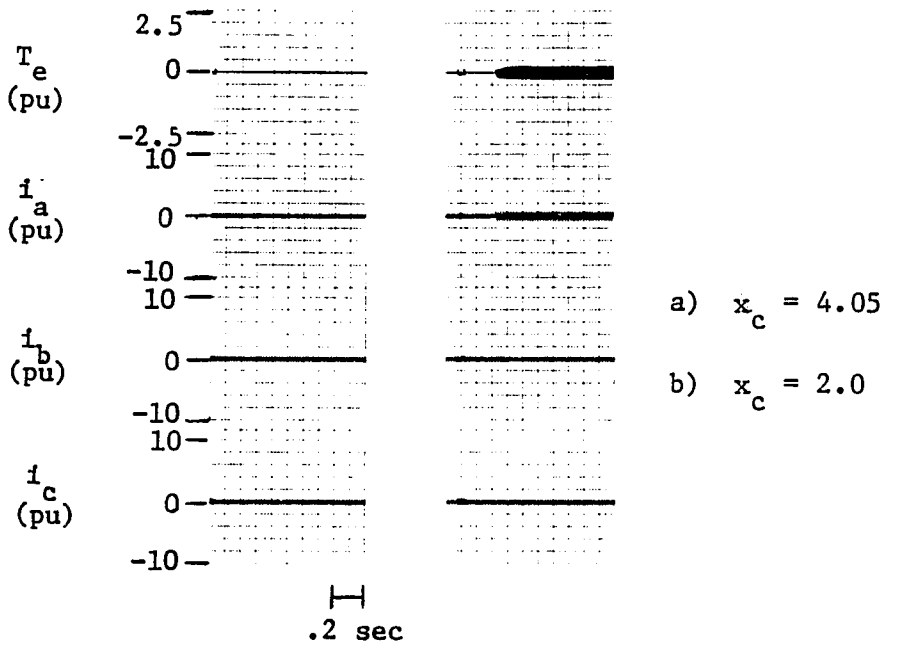

Figure 9.10 Motor M1 stator current and developed torque following sudden opening of A phase feed. T_m=0.0. Reactive compensation as noted. Electrical transient model predictions. Four rotor loops represented

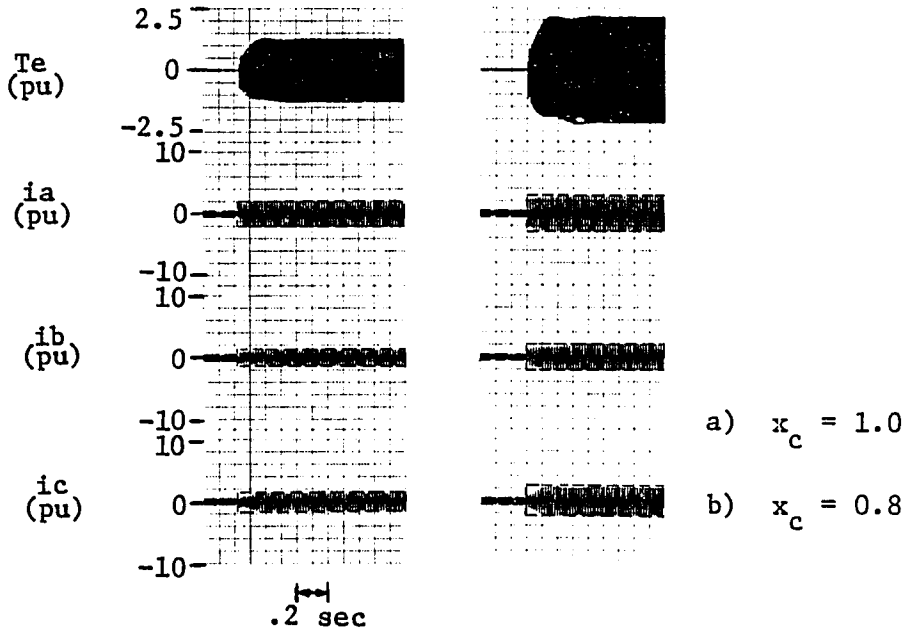

Figure 9.11 Motor M1 stator current and developed torque following sudden opening of A phase feed. T_m=0.0. Reactive compensation as noted. Four rotor loop representation used

torque oscillation levels must be fully investigated. The average torque prediction of the impedance model is not adequate in these cases.

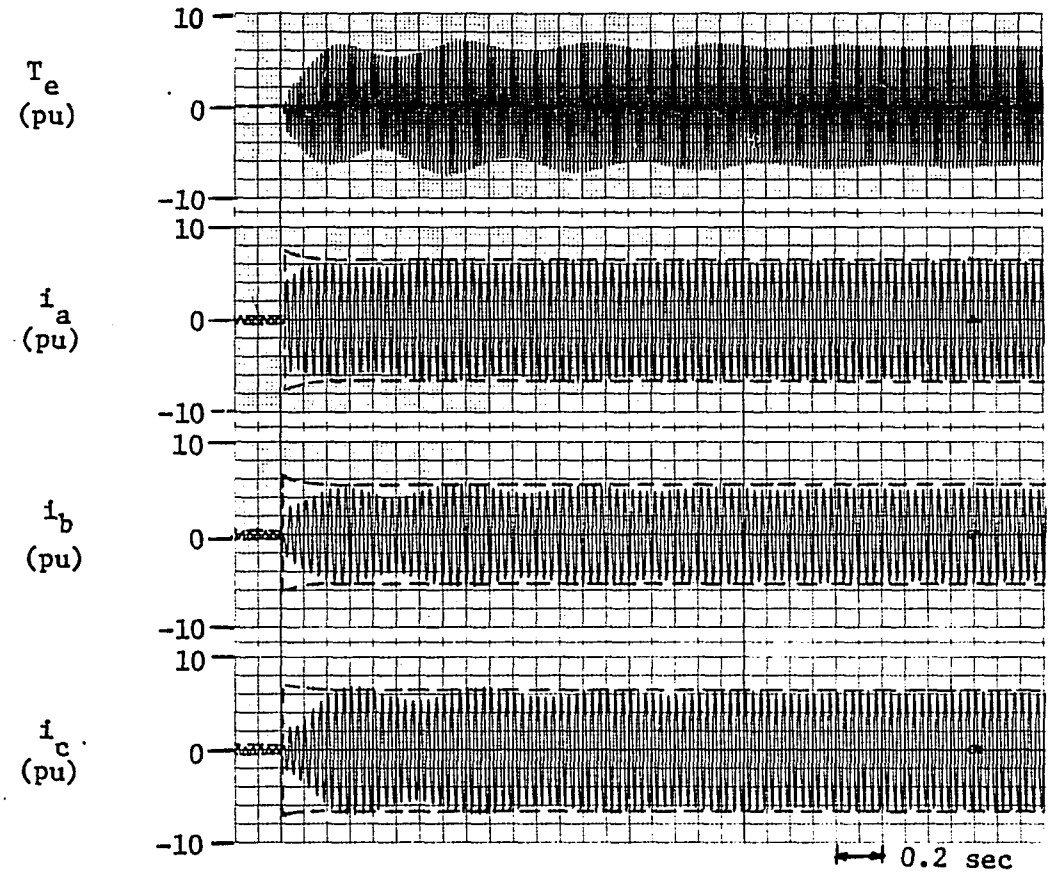

Figure 9.12 Motor M1 stator current and developed torque following sudden opening of A phase feed. T_m=0.0. Reactive compensation x_c=0.5. Four rotor loop representation used.

Comparisons of the skin effect model with models 1A and 1B are given in Table 9.5. Model 1A severely overestimates the current, while model

Table 9.5 Final operating conditions of motor M1 with shunt compensation of X_c=0.5 pu. Following the sudden opening of A phase. T_m=0.0

Model	Phase current (pu, rms) I_a	I_b	I_c	Sequence current (pu, rms) I_1	I_2	Rotor speed (pu) ω_r	Developed torque (pu) Pos. Seq.	Neg. Seq.	Terminal voltage (pu, rms) V_a
1A	7.789	6.638	7.257	.665	7.213	.997	.614	.614	2.295
1B	4.577	3.687	4.597	.582	4.286	.994	.657	.657	1.517
2	5.035	4.097	4.982	.591	4.687	.994	.676	.676	1.624
3	4.724	3.817	4.732	.589	4.406	.994	.672	.672	1.548
4	4.663	3.763	4.671	.584	4.347	.994	.662	.662	1.537
5	4.638	3.740	4.644	.582	4.322	.994	.657	.657	1.532
6	4.622	3.727	4.629	.581	4.307	.994	.654	.654	1.529
7	4.615	3.722	4.622	.580	4.302	.994	.653	.653	1.528
8	4.608	3.716	4.615	.579	4.295	.994	.652	.652	1.527

1B yields values which agree closely with the skin effect model. Because of the nature of model 1B, however, this agreement can only be expected for cases where the motional transient is limited to small values of slip.

Comments

These studies have shown the necessity of using the skin effect model of the induction motor in evaluating motor performance following the sudden opening of one phase of the motor feed. While motor models 1A and 1B in some cases are capable of predicting the motor transient, a wide variety of cases exist in which these models are unable to predict motor performance. The versatility of the skin effect model in predicting motor performance under all conditions overshadows the added complexity of these models.

The evaluation of reactive compensation at the motor terminals was shown to be important in evaluating the series fault transient. Damaging levels of current and torque can occur, depending on motor, power system, and capacitance parameters.

CHAPTER X. CONCLUSIONS

An investigation of induction machine operation has been conducted which is primarily concerned with the dynamic motor operation during unbalanced power system conditions. It was determined that the classical induction motor dynamic models do not provide accurate results during unbalanced conditions due to their failure to predict rotor bar skin effect. Several newly proposed models which present a more general description of the motor were analyzed. These models, however, present widely varying means of approaching the problem, and are further limited in that their use has been confined to cases involving balanced power system conditions.

For these reasons, an investigation into rotor bar skin effect was conducted. It was found that, for rectangular or nearly rectangular rotor bars, the basic equations of a conductor with certain simplifying assumptions may be used to obtain a reasonable dynamic rotor bar representation which accounts for rotor bar skin effect. The most important considerations involve the assumption of a constant current density across the rotor bar, the use of finite difference equations to approximate partial differential equations, and the treatment of the rotor bar as a filament in computing all mutual inductances.

The newly developed rotor bar representations were then incorporated into induction machine models. The first is a generalization of the two axis theory which is capable of predicting the rotor bar current distribution and the fast electrical transients which occur in the machine.

This model has been referred to as the skin effect electrical transient model.

The second model, the skin effect impedance model, predicts the rotor bar skin effect while neglecting the electrical transients in the machine. This unique motor representation, while being inherently less accurate than the skin effect electrical transient model, offers the advantages of computational efficiency and more readily interpretable results.

Three particularly important situations of dynamic motor operation with an unbalanced power system were studied using new skin effect electrical transient and skin effect impedance machine representations. In each instance, the necessity of considering the rotor bar skin effect was evaluated. Significant error was shown to occur when the skin effect is neglected and when the skin effect is improperly evaluated. It was also shown that the skin effect can be properly evaluated using a modest number of rotor bar segment representations.

In the first study, the starting of an induction motor fed through an open delta transformer bank was investigated using the two new skin effect models. The predictions of the impedance model agreed closely with the predictions of the electrical transient model for the motor run-up time, overall inrush current, and voltage dip. The major effect of using an open delta bank was shown to be the introduction of negative sequence currents. Cases studied involved both the starting of a motor-transformer combination of the same rating with no adjacent load, and the starting of a motor on a transformer which feeds several loads. The

open delta transformer bank does not appear to significantly affect motor run-up time, and, for most purposes, the oscillatory torque component can be neglected.

In the studies of single phase to ground faults, it was found that full evaluation of the electrical transients is important during the first few cycles following fault inception. The electrical transients during this period lead to large instantaneous values of motor current and developed torque. For faults of long duration, however, the skin effect electrical transient model and the skin effect impedance model yield similar results for the overall motor performance in most cases. One exception was seen to occur in the rotor speed predictions of the two models for a heavily loaded motor. Another exception occurs in studies for which evaluation of the oscillatory torque component is necessary. The necessity of evaluation of the skin effect was clearly shown in all cases.

It was observed that large currents exist in the unfaulted phases and high slip stable operating points are possible during faults of long duration. These are areas which may be of concern in the study of single phase to ground faults near induction motor terminals.

The single phase series fault is widely recognized to be a condition under which potentially harmful currents can flow which are high enough to be under the minimum sensitivity of fault sensing devices. The dynamic analysis of this study using the newly developed models shows generally smaller electrical transients following fault inception than in the case of single phase to ground faults. Both electrical transient and impedance models show good agreement in most cases, particularly in the prediction

of current levels. The presence of shunt compensation at the motor terminals was seen to be critical in the evaluation of the series fault. This capacitance, if present, must be modeled, and in extreme cases this capacitance can lead to conditions under which the impedance model becomes inaccurate. Severe levels of current and torque fluctuations can occur under these conditions.

REFERENCES

1. Adkins, B. and R. G. Harley. The General Theory of Alternating Current Machines. London: Chapman and Hall, 1975.

2. Alger, P. L. and J. H. Wray. "Double and Triple Squirrel Cages for Polyphase Induction Motors." Trans. Am. Inst. Electr. Engr. 72 part III (1953): 637-644.

3. Anderson, P. M. Analysis of Faulted Power Systems. Ames, Iowa: Iowa State University Press, 1973.

4. Anderson, P. M. and A. A. Fouad. Power System Control and Stability. Vol. 1. Ames, Iowa: Iowa State University Press, 1977.

5. Babb, D. S. and J. E. Williams. "Circuit Analysis Method for Determination of A-C Impedances of Machine Conductors." Trans. Am. Inst. Electr. Engr. 70 (1951): 661-666.

6. Berndt, M. M. and N. L. Schmitz. "Derating of Polyphase Induction Motors Operated with Unbalanced Line Voltages." IEEE Transactions PAS-82 (February 1963): 680-686.

7. Chang, S. S. L. "A Graphical Method for Determining the Impedance of Multiple-Cage Conductors." Trans. Am. Inst. Electr. Engr. 72 part III (1953): 621-624.

8. Clarke, Edith. Circuit Analysis of A-C Power Systems. Vol. 2. New York: John Wiley and Sons, Inc., 1950.

9. Clarke, Edith, H. A. Peterson, and P. H. Light. "Abnormal Voltage Conditions in Three-Phase Systems Produced by Single-Phase Switching." Trans. Am. Inst. Electr. Engr. 60 (1941): 329-339.

10. DeSarkar, A. K. and G. J. Berg. "Digital Simulation of Three-Phase Induction Motors." IEEE Transactions PAS-89 (1970): 1031-1036.

11. Douglas, J. F. H. "A Contribution to the Theory of the Deep-Bar Induction Motor." Trans. Am. Inst. Electr. Engr. 70 (1951): 863-866.

12. Douglas, J. F. H. "A Contribution to the Theory of the Double-Cage Induction Motor." Trans. Am. Inst. Electr. Engr. 72 part III (1953): 624-630.

13. Field, A. B. "Eddy Currents in Large Slot-Wound Conductors." Trans. Am. Inst. Electr. Engr. 24 (1905): 761-788.

14. Fitzgerald, A. E. and C. Kingsley. Electric Machinery. 2nd edition. New York: McGraw-Hill, Inc., 1961.

15. Fortescue, C. L. "Method of Symmetrical Coordinates Applied to the Solution of Polyphase Networks." Trans. Am. Inst. Electr. Engr. 37 (1918): 1027-1140.

16. Franklin, W. S. and R. B. Williamson. The Elements of Alternating Currents. 2nd edition. New York: The MacMillan Press, Ltd., 1901.

17. Gabbard, J. L. and J. E. Rowe. "Digital Computation of Induction Motor Transient Stability." Trans. Am. Inst. Electr. Engr. 76 (1957): 970-977.

18. Gafford, B. N., W. C. Duesterhoeff, and C. C. Mosher. "Heating of Induction Motors on Unbalanced Voltages." Trans. Am. Inst. Electr. Engr. 78 part III-A (1959): 282-286.

19. Goodman, J. "A Design Method for Double Squirrel-Cage Induction Motors." Trans. Am. Inst. Electr. Engr. 72 part III (1953): 645-650.

20. Greenwood, Allen. Electrical Transients in Power Systems. New York: John Wiley and Sons, Inc., 1971.

21. Griffith, M. S. "A Penetrating Gaze at One Open Phase: Analyzing the Polyphase Induction Motor Dilemma." IEEE Transactions Ind. Appl. IA-13 (1977): 504-516.

22. Harley, R. G., A. A. Mahmoud, and C. Calabrese. "Harmonic Distortion in 3-Phase Loads Supplied by Two Single-Phase Transformers." Paper A78 510-0. IEEE PES Summer Meeting, 1978.

23. Harley, R. G., A. A. Mahmoud, and T. H. Ortmeyer. "Computer Models for Induction Motor Drive Dynamics." Proceedings of IEEE Ind. Appl., Society Annual Meeting, October, 1977.

24. Humpage, W. D., K. E. Durrani, and V. F. Curvalho. "Synchronous - Asynchronous Machine Groups." Proceedings IEE 116 (1969): 2015-2027.

25. IEEE Committee. "Recommended Phasor Diagrams for Synchronous Machines." IEEE Transactions PAS-88 (1969: 1593-1610.

25. Jacobs, Paul. "Defining the Equivalent Circuit of the Double-Cage Motor." Trans. Am. Inst. Electr. Engr. 72 part III (1953): 651-657.

27. Jadrijevic, V. T. "Simulation of an Induction Machine and Switched Capacitor to Relieve Motor Starting Dip." M. S. Thesis, Iowa State University, Ames, Iowa, 1971.

28. Jordan, H. E. "Digital Computer Analysis of Induction Machines in Dynamic Systems." IEEE Transactions PAS-86 (1967): 722-727.

29. Jordan, H. E. "Synthesis of Double-Cage Induction Motor Design." Trans. Am. Inst. Electr. Engr. 78 part III (1959): 691-695.

30. Kalsi, S. S. "Switching Transients in Large Deep-Bar Squirrel Cage Induction Motors." IEEE Transactions PAS-92 (1973): 1266-1273.

31. Kalsi, S. S. and B. Adkins. "Transient Stability of Power Systems Containing both Synchronous and Induction Machines." Proceedings IEE 118 (1971): 1467-1474.

32. Kalsi, S. S., D. D. Stephan, and B. Adkins. "Calculation of System Fault Currents Due to Induction Motors." Proceedings IEE 118 (1971): 201-215.

33. Karapetoff, V. and B. C. Dennison. Experimental Electrical Engineering. Vol. 2, 4th edition. New York: John Wiley and Sons, Inc., 1941.

34. Klingshirn, E. A. and H. E. Jordan. "Simulation of Polyphase Induction Machines with Deep Rotor Bars." IEEE Transactions PAS-89 (1970): 1038-1043.

35. Krause, P. C. and C. H. Thomas. "Simulation of Symmetrical Induction Machinery." IEEE Transactions PAS-84 (November 1965): 1038-1053.

36. Lee, C. H. "A Design Method for Double Squirrel-Cage Induction Motors." Trans. Am. Inst. Electr. Engr. 72 part III (1953): 630-636.

37. Lewis, W. A. "A Basic Analysis of Synchronous Machines, Part 1." Trans. Am. Inst. Electr. Engr. PAS-77 part 3 (1958): 436-455.

38. Liwschitz-Garik, M. M. "Computation of Skin Effect in Bars of Squirrel-Cage Rotors." Trans. Am. Inst. Electr. Engr. 74 (1955): 768-771.

39. Lyon, W. V. Transient Analysis of Alternating Current Machinery. New York: John Wiley and Sons, Inc., 1954.

40. Maginniss, F. J. and N. R. Schultz. "Transient Performance of Induction Motors." Trans. Am. Inst. Electr. Engr. 63 (1944): 641-646.

41. Mamak, R. S. and E. R. Laithwaite. "Numerical Evaluation of Inductance and A.C. Resistance." Proceedings IEE 108 part C (1961): 252-258.

42. Neuenswander, J. R. Modern Power Systems. Scranton, Pennsylvania: International Textbook Co., 1971.

43. Ortmeyer, T. H. "A Comparison of Induction Motor Models for Starting Performance." M.S. Thesis, Ames, Iowa: Iowa State University, 1977.

44. Ortmeyer, T. H. and A. A. Mahmoud. "Mathematical Analysis of Induction Motor Starting Performance." Affiliate Research Program in Electric Power Annual Report. ISU-ERI-Ames-78287, Ames, Iowa: Iowa State University, 1978.

45. Ortmeyer, T. H. and A. A. Mahmoud. "Skin Effect Model of the Induction Motor." Affiliate Research Program in Electric Power Annual Report. ISU-ERI-Ames-79184, Ames, Iowa: Iowa State University, 1979.

46. Park, R. H. "Two Reaction Theory of Synchronous Machines, Part 1." Trans. Am. Inst. Electr. Engr. 48 (1929): 716-730.

47. Park, R. H. "Two Reaction Theory of Synchronous Machines, Part 2." Trans. Am. Inst. Electr. Engr. 52 (1933): 352-355.

48. Ramo, S., J. R. Whinnery, and T. Van Duzer. Fields and Waves in Communication Electronics. New York: John Wiley and Sons, Inc., 1965.

49. Robb, D. D. EE 540 Class Notes. Iowa State University, 1976.

50. Roberts, J. "Analogue Treatment of Eddy-Current Problems Involving Two-Dimensional Fields." Proceedings IEE 103 part C (1960): 11-18.

51. Rudenberg, Reinhold. Transient Performance of Electric Power Systems. Cambridge, Massachusetts: Massachusetts Institute of Technology Press, 1969.

52. Say, M. G. Alternating Current Machines. 4th edition. London: Pitman Publishing, 1976.

53. Seematter, S. C. and E. F. Richards. "Computer Analysis of 3-Phase Induction Motor Operation on Rural Open-Delta Distribution Systems." IEEE Transactions IA-12 (1976): 479-486.

54. Smith, R. and S. Sriharan. "Transient Performance of the Induction Motor." Proceedings IEE 113 (1966): 1173-1181.

55. Smith, R. F. and J. O. Nichols. "Analysis of a Deep Bar Induction Motor and Compressor Load During Start-Up." IEEE Transactions PAS-97 (1978): 1696-1705.

56. Stevenson, W. D. Elements of Power System Analysis. 3rd edition. New York: McGraw-Hill, Inc. 1975.

57. Swann, S. A. and J. W. Salmon. "Effective Resistance and Reactance of a Rectangular Conductor Placed in a Semi-Closed Slot." Proceedings IEE 110 (1963): 1656-1662.

58. Wagner, W. P. "Short-Circuit Contribution of Large Induction Motors." Proceedings IEE 116 (1969): 985-989.

59. Weinberger, H. F. A First Course in Partial Differential Equations. New York: John Wiley and Sons, Inc., 1965.

60. Williams, J. E. "Operation of 3-Phase Induction Motors on Unbalanced Voltages." Trans. Am. Inst. Electr. Engr. 73 part III-A (1954): 125-133.

ACKNOWLEDGMENTS

I wish to express my sincere appreciation to my major professor, Dr. Aly A. Mahmoud, for his guidance through all phases of this study. I also am indebted to all the many faculty members I have encountered at Iowa State University, particularly those on my program of study committee.

I would like to thank the Power Affiliate Research Program and the Engineering Research Institute for their support of this work.

I am grateful to my wife, Ann, whose patience and understanding has been essential.

I would also like to thank my typist, Gretchen Triplett.

APPENDIX A: PER UNIT SYSTEM

The per unit system used in this study is the same as that used in references 23 and 49. It is also similar to the per unit system used for synchronous machines in reference 4.

Base Time and Speed

The base speed is chosen as

$$\omega_b = \text{rated synchronous speed} \tag{A.1}$$

in electrical radians per second. The b subscript denotes a base quantity. In most applications in this country,

$$\omega_b = 377 \text{ radians/sec.} \tag{A.2}$$

It follows that

$$t_b = 1/\omega_b \text{ seconds} \tag{A.3}$$

If t_u is per unit time, then

$$\frac{d(\ )}{dt_u} = \frac{d(\ )}{d(t/t_b)} = t_b \frac{d(\ )}{dt} \tag{A.4}$$

Stator Bases

The stator voltage and current bases are chosen arbitrarily.

$$V_{sb} = \text{rated RMS line-to-neutral voltage} \tag{A.5}$$

$$I_{sb} = \text{rated RMS line current} \tag{A.6}$$

The remaining base stator quantities are functions of ω_b, V_{sb}, and I_{sb}.

base volt=amperes	$S_b = V_{sb} I_{sb}$	volt-amps
base resistance	$R_{sb} = V_{sb}/I_{sb}$	ohms

base inductance	$L_{sb} = R_{sb}/\omega_b$	henries	
base flux linkage	$\lambda_{sb} = L_{sb}I_{sb}$	weber-turns	(A.7)

Rotor Bases

The rotor bases are chosen so that the same volt-amp and time base are used in every winding, and the base mutual inductance is the geometric mean of the related base self-inductances. These choices are necessary for the dimensional and per unit electrical equations to be the same (37).

Of the remaining base quantities, there is one additional arbitrary choice for the rotor. This quantity is chosen in such a way that base rotor current will produce the same air-gap flux as base stator current. The d axis flux can be separated into three components as shown in Figure A.1. There are two components of flux linking the d winding of the stator --

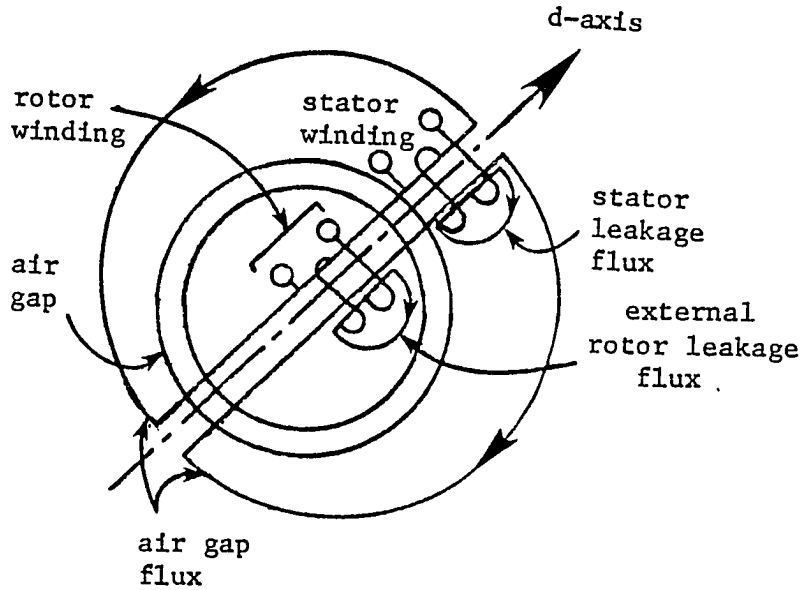

Figure A.1 d-axis flux paths and fictitious d-axis windings

the air-gap flux and the stator leakage flux. Therefore, the flux linkage λ_{ds} can be rewritten from Eq. 5.27 as

$$\lambda_{dls} + \lambda_{mds} = (L_s + L_{sm})i_{ds} + \frac{3}{2} L_{sr} i_{dr1} \tag{A.8}$$

where λ_{dls} is the stator flux linkage due to leakage flux and λ_{mds} is stator flux linkage due to air-gap flux. Because it is assumed that the machine contains linear magnetic circuits, and λ_{dls} is a function only of i_{ds},

$$\lambda_{dls} = l_s i_{ds} \tag{A.9}$$

and l_s is the stator leakage inductance. If equation A.9 is subtracted from A.8, Eq. A.10 results.

$$\lambda_{mds} = (L_s + L_{sm} - l_s)i_{ds} + \frac{3}{2} L_{sr} i_{dr1} \tag{A.10}$$

When I_{sb} flows in the stator d axis winding with the rotor open circuited,

$$\lambda'_{mds} = (L_s + L_{sm} - l_s)I_{sb} \tag{A.11}$$

For rotor current alone to produce the same flux,

$$\lambda'_{mds} = \frac{3}{2} L_{sr} i'_{dr} \tag{A.12}$$

Since this is the desired rotor base current, it follows that

$$I_{br} = i'_{dr} = \frac{L_s + L_{sm} - l_s}{\frac{3}{2} L_{sr}} I_{sb} \tag{A.13}$$

Because of the symmetrical nature of the induction machine, the same analysis of the q axis would produce the same results.

The remainder of the rotor bases are functions of ω_b, S_b, and I_{br}.

rotor base voltage	$V_{br} = S_b/I_{br}$	volts
rotor base resistance	$R_{br} = V_{br}/I_{br}$	ohms

rotor base inductance	$L_{br} = R_{br}/\omega_b$	henries	
rotor base flux linkage	$\lambda_{br} = L_{br} I_{br}$	weber-turns	(A.14)

The stator to rotor base inductance is then

$$M_{bsr} = \sqrt{L_{bs} L_{br}} \tag{A.15}$$

Magnetizing Inductance

By comparing equation 5.27 with Figure A.1, it can be seen that an equation can be written for the rotor which corresponds to Eq. A.10 for the stator. The rotor flux linkage due to air-gap flux is

$$\lambda_{mdr} = \frac{3}{2} L_{sr} i_{ds} + (L_r + L_{rm} - l_r) i_{dr1} \tag{A.16}$$

When $i_{ds} = I_{sb}$ and $i_{dr1} = 0$, $\lambda_{mds} = \lambda'_{mds}$ from Eq. A.11. For this condition, Eq. A.16 becomes

$$\lambda'_{mdr} = \frac{3}{2} L_{sr} I_{sb} \tag{A.17}$$

However, when $i_{dr1} = I_{br}$, the air-gap flux is the same, so the rotor flux linkage due to the air-gap flux again is

$$\lambda'_{mdr} = (L_r + L_{rm} - l_r) I_{br} \tag{A.18}$$

These equations are valid in either dimensional units or per unit, because of the choice of base quantities. In per unit, however, Eq. A.11 becomes

$$\lambda'_{mds} = (L_s + L_{sm} - l_s)(1.0) \tag{A.19}$$

since $i_{ds} = I_{sb} = 1.0$ in per unit. Similarly, Eq. A.12 becomes

$$\lambda'_{mds} = \frac{3}{2} L_{sr}(1.0) \tag{A.20}$$

when $i_{dr1} = 1.0$ in per unit. Therefore,

$$L_s + L_{sm} - l_s = \frac{3}{2} L_{sr} \tag{A.21}$$

in per unit values. Similar treatment of Equations A.17 and A.18 show that

$$\frac{3}{2} L_{sr} = L_r + L_{rm} - 1_r \tag{A.22}$$

A new term M, known as the magnetizing inductance, can be defined as

$$M \triangleq \frac{3}{2} L_{sr} = L_r + L_{rm} - 1_r = L_s + L_{sm} - 1_s \tag{A.23}$$

Further analysis of A.10 and A.16 shows that, in per unit values,

$$\lambda_{mds} = \lambda_{mdr} \triangleq \lambda_{md} \tag{A.24}$$

Eq. 5.27 therefore becomes, in per unit values only,

$$\begin{bmatrix} \lambda_{ds} \\ \lambda_{drl} \\ \hline \lambda_{qs} \\ \lambda_{qrl} \end{bmatrix} = \left[\begin{array}{cc:cc} M + 1_s & M & 0 & 0 \\ M & M + 1_r & 0 & 0 \\ \hdashline 0 & 0 & M + 1_s & M \\ 0 & 0 & M & M + 1_r \end{array}\right] \begin{bmatrix} i_{ds} \\ i_{drl} \\ \hline i_{qs} \\ i_{qrl} \end{bmatrix} \tag{A.25}$$

Mechanical Bases and Per Unit Equations

Since power is the product of torque and speed, base torque can be taken as rated three-phase power divided by rated mechanical speed. Since S_b (Eq. A.7) is based on single phase rated power, and ω_b (Eq. A.1) is rated speed in electrical radians per second, the expression for base torque in terms of S_b and ω_b is:

$$T_b = \frac{P}{2} \frac{3S_b}{\omega_b} \tag{A.26}$$

P is the number of poles of the machine.

The electrically developed torque in dimensional units is:

$$T_e = \frac{P}{2} (\lambda_{qs} i_{ds} - \lambda_{ds} i_{qs}) \tag{A.27}$$

By dividing Eq. A.27 by Eq. A.26, the per unit electrical torque is found to be:

$$T_e = \frac{1}{3}(\lambda_{qs} i_{ds} - \lambda_{ds} i_{qs}) \tag{A.28}$$

If T_m is the mechanical load torque, the dimensional equations for rotor acceleration is

$$\frac{2}{P} J \frac{d\omega_r}{dt} = T_e - T_m \tag{A.29}$$

where J is the moment of inertia and ω_r is the rotor speed in electrical radians/sec. Since the kinetic energy of a rotating body is

$$W = \frac{1}{2} J\omega_m^2 \tag{A.30}$$

the stored energy at rated speed is

$$W_R = \frac{1}{2} J(\frac{2}{P} \omega_b)^2 \tag{A.31}$$

because the mechanical speed is $\omega_m = \frac{2}{P} \omega_b$,

Eq. A.29 with W_R substituted for J is

$$\frac{2W_R}{\frac{2}{P}^2 \omega_b} \frac{d\omega_r}{dt} = T_e - T_m \tag{A.32}$$

When Eq. A.32 is divided by Eq. A.26, the relationship between rotor acceleration and per unit torque is found to be

$$\frac{2W_R}{\omega_b 3S_b} \frac{d\omega_r}{dt} = T_e - T_m \tag{A.33}$$

The inertia constant H has been defined to be the ratio of inertially stored energy to rated three phase volt amperes, or

$$H = \frac{W_R}{3S_b} \tag{A.34}$$

and Eq. A.33 is rewritten to be

$$\frac{2H}{\omega_b} \frac{d\omega_r}{dt} = T_e - T_m \tag{A.35}$$

where H and t are in seconds, ω_r and ω_b are in radians/sec., and torque is in per unit.

APPENDIX B: TRANSFORMATION TO THE o-d-q AXIS QUANTITIES

Simplification of the a, b, and c phase equations for flux linkage and voltage can be achieved by transformation of variables from abc quantities to odq axis quantities. This is accomplished by using an orthogonal version (37) of the original Park's transformation (46) (47). This transformation transforms all variables onto the direct (d) and quadrature (q) axes, shown in Figure 5.4, and the o axis, which is stationary.

Because of the symmetry of the induction motor, no reference frame is suggested by the motor itself, as is the case with the field winding of the synchronous machine rotor. The most commonly used reference frames are known as the synchronously rotating reference frame, the rotor reference frame, the stationary or stator reference frame, and the arbitrary reference frame. In the synchronously rotating reference frame, the d and q axes rotate with the same speed as synchronous speed. The d and q axes are fixed to the rotor in the rotor reference frame. In the stationary reference frame, the d and q axes are stationary, and thus fixed to constant positions on the stator. The arbitrary reference frame is an intermediate step which is useful because of its generality (35). In Figure 5.4, the angles Θ and β are defined as the angles between the d axis and the A phase magnetic axis of the stator and rotor, respectively. The speed ω is the speed of the reference frame. Θ, β, and ω are the variables of the arbitrary reference frame. The machine equations can be transformed into the arbitrary reference frame, then by choosing specific values of Θ, β, and ω the machine equations can be represented in the

stationary, rotor, or synchronous reference frames as would be desired.

Parks's Transformation

Transformation from the abc phase quantities to the arbitrary reference frame odq axis quantities is accomplished by Equations B.1.

$$\text{For stator quantities } [F_{odqs}] = [P_{\theta}][F_{abcs}]$$
$$\text{For rotor quantities } [F_{odqr}] = [P_{\beta}][F_{abcr}] \tag{B.1}$$

where

$$[P_{\theta}] = \sqrt{\frac{2}{3}} \begin{bmatrix} \sqrt{\frac{1}{2}} & \sqrt{\frac{1}{2}} & \sqrt{\frac{1}{2}} \\ \cos\theta & \cos(\theta - \frac{2\pi}{3}) & \cos(\theta + \frac{2\pi}{3}) \\ \sin\theta & \sin(\theta - \frac{2\pi}{3}) & \sin(\theta + \frac{2\pi}{3}) \end{bmatrix}$$

$$[P_{\beta}] = \sqrt{\frac{2}{3}} \begin{bmatrix} \sqrt{\frac{1}{2}} & \sqrt{\frac{1}{2}} & \sqrt{\frac{1}{2}} \\ \cos\beta & \cos(\beta - \frac{2\pi}{3}) & \cos(\beta + \frac{2\pi}{3}) \\ \sin\beta & \sin(\beta - \frac{2\pi}{3}) & \sin(\beta + \frac{2\pi}{3}) \end{bmatrix} \tag{B.2}$$

$[F_{abc}]$ is the set of three phase quantities: current, voltage, or flux linkage; and $[F_{odq}]$ is the corresponding set of axis quantities.

Since the transformation is orthogonal, it follows that

$$[P_{\theta}]^{-1} = [P_{\theta}]^{T}, \quad [P_{\beta}]^{-1} = [P_{\beta}]^{T} \tag{B.3}$$

Transformation of Equations

Eq. B.4 describes a general system of three phase voltages.

$$\begin{bmatrix} v_a \\ v_b \\ v_c \end{bmatrix} = \begin{bmatrix} R & 0 & 0 \\ 0 & R & 0 \\ 0 & 0 & R \end{bmatrix} \begin{bmatrix} i_a \\ i_b \\ i_c \end{bmatrix} + \begin{bmatrix} p\lambda_a \\ p\lambda_b \\ p\lambda_c \end{bmatrix} \tag{B.4}$$

In matrix notation, Eq. B.4 becomes

$$[v_{abc}] = [R_{abc}][i_{abc}] + [p\lambda_{abc}] \tag{B.5}$$

In order to obtain the odq axis voltages, Eq. B.5 is multiplied by Eq. B.2.

$$[P_\theta][v_{abc}] = [P_\theta][R_{abc}][P_\theta]^{-1}[P_\theta][i_{abc}] + [P_\theta][p\lambda_{abc}] \tag{B.6}$$

Because of the identities of Eq. B.1, Eq. B.6 can be rewritten as

$$[v_{odq}] = [P_\theta][R_{abc}][P_\theta]^{-1}[i_{odq}] + [P_\theta][p\lambda_{abc}] \tag{B.7}$$

If the odq axis resistances are defined as

$$[R_{odq}] = [P_\theta][R_{abc}][P_\theta]^{-1} \tag{B.8}$$

Eq. B.7 becomes

$$[v_{odq}] = [R_{odq}][i_{odq}] + [P_\theta][p\lambda_{abc}] \tag{B.9}$$

Eq. B.8 is known as the similarity transformation.

The derivative of Eq. B.1 is

$$[pf_{odq}] = [pP_\theta][f_{abc}] + [P_\theta][pf_{abc}] \tag{B.10}$$

or

$$[P_\theta][pf_{abc}] = [pf_{odq}] - [pP_\theta][f_{abc}] \tag{B.11}$$

Since $[f_{abc}] = [P_\theta]^{-1}[f_{odq}]$,

$$[P_\theta][pf_{abc}] = [pf_{odq}] - [pP_\theta][P_\theta]^{-1}[f_{odq}] \tag{B.12}$$

Using Eq. B.2,

$$[pP_\theta][P_\theta]^{-1} = \begin{bmatrix} 0 & 0 & 0 \\ 0 & 0 & -p\theta \\ 0 & p\theta & 0 \end{bmatrix} \tag{B.13}$$

Similarly, for rotor quantities,

$$[pP_\beta][P_\beta]^{-1} = \begin{bmatrix} 0 & 0 & 0 \\ 0 & 0 & -p\beta \\ 0 & p\beta & 0 \end{bmatrix} \tag{B.14}$$

By substituting the results of Equations B.12 and B.13 into Eq. B.9, the odq axis voltages can be written in terms of odq axis variables only.

$$[v_{odq}] = [R_{odq}][i_{odq}] + [p\lambda_{odq}] + \begin{bmatrix} 0 \\ -\lambda_q p\theta \\ \lambda_d p\theta \end{bmatrix} \tag{B.15}$$

Similarity Transformations

The 3 by 3 matrix which relates the three phase currents to the three phase voltages can contain resistances, inductances, or capacitances. A wide variety of forms of these matrices is needed to represent different components of the power system. These matrices can be transformed into odq quantities by the similarity transformation given by Eq. B.8. The similarity transformations which were used in this study are given below. Since the results are identical whether the stator or rotor transformation is used, these results are given in terms of the general Park's transformation [P].

When each phase has the same resistance,

$$[R_{odq}] = [P] \begin{bmatrix} R & 0 & 0 \\ 0 & R & 0 \\ 0 & 0 & R \end{bmatrix} [P]^{-1} = \begin{bmatrix} R & 0 & 0 \\ 0 & R & 0 \\ 0 & 0 & R \end{bmatrix} \quad \text{(B.16)}$$

The same results are obtained for balanced inductances and capacitances.

Many transmission or distribution lines can be assumed to have equal self inductances and equal mutual inductances (56), or

$$[L_{abc}] = \begin{bmatrix} L_1 & L_2 & L_2 \\ L_2 & L_1 & L_2 \\ L_2 & L_2 & L_1 \end{bmatrix} \quad \text{(B.17)}$$

The odq axis inductances are then

$$[L_{odq}] = [P][L_{abc}][P]^{-1} = \begin{bmatrix} L_1+2L_2 & 0 & 0 \\ 0 & L_1-L_2 & 0 \\ 0 & 0 & L_1-L_2 \end{bmatrix} \quad \text{(B.18)}$$

APPENDIX C: ANALOG COMPUTER SIMULATION OF THE SKIN EFFECT ELECTRICAL TRANSIENT MODEL

The equations of the skin effect electrical transient model are presented in Chapter 5. These equations are presented for a general N-loop rotor bar approximation in the arbitrary reference frame. In order to solve these equations, the number of rotor loops and the specific reference frame must be specified. The analog computer patching diagrams presented below consider four rotor loops in the stationary reference frame.

The d axis flux linkages are, from Eq. 5.39,

$$\begin{aligned}
\lambda_{ds} &= \ell_s i_{ds} + M(i_{ds} + i_{dr1}) \\
\lambda_{dr1} &= (L_0 + L_1)\, i_{dri} + M(i_{ds} + i_{dr1}) \\
\lambda_{dr2} &= L_2 i_{dr2} \\
\lambda_{dr3} &= L_3 i_{dr3} \\
\lambda_{dr4} &= L_4 i_{dr4}
\end{aligned} \tag{C.1}$$

Define a d axis mutual flux linkage to be

$$\lambda_{md} = M(i_{ds} + i_{dr1}) \tag{C.2}$$

Then the d axis currents are

$$\begin{aligned}
i_{ds} &= \frac{\lambda_{ds} - \lambda_{md}}{\ell_s} \\
i_{dr1} &= \frac{\lambda_{dr1} - \lambda_{md}}{L_0 + L_1}
\end{aligned} \tag{C.3}$$

If Eq. C.3 is substituted into Eq. C.2, the d axis mutual flux linkage is found to be

$$\lambda_{md}\left[\frac{1}{M}+\frac{1}{\ell_s}+\frac{1}{L_0+L_1}\right]=\frac{\lambda_{ds}}{\ell_s}+\frac{\lambda_{dr1}}{L_0+L_1} \tag{C.4}$$

Define

$$\frac{1}{L_m}=\frac{1}{M}+\frac{1}{\ell_s}+\frac{1}{L_0+L_1} \tag{C.5}$$

Then

$$\lambda_{md}=L_m\left(\frac{\lambda_{ds}}{\ell}+\frac{\lambda_{dr1}}{L_0+L_1}\right) \tag{C.6}$$

Similarly, for the q axis,

$$\lambda_{mq}=L_m\left(\frac{\lambda_{qs}}{\ell_s}+\frac{\lambda_{qr1}}{L_0+L_1}\right) \tag{C.7}$$

$$i_{qs}=\frac{\lambda_{qs}-\lambda_{mq}}{L_0+L_1}$$

The d axis voltages are, from Equations 5.38,

$$\begin{aligned}
v_{ds} &= r_s i_{ds} + p\lambda_{ds} + \lambda_{qs}p\theta \\
0 &= R_1(i_{dr1}-i_{dr2}) + p\lambda_{dr1} + \lambda_{qr1}p\beta \\
0 &= R_1(i_{dr2}-i_{dr1}) + R_2(i_{dr2}-i_{dr3}) + p\lambda_{dr2} + \lambda_{qr2}p\beta \\
0 &= R_2(i_{dr3}-i_{dr2}) + R_3(i_{dr3}-i_{dr4}) + p\lambda_{dr3} + \lambda_{qr3}p\beta \\
0 &= R_3(i_{dr4}-i_{dr3}) + R_4 i_{dr4} + p\lambda_{dr4} + \lambda_{qr4}p\beta
\end{aligned} \tag{C.8}$$

In the stationary reference frame,

$$\begin{aligned}
p\theta &= 0 \\
p\beta &= -p\theta_r = -\omega_r
\end{aligned} \tag{C.9}$$

After substituting Equations C.1, C.3, and C.9 into Eq. C.8, the expressions may be integrated to obtain

$$\lambda_{ds} = \int\left[v_{ds} - \frac{r_s}{\ell_s}(\lambda_{ds}-\lambda_{md})\right] dt$$

$$\lambda_{dr1} = -\int\left[\frac{R_1}{L_0+L_1}(\lambda_{dr1}\lambda_{md}) - \frac{R_1}{L_2}\lambda_{dr2} - \omega_r\lambda_{qr1}\right] dt$$

$$\lambda_{dr2} = -\int\left[\left(\frac{R_1}{L_2}+\frac{R_2}{L_2}\right)\lambda_{dr2} - \frac{R_1}{L_0+L_1}(\lambda_{dr1}-\lambda_{md}) - \frac{R_2}{L_3}\lambda_{dr3} - \omega_r\lambda_{qr2}\right] dt$$

$$\lambda_{dr3} = -\int\left[\frac{R_2+R_3}{L_3}\lambda_{dr3} - \frac{R_2}{L_2}\lambda_{dr2} - \frac{R_3}{L_4}\lambda_{dr4} - \omega_r\lambda_{qr3}\right] dt$$

$$\lambda_{dr4} = -\int\left[\frac{R_3+R_4}{L_4}\lambda_{dr4} - \frac{R_3}{L_3}\lambda_{dr3} - \omega_r\lambda_{qr4}\right] dt \qquad (C.10)$$

These equations are valid in per unit quantities. It is more desirable, however, to express the electrical parameters in per unit and the time and speed in dimensional units. The relationships A.2-A.4, and the d axis flux linkages become

$$\lambda_{ds} = \omega_b\int\left[v_{ds} + \frac{r_s}{\ell_s}\lambda_{md} - \frac{r_s}{\ell_s}\lambda_{ds}\right] dt$$

$$\lambda_{dr1} = \omega_b\int\left[-\frac{R_1}{L_0+L_1}(\lambda_{dr1}-\lambda_{md}) + \frac{R_1}{L_2}\lambda_{dr2} + \omega_r\lambda_{qr1}\right] dt \qquad (C.11)$$

with similar changes for λ_{dr2} through λ_{dr4}. The q axis equations are treated similarly.

The torque and rotor speed of the machine are given in Equations 5.41 and 5.42.

The Analog Simulation

The particulars of the analog solutions used in this study are presented below. The analog patching diagrams for the motor are shown in Figure C.1. Table C.1 lists the device numbers, their function, and their specific use. The scaling factors used for this study are in Table C.2. The potentiometers used for the study are given in Table C.3, along with their coefficients. The particular values given are for the motor M1 with typical values of system impedance.

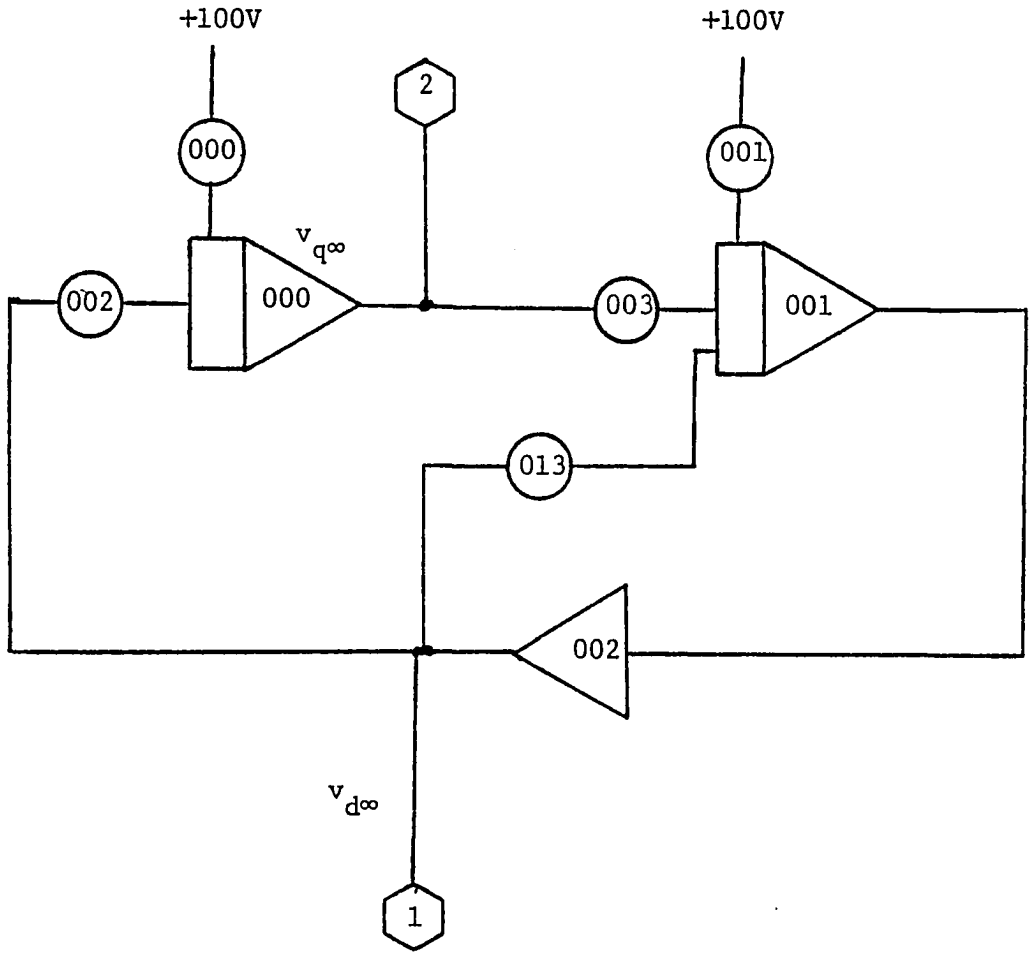

Figure C.1 Analog computer patching diagram

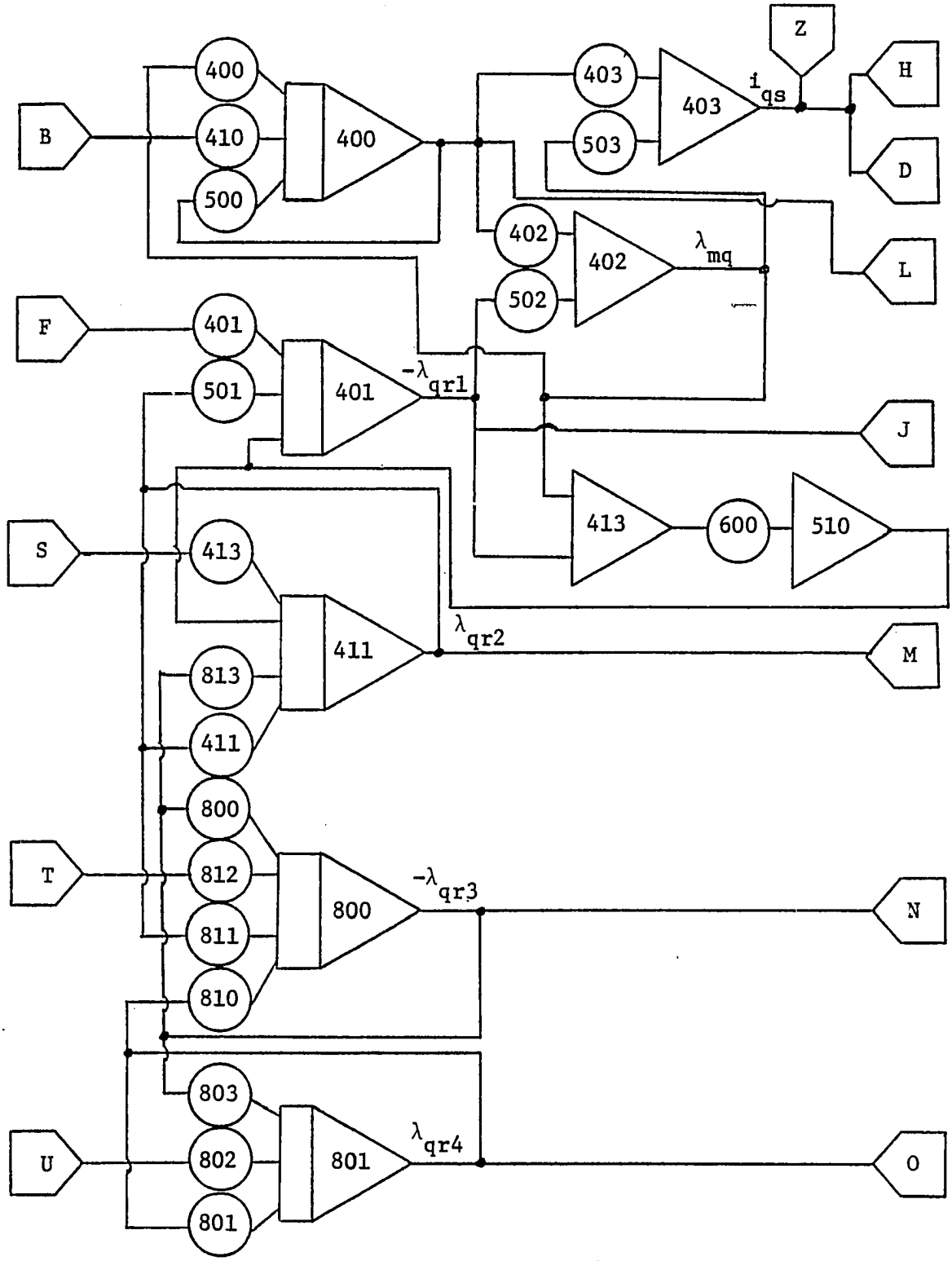

Figure C.1 Continued

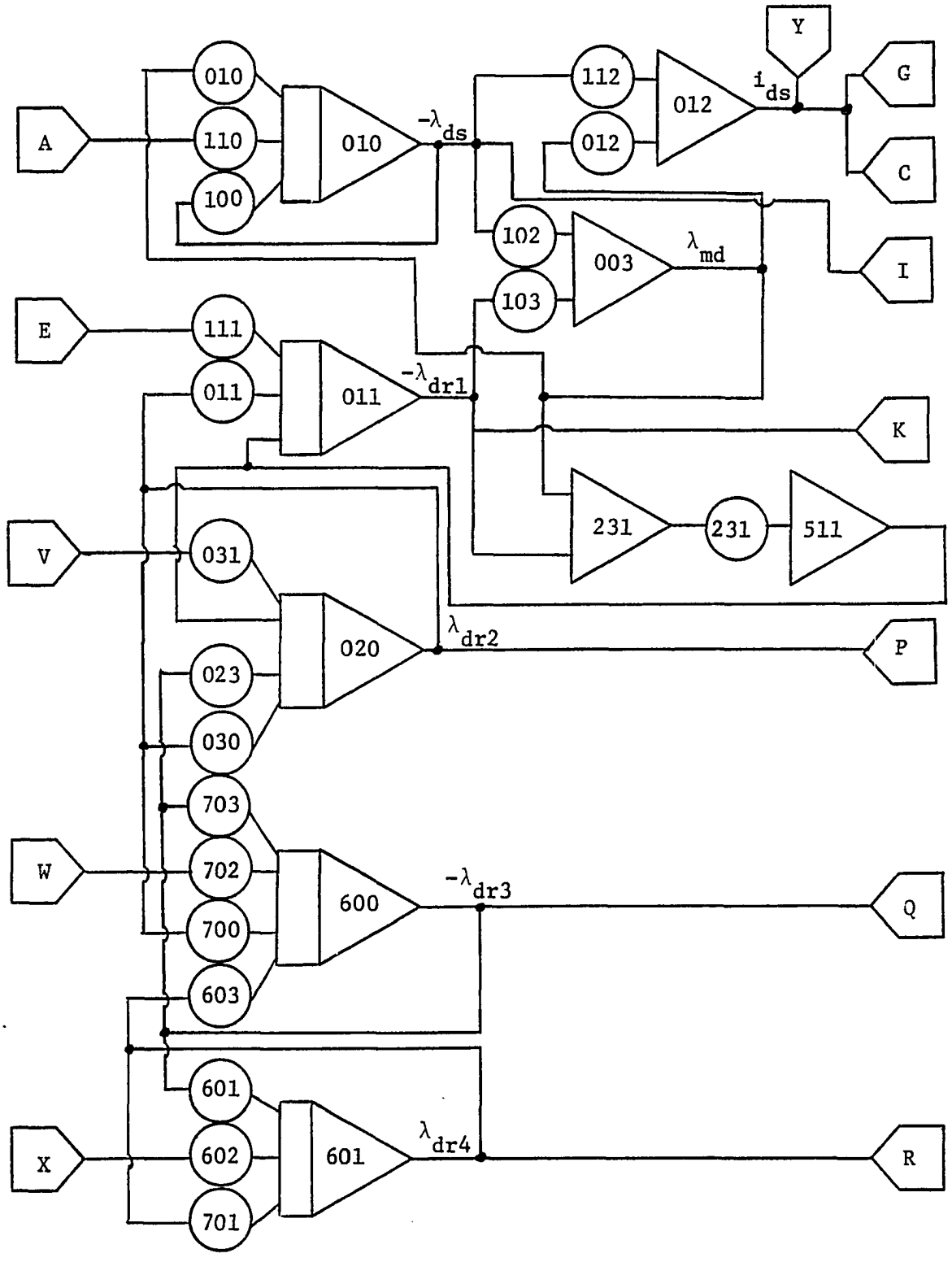

Figure C.1 Continued

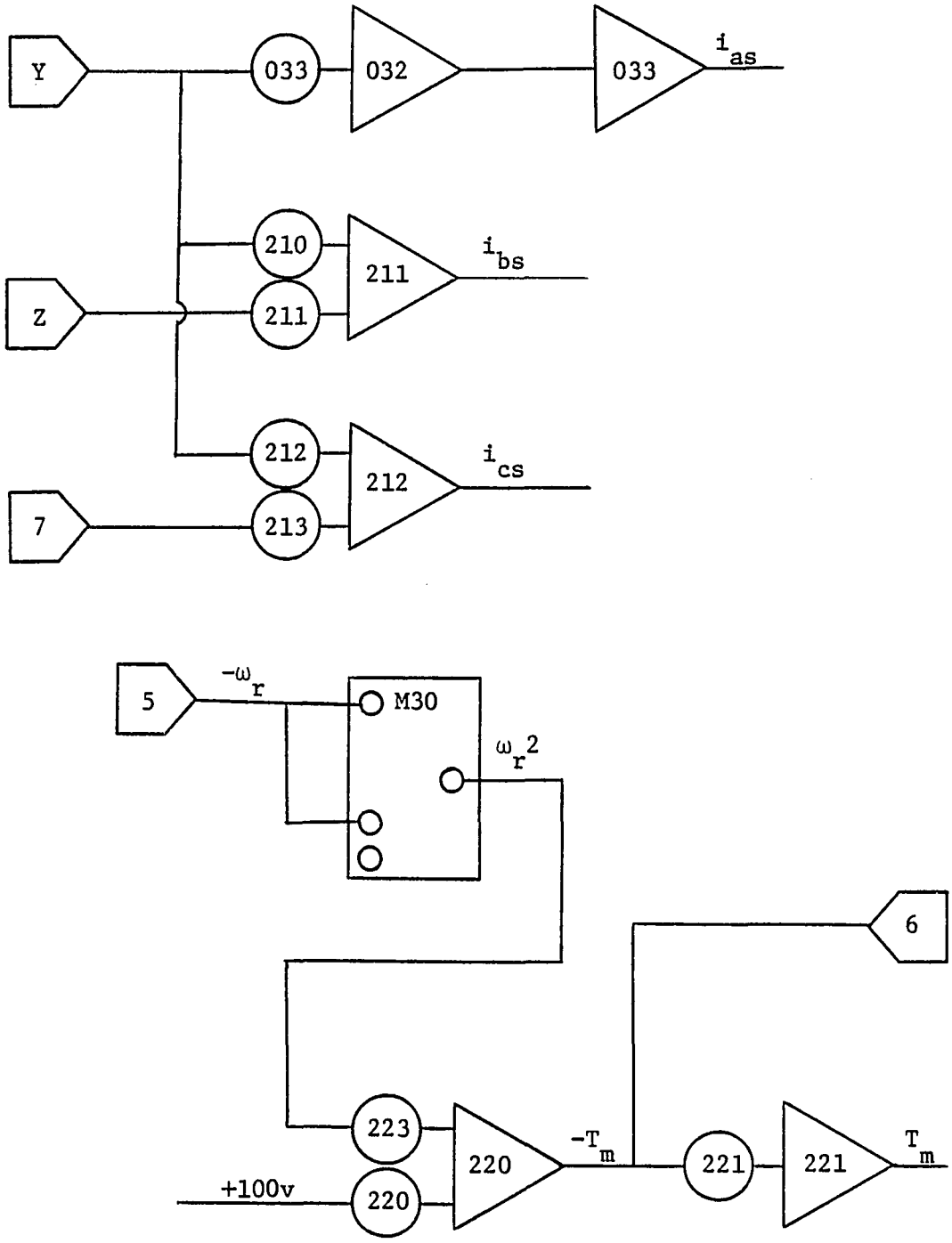

Figure C.1 Continued

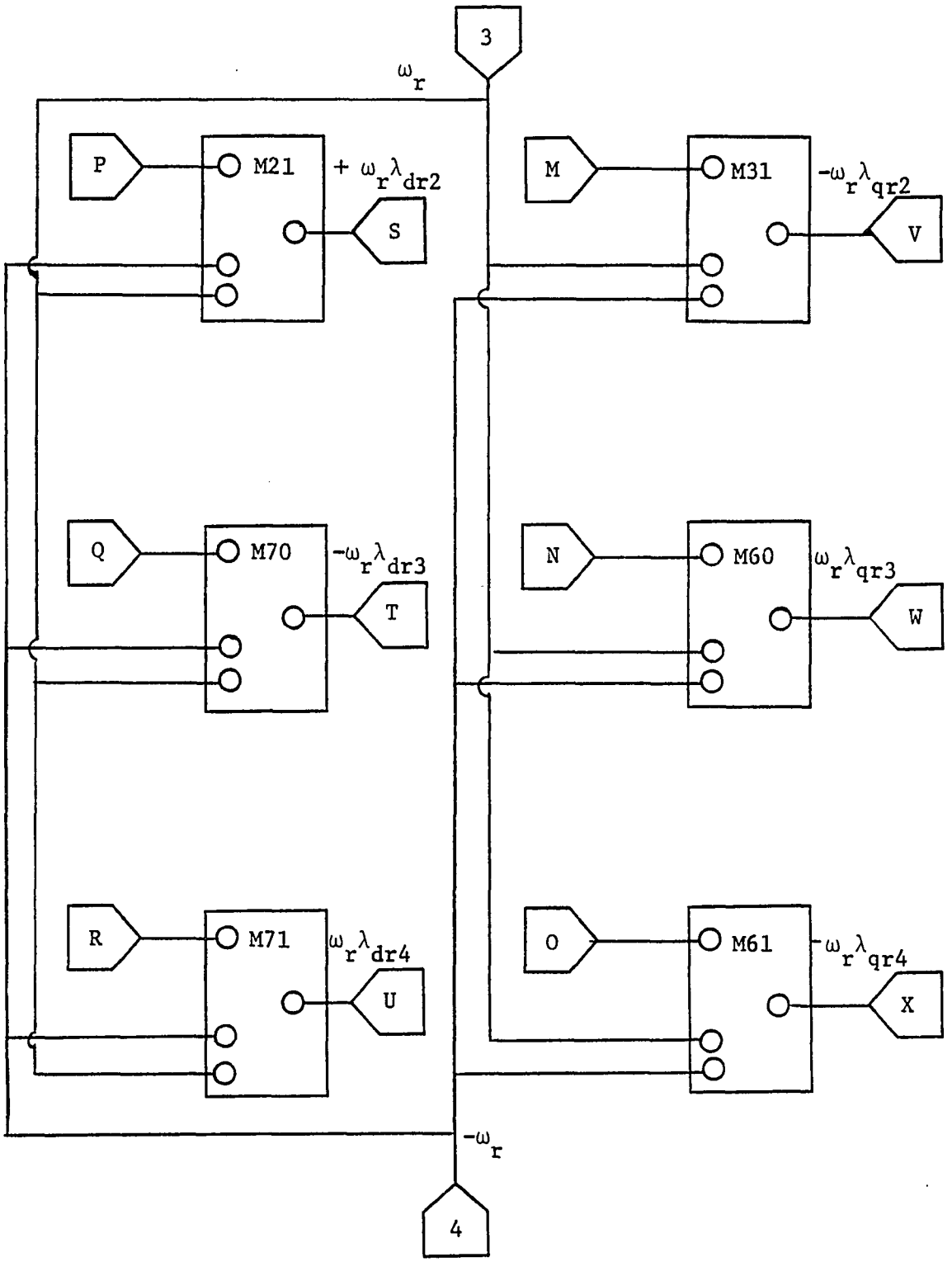

Figure C.1 Continued

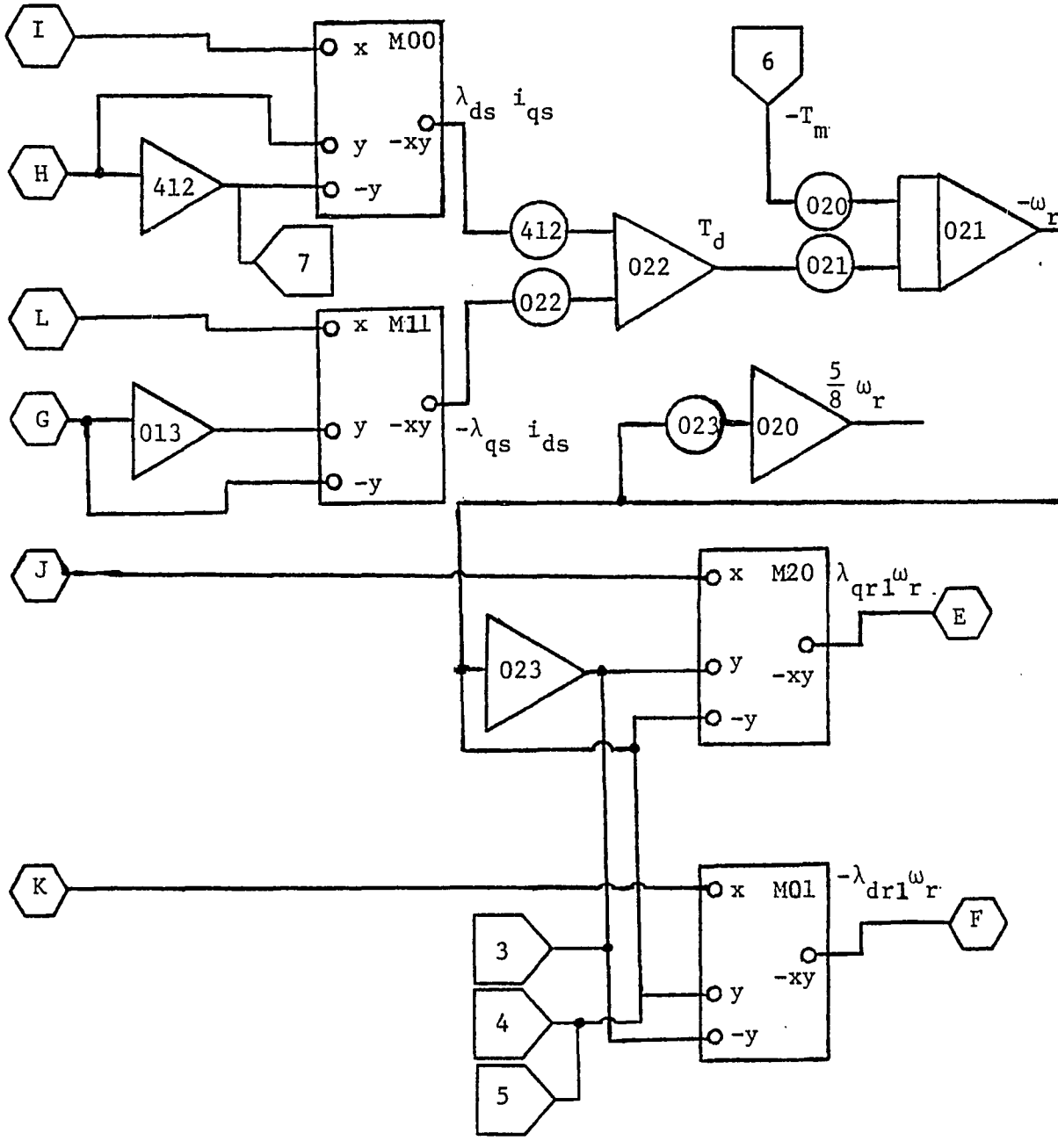

Figure C.1 Continued

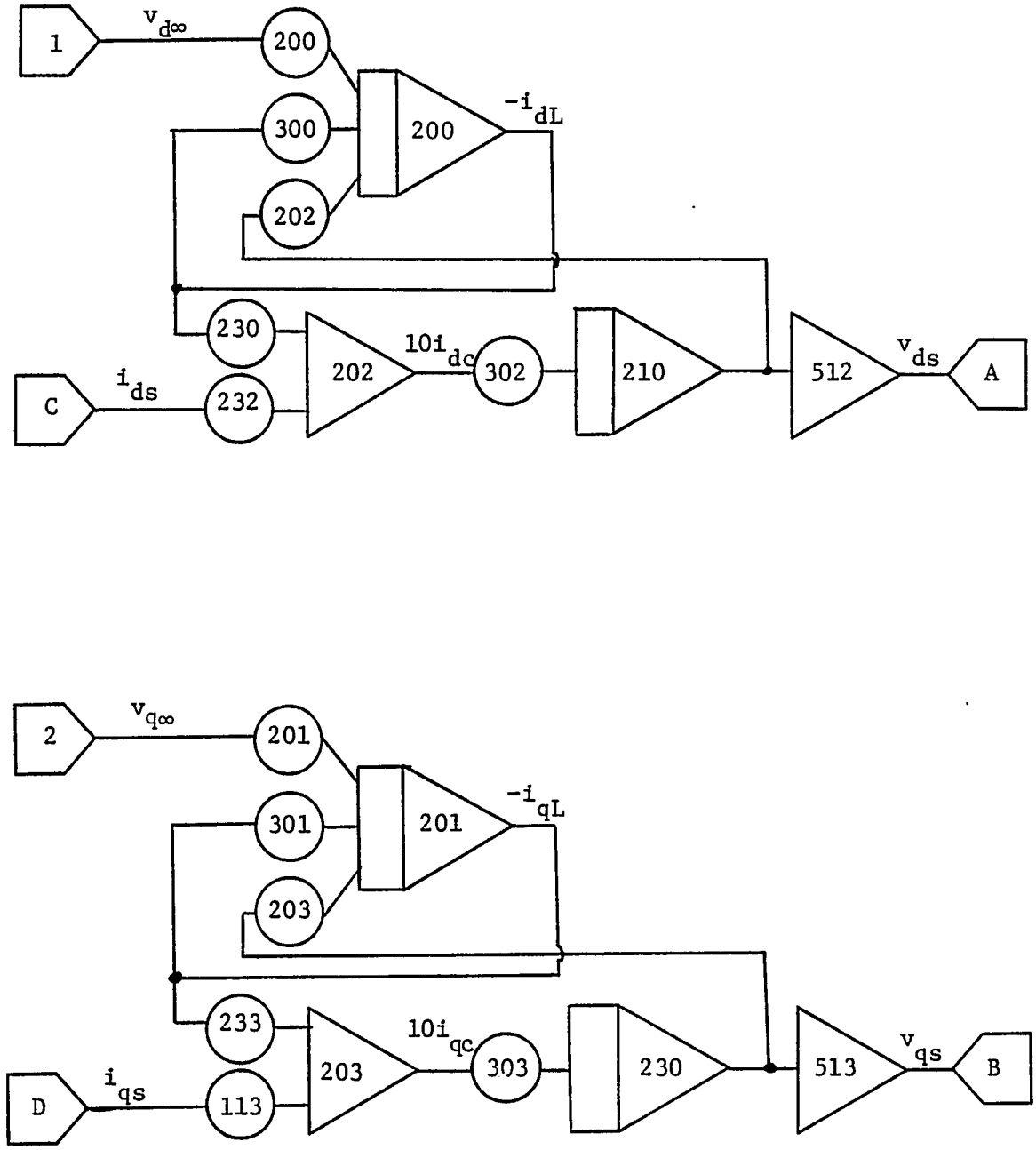

Figure C.1 Continued

Table C.1 Analog device functions

REFERENCE NUMBER	FUNCTION[a,b]	OUTPUT
000	I	$v_{q\infty}$
001	I	$-v_{d\infty}$
002	S	$v_{d\infty}$
003	S	λ_{md}
004	M	$\lambda_{ds}i_{qs}$
010	I	$-\lambda_{ds}$
011	I_{100}	$-\lambda_{dr1}$
012	S	i_{ds}
013	S	i_{ds}
014	M	$-\omega_r\lambda_{dr1}$
020	I_{100}	λ_{dr2}
021	$I_{.1}$	$-\omega_r$
022	S	T_e
023	S	ω_r
031	S	$5/8\omega_r$
032	S	$-i_{as}$
033	S	i_{as}

[a]Functions: I - integrator
S - summer
M - multiplier

[b]Subscripts: .1 - integrator includes x0.1 tap
100 - integrator includes x100 tap

Table C.1 Continued

REFERENCE NUMBER	FUNCTION	OUTPUT
114	M	$-\lambda_{qs} i_{ds}$
200	I_{100}	$-i_{dL}$
201	I_{100}	$-i_{qL}$
202	S	$5i_{dc}$
203	S	$5i_{qc}$
204	M	$\omega_{r\ qrl}$
210	I_{100}	$-v_{ds}$
211	S	i_{bs}
212	S	i_{cs}
214	M	$\omega_r \lambda_{dr2}$
220	S	$-T_m$
221	S	T_m
230	I_{100}	$-v_{qs}$
231	S	$\lambda_{drl} - \lambda_{md}$
304	M	ω_r^2
314	M	$\omega_r \lambda_{qr2}$
400	I	$-\lambda_{qs}$
401	I_{100}	$-\lambda_{qrl}$
402	S	λ_{mq}
403	S	i_{qs}
411	I_{100}	λ_{qr2}
412	S	$-i_{qs}$

Table C.1 Continued

REFERENCE NUMBER	FUNCTION	OUTPUT
413	S	$\lambda_{qr1}-\lambda_{mq}$
510	S	$\lambda_{mq}-\lambda_{qr1}$
511	S	$\lambda_{md}-\lambda_{dr1}$
512	S	v_{ds}
513	S	v_{qs}
600	I_{100}	$-\lambda_{dr3}$
601	I_{100}	λ_{dr4}
604	M	$\omega_r\lambda_{qr3}$
614	M	$-\omega_r\lambda_{qr4}$
704	M	$-\omega_r\lambda_{dr3}$
714	M	$\omega_r\lambda_{dr4}$
800	I_{100}	$-\lambda_{qr3}$
801	I_{100}	λ_{qr4}
812	S	$-\omega_r$
813	S	ω_r

Table C.2 Scale factors used

V_{max}	I_{max}	λ_{max}	T_{max}	ω_{max}	a (time scaling)
3 p.u.	20 p.u.	5 p.u.	10 p.u.	1.25 p.u.	50

Table C.3 Potentiometers

Potentiometer Number	Coefficient	Scaling Factor	S.V. Value[a]	Pot Setting[a]	Multiplier[a]
000	$\sqrt{3}$ V sinα	1/V	.3333	.0000	-
001	$\sqrt{3}$ V cosα	1/V	.3333	.5774	-
002	ω_b	1/a	.02	.7540	10
003	ω_b	1/a	.02	.7540	10
010	$\omega_b r_s/\ell_s$	1/a	.02	.1885	10
011	$\omega_b R_1/L_2$	1/a	.02	.5818	100
012	$1/\ell_s$	$\lambda./I.$	.25	.3125	10
013	oscillator positive feedback			.0016	-
020	1/2H	T/ a	.16	.8000	0.1
021	1/2H	T/ωa	.16	.8000	0.1
022	1/3	λI/T	10.0	.3333	10
023	$\omega_b R_2/L_3$	1/a	.02	.1745	100
030	$\omega_b(R_1+R_2)/L_2$	1/a	.02	.8727	100
031	ω_b	ω/a	.02	.9425	10
032	scaling pot----ω_r recording			.6250	1

033	$\sqrt{2/3}$	1	1.0	.8165	1
100	$\omega_b r_s/\ell_s$	1/a	.02	.1885	10
101	ω_{r0}	1/ω	.8	$.8 \times \omega_{r0}$	-
102	L_m/ℓ_s	1	1.0	.4200	1
103	L_m/L_1	1	1.0	.5714	1
110	ω_b	V/λa	.012	.4524	10
111	ω_b	ω/a	.025	.9425	10
112	$1/\ell_s$	λ/I	.25	.3125	10
113	1.0	1/2	.5	.5000	1
200	ω_b/L_e	V/Ia	.003	.2262	100
201	ω_b/Le	V/Ia	.003	.2262	100
202	ω_b/Le	V/Ia	.003	.2262	100
203	ω_b/Le	V/Ia	.003	.2262	100
120	$1/\sqrt{6}$	1	1	.4082	1
211	$1/\sqrt{2}$	1	1	.7071	1
212	$1/\sqrt{6}$	1	1	.4082	1
213	$1/\sqrt{2}$	1	1	.7071	1

[a]Values for motor M1 with typical source impedance Z_e = .025 + j.05.

Table C.3 Continued

Potentiometer Number	Coefficient	Scaling Factor	S.F. Value[a]	Pot Setting[a]	Multiplier[a]
220	T_{m0}	1/T	.1	$.1xT_{m0}$	1
221	1.1	1/2	.5	.5000	1
222	$\sqrt{2}/3$	1	1.0	.8165	1
223	T_{m2}	$^2/T$	.156	$.156xT_{m2}$	1
230	1.0	1/2	.5	.5000	1
231	$\omega_b R_1/L_1 a$	1.0	1.0	.3206	1
232	1.0	1/2	.5	.5000	1
233	1.0	1/2	.5	.5000	1
300	$\omega_b R_e/L_e$	1/a	.02	.3770	10
301	$\omega_b R_e/L_e$	1/a	.02	.3770	10
302	ω_b/C	I/5Va	.0267	.1007xc	100
303	ω_b/C	I/5Va	.0267	.1007xc	100
400	$\omega_b r_s/\ell_s$	1/a	.02	.1885	10
401	ω_b	ω/a	.025	.9425	10
402	L_m/ℓ_s	1.0	1.0	.4200	1

403	$1/\ell_s$	λ/I	.25	.3125	10
410	ω_b	$V/\lambda a$	.012	.4524	10
411	$\omega_b(R_1+R_2)/L_2$	1/a	.02	.8727	100
412	1/3	$\lambda I/T$	10.0	.3333	10
413	ω_b	ω/a	.025	.9425	10
500	$\omega_b r_s/\ell_s$	1/a	.02	.1885	10
501	$\omega_b R_1/L_2$	1/a	.02	.5818	100
502	L_m/L_1	1.0	1.0	.5714	1
503	$1/\ell_s$	λ/I	.25	.3125	10
600	$\omega_b R_1/L_1 a$	1.0	1.0	.3206	1
601	$\omega_b R_3/L_3$	1/a	.02	.1163	100
602	ω_b	ω/a	.025	.9425	10
603	$\omega_b R_3/L_4$	1/a	.02	.8308	10
700	$\omega_b R_2/L_2$	1/a	.02	.2909	100
701	$\omega_b(R_3+R_4)/L_4$	1/a	.02	.1454	100
702	ω_b	ω/a	.025	.9425	10
703	$\omega_b(R_2+R_3)/L_3$	1/a	.02	.2908	100
800	$\omega_b(R_2+R_3)/L_3$	1/a	.02	.2908	100

Table C.3 Continued

Potentiometer Number	Coefficient	Scaling Factor	S.F. Value[a]	Pot Setting[a]	Multiplier[a]
801	$\omega_b(R_3+R_4)/L_4$	1/a	.02	.1454	100
802	ω_b	ω/a	.025	.9425	10
803	$\omega_b R_3/L_3$	1/a	.02	.1163	100
810	$\omega_b R_3/L_4$	1/a	.02	.8308	10
811	$\omega_b R_2/L_2$	1/a	.02	.2909	100
812	ω_b	ω/a	.025	.9425	10
813	$\omega_b R_2/L_3$	1/a	.02	.1745	100

APPENDIX D: DIGITAL COMPUTER REPRESENTATION OF THE SKIN EFFECT IMPEDANCE MODEL

Time solutions of the skin effect impedance model involve the positive and negative sequence equivalent circuits of the motor (Figures 6.1 and 6.2), the positive and negative sequence torque (Equations 6.57 and 6.59) and the rotor speed (Eq. 5.42).

The step-by-step time solution of these equations is undertaken by first solving the electrical equations with the correct value of rotor slip. The developed torque is then found from the rotor current. Eq. 5.42 is then solved over a time step of integration by the first order Kutta-Merson (23) integration subroutine. A time step of .025 seconds was used in this study, except in cases involving low rotor inertia constants. The rotor speed is then used to find the slip for the next iteration.

The digital program used to solve the skin effect impedance model in this study is presented in Table D.1. Several different forms of subroutine CALCI are given. These forms account for the various power system configurations studied. Table D.2 contains a list of computer variables and constants and the equivalent expressions used in the text. A simplified flow chart of the computer program is given in Figure D.1.

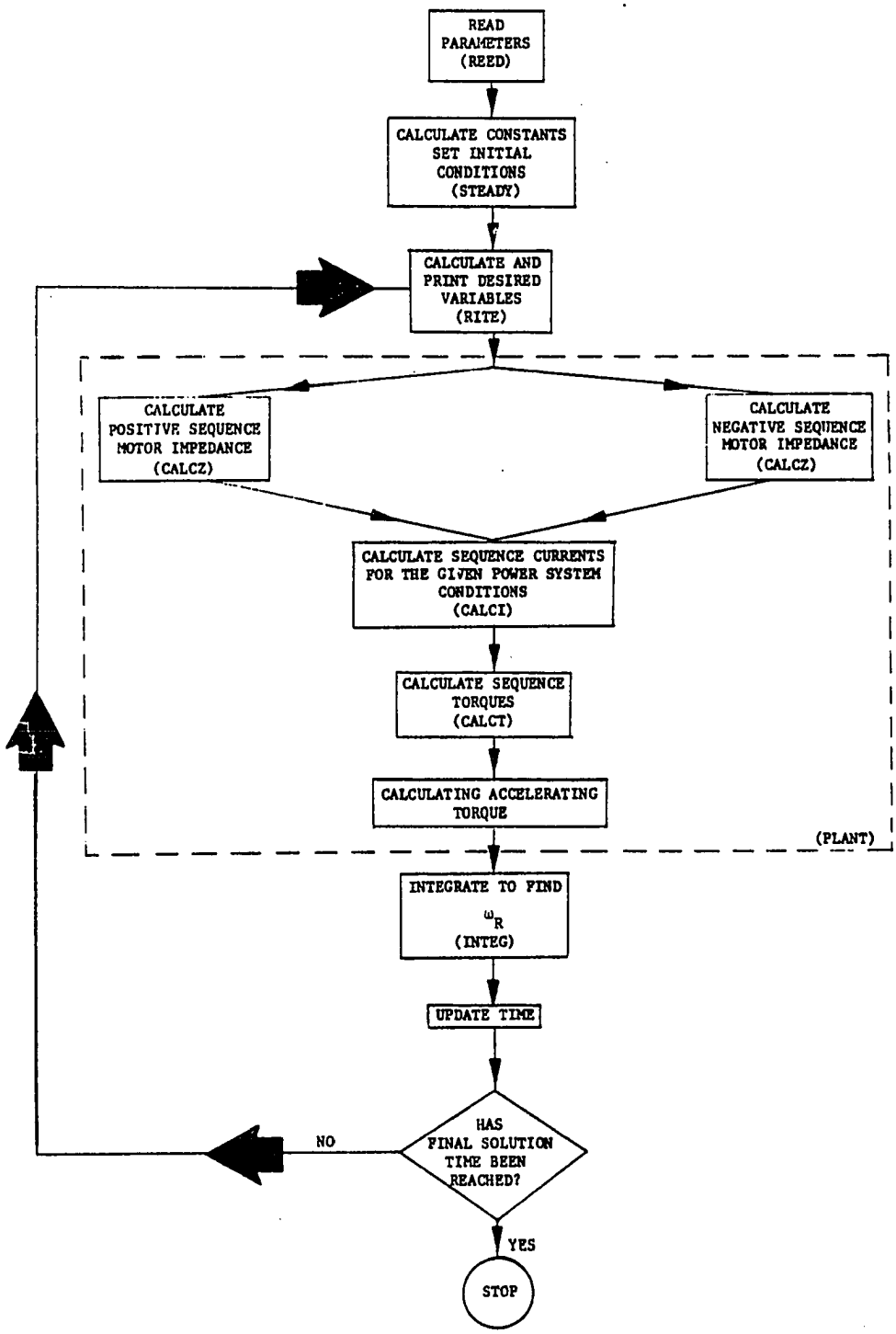

Figure D.1 Simplified flow chart of skin effect impedance model digital program.

Table D.1 Skin effect impedance model digital program listing

```
C         INDUCTION MOTOR PERFORMANCE EVALUATION UNDER VARIOUS
C          UNBALANCED CONDITIONS.  SKIN EFFECT MODEL OF THE INDUCTION MOTOR
C         IS USED.
C  - - - - - - - - - - - - - - - - - - - - - - - - - - - - - - - - - - - - -
C  "REED"  READS IN AND PRINTS OUT DATA
C  "STEADY"  FINDS PRE-DISTURBANCE INITIAL VALUES OF VARIABLES.
C  "INTEG"  IS NUMERICAL INTEGRATING ROUTINE WHICH IN TURN CALLS
C   "PLANT". "PLANT"CONTAINS DIFFERENTIAL EQUNS. AND "INTEG" RETURNS
C   NEW INTEGRATED VALUES TO "MAIN PROGRAM".
C  "RITE"  PRINTS OUT COLUMNS OF INTEGRATION RESULTS
C     "MSTART" SETS INITIAL VALUES FOR STARTING THE MOTOR.
C     "NDIFF" IS THE NUMBER OF DIFFERENTIAL EQUNS TO SOLVE IN "XY".
C        "CALCZ" CALCULATES POSITIVE AND NEGATIVE SEQUENCE MOTOR IMPEDANCES
C        "CALCI" CALCULATES SEQUENCE CURRENCTS
C        "CALCT" CALCULATES SEQUENCE EM TORQUE
C
      IMPLICIT COMPLEX (I,V,Z)
      COMMON/BL5/  RR(8), XR(8), NCIRC, ZMAG, ZSTAT
      COMMON /BL1/  XY(6), XDOT(6), T, DELT, LINES, L, N, TFINAL, NDIFF
      CALL REED
      CALL STEADY
      WRITE(6,60)
C  DISTURBANCE  STARTS#####DISTURBANCE  STARTS######
      CALL MSTART
      WRITE(6,10)
   10 FORMAT ('- TIME', 3X, 'POSITIVE SEQUENCE', 7X, 'NEGATIVE SEQUENCE'
     2  , 7X, /                          10X, 'VPM', 5X, 'IPS', 6X, 'TP',
     3         5X, 'VNM', 5X, 'INS', 6X, 'TN', 6X, 'WR', 5X, 'SLIP',
     4      4X, 'TEM', 5X, 'TLM', 5X, 'VAPK', 5X, 'IAPK',4X,'IBPK',4X,
     5  'ICPK')
      CALL RITE
   84 CONTINUE
      CALL INTEG(T, DELT,NDIFF, XY, XDOT  )
      IF(L-N) 77,78,77
   78 L=0
```

Table D.1 Continued

```
      LINES= LINES+1
      IF( LINES-5) 38,37,37
   37 WRITE(6,60)
      LINES= 0
   38 CALL RITE
   77 L=L+1
      IF(T.GT. TFINAL ) GO TO 85
      GO TO 84
   85 CALL RITE
   86 CONTINUE
    3 CONTINUE
  100 FORMAT   (8F9.4)
  105 FORMAT  (I3,F9.4)
  106 FORMAT  (20X, I3, 10X, F9.4, 5X, F9.4 )
  110 FORMAT (' ROTOR IMPEDANCES    CKT NO.', 5X, 'RESISTANCE', 5X,
     2    'REACTANCE', 'GAP REACTANCE XG=',  F9.4)
   60 FORMAT(2X,'-------------------------------------------------------
     2-------------------------------------------------------')
      STOP
      END
C- - - - - - - - - - - - - - - - - - - - - - - - - - - - - - - - - - - -
      SUBROUTINE REED
      IMPLICIT COMPLEX (I,V,Z)
      COMMON /BL1/  XY(6), XDOT(6), T, DELT, LINES, L, N, TFINAL, NDIFF
      COMMON/BL2/  IP,IN, VPM,VNM,TP,TN,TEM,TLM,WR,SLIP , ZPM, ZNM,WRO
      COMMON/BL3/  RL,  XL,  UP, UN, PHIPN, F, RT, XT, NPHASE, RS, XS,
     2    XM, H, TL0, TL2, XCAP
      COMMON/BL5/  RR(8), XR(8), NCIRC, ZMAG, ZSTAT
      READ (5,100) RL, XL, UP, UN, PHIPN, F, XCAP
      WRITE (6,101) RL, XL, UP, UN, PHIPN, F, XCAP
      READ (5,102)  RT, XT, NPHASE
      WRITE (6,103)   RT, XT, NPHASE
      READ (5,100) RS,XS,XM,RM
      WRITE (6,104) RS,XS,XM,RM
      ZMAG = CMPLX(RM,XM)
      ZSTAT = CMPLX(RS,XS)
```

Table D.1 Continued

```
      READ (5,105)   NCIRC,  XG
      WRITE (6,110)   XG
      DO 1 J = 1,NCIRC
      READ (5,100)       RR(J),    XR(J)
    1 WRITE (6,106)   J, RR(J), XR(J)
      XR(NCIRC)  =XR(NCIRC)  +  XG
      READ (5,100) H, TL0, TL2, WR
      WRITE (6,107)  H,TL0,TL2,WR
      WRD = WR
      READ (5,108)   DELT,  N,  TFINAL
      WRITE (6,109)  DELT,  N,  TFINAL
  100 FORMAT   (8F9.4)
  101 FORMAT  (' SYSTEM DATA  RL=', F9.4, 2X, 'XL=', F9.4, 2X,
     2   'BUS VOLTAGE-POS. SEQ', F9.4, 2X, 'NEG SEQ', F9.4, 2X,
     3  'PHIPN=', F9.4, 2X, 'F=',  F9.4,2X,/,'XCAP=',F9.4)
  103 FORMAT  (' TRANSFORMER DATA  RT=',F9.4, 2X, 'XT=', F9.4, 2X,
     2     '2 OR 3 PHASE BANK', I3)
  102 FORMAT (2F9.4, I3)
  104 FORMAT (' STATOR DATA  RS=',F9.4, 2X, 'XS=', F9.4, 2X,
     2 'MAG IND XM=', F9.4, 'MAG BRANCH RES RM=', F9.4)
  107 FORMAT (' MECHANICAL DATA  H=', F9.4,  2X, 'TL0=',F9.4, 2X,
     2  'TL2=', F9.4, 'INITIAL SPEED WR=', F9.4)
  108 FORMAT  (F9.4, I3, F9.4)
  109 FORMAT (' DELT=', F9.4, 2X, 'N=', I3, 2X, 'TFINAL=', F9.4)
      RETURN
      END
C- - - - - - - - - - - - - - - - - - - - - - - - - - - - - - - - - - -
C
      SUBROUTINE STEADY
      IMPLICIT COMPLEX (I,V,Z)
      COMMON /BL1/  XY(6), XDOT(6), T, DELT, LINES, L, N, TFINAL, NDIFF
      COMMON/BL2/  IP,IN, VPM,VNM,TP,TN,TEM,TLM,WR,SLIP , ZPM, ZNM,WRD
      COMMON/BL3/  RL,  XL,  UP, UN, PHIPN, F, RT, XT, NPHASE, RS, XS,
     2    XM, H, TL0, TL2, XCAP
      COMMON/BL4/ ACF, VPB, VNB, IO
      COMMON/BL6/ ZCAP, ZL, VPBS, VNBS, Z11, Z22, Z12, VOM
```

Table D.1 Continued

```
      SQ2= SQRT(2.0)
      SQ3= SQRT(3.0)
      SQ32 = SQ3/2.0
      PAI= 3.141593
      WZ= 2.0*PAI*F
      ACF =  0.5/H
      T=0.0
      LINES = 1
      L=1
      ZA = CMPLX(-0.5,SQ32)
      ZASQ = CMPLX(-0.5,-SQ32)
      NDIFF= 1
      DO 300 J=1,6
      XY(J) =0.0
  300 XDOT(J)= 0.0
      XY(1) = WRO
      IF (XY(1).GT.0.999) XY(1) = 0.999
      VPB = CMPLX(UP,0.0)
      PHIPNR = PHIPN * PAI /180.0
      A =  UN * COS(PHIPNR)
      B = UN * SIN(PHIPNR)
      VNB = CMPLX(A,B)
      ZL = CMPLX(RL,XL)
      X = -XCAP
      ZCAP = CMPLX(0.0,X)
      Z11 = CMPLX(RT, XT)
      Z12 = -Z11/3.0
      Z22 = Z11*2.0/3.0 + CMPLX(RL,XL)
      Z11 = Z22
      A = 2.0*UP/3.0
      VPBS = CMPLX(A,0.0)
      A = -A/2.0
      VNBS = CMPLX(A,0.0)
      RETURN
C - - - - - - - - - - - - - - - - - - - - - - - - - - - - - - - - - - - - - -
```

Table D.1 Continued

```
      ENTRY RITE
      RIM = REAL (IP)
      AIMI = AIMAG(IP)
      CPRMS = SQRT(RIM*RIM + AIMI*AIMI)
      RIM = REAL(IN)
      AIMI = AIMAG(IN)
      CNRMS = SQRT(RIM*RIM + AIMI*AIMI)
      VPM = IP*ZPM
      RV = REAL(VPM)
      AIV = AIMAG(VPM)
      UPM = SQRT(RV*RV + AIV*AIV)
      VNM = IN * ZNM
      RV = REAL(VNM)
      AIV = AIMAG (VNM)
      UNM = SQRT(RV*RV + AIV*AIV)
      IA = IP + IN
      VAM = VPM + VNM + VOM
      R = REAL(IA)
      AI = AIMAG(IA)
      CA = SQRT(R*R+ AI*AI) * SQ2
      R = REAL(VAM)
      AI = AIMAG(VAM)
      UA = SQRT(R*R+AI*AI) * SQ2
      IB = IP*ZASQ + IN*ZA
      IC = IP * ZA + IN * ZASQ
      AI = AIMAG(IB)
      R = REAL(IB)
      CB = SQRT(R*R+AI*AI)*SQ2
      R = REAL(IC)
      AI = AIMAG(IC)
      CC = SQRT(R*R+AI*AI)*SQ2
      WRITE(6,301) T,UPM,CPRMS,TP,UNM,CNRMS,TN,WR,SLIP,TEM,TLM,UA,CA
     2    , CB,CC
  301 FORMAT (15F8.3)
      RETURN
      END
```

Table D.1 Continued

```
C - - - - - - - - - - - - - - - - - - - - - - - - - - - - - - - - - - -
      ENTRY MSTART
      CALL PLANT( T, XY, XDOT )
      RETURN
C- - - - - - - - - - - - - - - - - - - - - - - - - - - - - - - - - - -
C - - - - - - - - - - - - - - - - - - - - - - - - - - - - - - - - - - -
C
      SUBROUTINE PLANT(TDUM, YV, YDOT)
      IMPLICIT COMPLEX (I,V,Z)
      DIMENSION YV(6),  YDOT(6)
      COMMON/BL2/  IP,IN, VPM,VNM,TP,TN,TEM,TLM,WR,SLIP , ZPM, ZNM,WRO
      COMMON/BL3/  RL,  XL,  UP, UN, PHIPN, F, RT, XT, NPHASE, RS, XS,
     2    XM, H, TL0, TL2, XCAP
      COMMON/BL4/ ACF, VPB, VNB, IO
      WR =  YV(1)
      SLIP = 1.0-WR
      CALL CALCZ (SLIP, ZPM, ZPR)
      BSLIP = 2.0 - SLIP
      CALL CALCZ (BSLIP, ZNM, ZNR)
      CALL CALCI (ZPM,ZNM,IP,IN,IO,VPB,VNB)
      CALL CALCT(IP,ZPR,XM,TP)
      CALL CALCT (IN,ZNR,XM,TN)
      TEM = TP-TN
      TLM = TL0 + TL2 * WR * WR
      YDOT(1)  = ACF * (TEM - TLM)
      RETURN
      END
```

Table D.1 Continued

```
      SUBROUTINE CALCZ (S,Z,ZR)
      IMPLICIT COMPLEX (I,V,Z)
      DIMENSION R(8)
      COMMON/BL5/  RR(8), XR(8), NCIRC, ZMAG, ZSTAT
      DO 10  J = 1,NCIRC
   10 R(J) =  RR(J) / S
      RM =  R(1)
      XM = XR(1)
      DO 11 J = 2,NCIRC
      DMI = (RM + R(J))**2 + XM*XM
      RM = R(J) * (RM*(RM + R(J)) + XM*XM)/DMI
      XM = XM*R(J)*R(J)/DMI + XR(J)
   11 CONTINUE
      ZR = CMPLX(RM,XM)
      Z = ZSTAT + ZMAG*ZR/(ZMAG+ZR)
      RETURN
      END
      SUBROUTINE CALCT (IEQ, ZEQ, XM, T)
      IMPLICIT COMPLEX (I,V,Z)
      COMMON/BL5/ RR(8), XR(8), NCIRC, ZMAG, ZSTAT
      REQ = REAL(ZEQ)
      IR = IEQ*ZMAG/(ZMAG+ZEQ)
      A = REAL(IR)
      B = AIMAG(IR)
      CROTOR = SQRT(A*A+B*B)
      T = REQ*CROTOR*CROTOR
      RETURN
      END
```

Table D.1 Continued

```
      SUBROUTINE INTEG(T,DELT,N,X,YDOT  )
C     FIXED KUTTA MERSON OVERRIDING THE VARIABLE TIME STEP
      DIMENSION  X(6), YDOT(6), XN(6)
      DIMENSION FK1(8), FK2(8), FK3(8), FK4(8),  FK5(8)
C     N IS LIMITED BY CORE STORAGE AND IS THE NUMBER OF DIFFERENTIAL EQN
      DELT2=DELT/2.
      DELT3=DELT/3.
      CALL PLANT(T, X , YDOT )
      DO 10 M=1,N
      FK1(M)=DELT3*YDOT(M)
      XN(M)=X(M)+FK1(M)
   10 CONTINUE
      T3=T+DELT3
      CALL PLANT(T3, XN, YDOT )
      DO 20M =1,N
      FK2(M)=DELT3*YDOT(M)
      XN(M)=X(M)+(FK2(M)+FK1(M))/2.
   20 CONTINUE
      CALL PLANT(T3, XN, YDOT )
      DO 30 M=1,N
      FK3(M)=DELT3*YDOT(M)
      XN(M)=X(M)+(FK3(M) *9.+3.*FK1(M))/8.
   30 CONTINUE
      T2=T+DELT2
      CALL PLANT(T2, XN, YDOT )
      DO 40M=1,N
      FK4(M)=DELT3*YDOT(M)
      XN(M) = X(M) +( 3.*FK1(M) -9.*FK3(M) +12.*FK4(M) )/2.
   40 CONTINUE
      T=T+DELT
      CALL PLANT(T, XN, YDOT )
      DO 50M=1,N
      FK5(M)=DELT3*YDOT(M)
   50 CONTINUE
      DO 60M=1,N
```

Table D.1 Continued

```
      X(M)=X(M)+(FK1(M)+4.*FK4(M)+FK5(M))/2.
   60 CONTINUE
      RETURN

      SUBROUTINE CALCI(ZPM,ZNM,IP,IN,IO,VPB,VNB)
      IMPLICIT COMPLEX (I,V,Z)
C     MOTOR PERFORMANCE WITH A PHASE SUDDENLY OPEN-----
C           SHUNT CAPACITOR (UNGROUNDED) AT MOTOR TERMINALS
      COMMON/BL6/ ZCAP, ZL, VPBS, VNBS, Z11, Z22, Z12, VOM
      ZP = ZPM*ZCAP/(ZPM+ZCAP)
      ZN = ZNM*ZCAP/(ZNM+ZCAP)
      Z = ZL + ZN
      ZEQ = Z + ZL + ZP
      I = VPB/ZEQ
      IP = I*ZCAP/(ZPM+ZCAP)
      INS = -I
      IN = INS*ZCAP/(ZNM+ZCAP)
      VOM = -INS*Z
      RETURN
      END
C  - - - - - - - - - - - - - - - - - - - - - - - - - - - - - - - - - - - - -
C
```

Table D.1 Continued

```
      SUBROUTINE CALCI(ZPM,ZNM,IP,IN,IO,VPB,VNB)
      IMPLICIT COMPLEX (I,V,Z)
C        MOTOR PERFORMANCE WITH SHORT CIRCUIT ON A PHASE MOTOR TERMINAL
      COMMON/BL6/ ZCAP, ZL, VPBS, VNBS, Z11, Z22, Z12, VOM
      IP = VPBS/ZPM
      IN = VNBS/ZNM
      VOM = VNBS
      RETURN
      END
      SUBROUTINE CALCI(ZPM,ZNM,IP,IN,IO,VPB,VNB)
C        MOTOR  STARTING PERFORMANCE WITH OPEN DELTA TRANSFORMER
      IMPLICIT COMPLEX (I,V,Z)
      COMMON/BL6/ ZCAP, ZL, VPBS, VNBS, Z11, Z22, Z12
      ZP = Z11 + ZPM
      ZN = Z22 + ZNM
      ZDET = ZP*ZN - Z12*Z12
      IP = (ZN*VPB - Z12*VNB)/ZDET
      IN = (ZP*VNB-Z12*VPB)/ZDET
      IO = CMPLX(0.0,0.0)
      RETURN
      END
      SUBROUTINE CALCI(ZPM,ZNM,IP,IN,IO,VPB,VNB)
      IMPLICIT COMPLEX (I,V,Z)
      COMMON/BL6/ ZCAP, ZL, VPBS, VNBS, Z11, Z22, Z12, VOM
C        MOTOR PERFORMANCE WITH A PHASE SUDDENLY OPEN----
      ZEQ = ZPM + ZNM + 2.0*ZL
      I = VPB/ZEQ
      IP = I
      IN = -I
      VOM = -I*(ZNM+ZL)
      RETURN
      END
```

Table D.2 Equivalent parameters

TEXT	COMPUTER PROGRAM
r_s	RS
$\omega_o \ell_s$	XS
$w_0 M$	XM
R_k	RR(k)
$\omega_0 L_0$	XG
$\omega_0 L_k$	XR(k)
H	H
ω_r	WR
S	SLIP
T_e	TEM
T_m	TLM
$\overline{I}_1$	IP
$\overline{I}_2$	IN
$\overline{V}_1$	VPM
$\overline{V}_2$	VNM

APPENDIX E: DEVELOPED TORQUE IN THE MOTOR

As the electrical machine properties have been expressed in terms of phasor quantities, it is desirable to also derive a relationship between these phasor quantities and the developed torque. In order to do this, the torque equation of Chapter 5 must be expressed in terms of rotor quantities rather than stator quantities.

The per unit torque developed by the motor is, from Chapter 5,

$$T_e = \frac{1}{3}(\lambda_{qs} i_{ds} - \lambda_{ds} i_{qs}) \tag{E.1}$$

An alternate expression for this torque is Equation E.2, which is found by substituting the equations for λ_{qs} and λ_{ds} into Equation E.1.

$$T_e = \frac{M}{3}(i_{qr1} i_{ds} - i_{dr1} i_{qs}) \tag{E.2}$$

In order to express the torque strictly in terms of rotor quantitites, it is helpful to define currents in each bar segment, as shown in Figure E.1. Then

$$i_{dr1} = \sum_{k=1}^{N} i_{dbk} \tag{E.3}$$

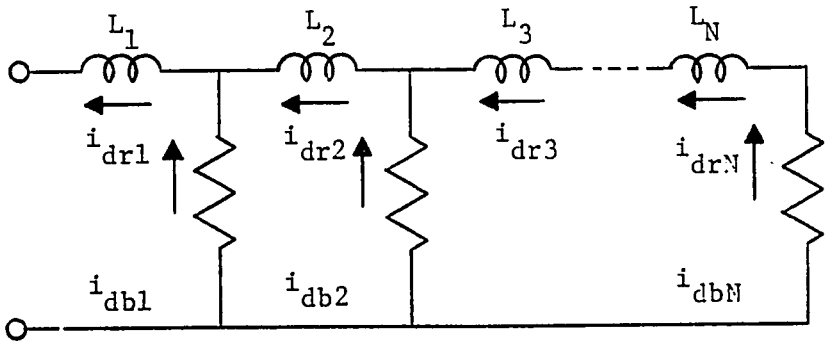

Fig. E.1 d-axis rotor bar equivalent circuit defining rotor bar segment segment currents

Also, from Figure E.1

$$i_{dbk} = i_{drk} - i_{drk+1} \tag{E.4}$$

except for k=N when

$$i_{dbN} = i_{drN} \tag{E.5}$$

Similar defininitions are also taken for q axis quantities. Equation E.2 now can be written in terms of the individual bar segments currents as

$$T_e = \frac{M}{3} \sum_{k=1}^{N} (i_{qbk} i_{ds} - i_{dbk} i_{qs}) \tag{E.6}$$

For any segment m,

$$i_{drm} i_{qrm} - i_{qrm} i_{drm} = 0 \tag{E.7}$$

can be rewritten as

$$\sum_{k=m}^{N} (i_{drm} i_{qbk} - i_{qrm} i_{dbk}) = 0 \tag{E.8}$$

Then

$$T_e = \frac{M}{3} \sum_{k=1}^{N} (i_{qbk} i_{ds} - i_{dbk} i_{qs}) + \frac{M+L_0+L_1}{3} \sum_{k=1}^{N} (i_{dr1} i_{qbk} - i_{qr1} i_{dbk})$$

$$+ \sum_{m=2}^{N} \frac{L_m}{3} \sum_{k=m}^{N} (i_{drm} i_{qbk} - i_{qrm} i_{dbk}) \tag{E.9}$$

While this expression appears to overly complicate the torque equation, actually it will lead to the evaluation of developed torque in terms of rotor bar currents and the flux linking that bar segment. Recall that in defining the rotor flux linkages, λ_{r1} linked the entire bar, λ_{r2}

linked only segments 2 through N, and similarly on to λ_{rN}, which linked only the final rotor segment N. Then, in general, the flux linking the k^{th} rotor bar segment is

$$\sum_{m=1}^{k} \lambda_m \tag{E.10}$$

The torque can now be separated into N components,

$$T_e = T_{e1} + T_{e2} + \cdots + T_{eN} \tag{E.11}$$

where T_{ej} is the sum of all components of Equation E.9 where j=k. Then

$$T_{e1} = \frac{1}{3} \left\{ \left[Mi_{ds} + (M+L_0+L_1) i_{dr1} \right] i_{qb1} - \left[Mi_{qs} + (M+L_0+L_1) i_{qr1} \right] i_{db1} \right\} \tag{E.12}$$

From the set of equations relating flux linkage and currents, Equation 5.39,

$$T_{e1} = \frac{1}{3} (\lambda_{dr1} i_{qb1} - \lambda_{qr1} i_{db1}) \tag{E.13}$$

Similarly,

$$\begin{aligned} T_{e2} &= \frac{1}{3} \left\{ \left[Mi_{ds} + (M+L_0+L_1) i_{dr1} + L_2 i_{dr2} \right] i_{qb2} \right. \\ &\quad \left. - \left[Mi_{qs} + (M+L_0+L_1) i_{dr1} + L_2 i_{qr2} \right] i_{db2} \right\} \\ &= \frac{1}{3} \left[(\lambda_{dr1} + \lambda_{dr2}) i_{qb2} - (\lambda_{qr1} + \lambda_{qr2}) i_{db2} \right] \end{aligned} \tag{E.14}$$

In general, from Equation 6.36 and the flux linkage relationships

$$T_{ek} = \frac{1}{3} \left(\sum_{m=1}^{N} \lambda_{drm} \right) i_{qbk} - \left(\sum_{m=1}^{k} \lambda_{qrm} \right) i_{dbk} \tag{E.15}$$

which states that developed torque related to a rotor bar segment is a function of the current in the segment and the total flux linking that segment. The developed torque of the motor is the sum of these individual torques

$$T_e = \frac{1}{3} \sum_{k=1}^{N} \sum_{m=1}^{k} (\lambda_{drm} i_{qbk} - \lambda_{qrm} i_{dbk}) \qquad \text{(E.16)}$$

Sequence torques: Equation E.16 is a general expression for the developed torque of the motor. This equation is valid in any reference frame. It is, however, written in terms of d and q axis components. For the simplified analysis of this chapter, it is necessary to obtain a relationship between torque and positive and negative sequence phasor quantities.

Consider a machine fed from a positive sequence source. Equations 6.1 and 6.9 relate the motor variables. In the steady state, the currents and flux linkages are constants. The rotor equations are

$$\begin{aligned}
0 &= R_1(i_{dr1} - i_{dr2}) + s\omega_0 \lambda_{qr1} \\
0 &= R_1(i_{qr1} - i_{qr2}) - s\omega_0 \lambda_{dr1} \\
0 &= R_1(i_{dr2} - i_{dr1}) + R_2(i_{dr2} - i_{dr3}) + s\omega_0 \lambda_{qr2} \\
0 &= R_1(i_{qr2} - i_{qr1}) + R_2(i_{qr2} - i_{qr3}) - s\omega_0 \lambda_{dr2} \\
&\vdots \\
0 &= R_{N-1}(i_{drN} - i_{drN-1}) + R_N i_{drN} + s\omega_0 \lambda_{qrN} \\
0 &= R_{N-1}(i_{qrN} - i_{qrN-1}) + R_N i_{qrN} - s\omega_0 \lambda_{drN}
\end{aligned} \qquad \text{(E.17)}$$

The flux linkages are, using the relationships of Equations E.4 and E.17

$$\lambda_{qr1} = -\frac{R_1}{s\omega_0} i_{db1}$$

$$\lambda_{dr1} = \frac{R_1}{s\omega_0} i_{qb1}$$

$$\lambda_{qr1} + \lambda_{qr2} = -\frac{R_2}{s\omega_0} i_{db2}$$

$$\lambda_{dr1} + \lambda_{dr2} = \frac{R_2}{s\omega_0} i_{qb2}$$

$$\vdots$$

$$\sum_{k=1}^{N} \lambda_{qrk} = -\frac{R_N}{s\omega_0} i_{dbN}$$

$$\sum_{k=1}^{N} \lambda_{drk} = \frac{R_N}{s\omega_0} i_{qbN} \qquad \text{(E.18)}$$

These flux linkages can be substituted into Equation E.16 to find

$$T_e = \frac{1}{3} \sum_{k=1}^{N} \frac{R_k}{s\omega_0} (i_{qbk}^2 + i_{dbk}^2) \qquad \text{(E.19)}$$

Equation 6.17 relates the axis quantities to the positive sequence phase quantities. Using this relationship, the positive sequence torque is

$$T_{ep} = \sum_{k=1}^{N} \frac{R_k}{s\omega_0} I_{bkp}^2 \qquad \text{(E.20)}$$

The developed torque due to positive sequence currents is therefore equal to the sum of the square of the individual bar segment current

magnitude times the bar segment resistance all divided by the per unit slip of the motor.

The negative sequence torque can be found in a similar manner by using the negative sequence reference frame Equations 6.24 and 6.28 rather than the synchronously rotating reference frame Equations 6.9 and 6.17. A machine fed by negative sequence voltages operating in the steady state will have constant currents and flux linkages.

$$\lambda_{qr1} = \frac{R_1}{(2-s)\omega_0} \; i_{db1}$$

$$\lambda_{dr1} = -\frac{R_1}{(2-s)\omega_0} \; i_{qb1}$$

$$\lambda_{qr1} + \lambda_{qr2} = \frac{R_2}{(2-s)\omega_0} \; i_{db2}$$

$$\lambda_{dr1} + \lambda_{dr2} = -\frac{R_2}{(2-s)\omega_0} \; i_{qb2}$$

$$\vdots$$

$$\sum_{k=1}^{N} \lambda_{qrk} = \frac{R_N}{(2-s)\omega_0} \; i_{dbN}$$

$$\sum_{k=1}^{N} \lambda_{drk} = -\frac{R_N}{(2-s)\omega_0} \; i_{qbN} \qquad \text{(E.21)}$$

and the negative sequence torque will be

$$T_{eN} = -\sum_{k=1}^{N} \frac{R_k}{(2-s)\omega_0} \; I_{bkn}^2 \qquad \text{(E.22)}$$

Normally, the motor will contain both positive and negative sequence currents. Under these conditions, the total torque is not the sum of the positive sequence torque and the negative sequence torque. A third component of torque is also present which arises from the interaction of the positive and negative sequence currents. This torque oscillates at the frequency which the positive and negative sequence flux waves pass each other in the air-gap, which is 120 hertz. As this torque component has an average value of zero, it should not significantly affect the overall motor performance. Therefore, it is generally neglected in studying the positive and negative sequence performance of the induction motor.